MOLTEN SALT ASSISTED SELF-ASSEMBLY (MASA): SYNTHESIS OF MESOPOROUS SILICA-ZnO AND MESOPOROUS CdO THIN FILMS

A DISSERTATION SUBMITTED TO

THE DEPARTMENT OF CHEMISTRY

AND

THE GRADUATE SCHOOL OF ENGINEERING AND SCIENCE

OF

BILKENT UNIVERSITY

IN PARTIAL FULFILLMENT OF THE REQUIREMENTS

FOR THE DEGREE OF

MASTER OF SCIENCE

By

CÜNEYT KARAKAYA

January 2012

I certify that I have read this thesis and have found that it is fully adequate, in scope and in quality, as a thesis for the degree of Master of Science.

Prof. Dr. Ömer Dağ
Supervisor

I certify that I have read this thesis and have found that it is fully adequate, in scope and in quality, as a thesis for the degree of Master of Science.

Prof. Dr. Saim Özkar
Examining Committee Member

I certify that I have read this thesis and have found that it is fully adequate, in scope and in quality, as a thesis for the degree of Master of Science.

Assoc. Prof. Dr. Margarita Kantcheva
Examining Committee Member

I certify that I have read this thesis and have found that it is fully adequate, in scope and in quality, as a thesis for the degree of Master of Science.

Assist. Prof. Dr. Erman Bengü
Examining Committee Member

I certify that I have read this thesis and have found that it is fully adequate, in scope and in quality, as a thesis for the degree of Master of Science.

Assist. Prof. Dr. Emrah Özensoy
Examining Committee Member

Approval of the Graduate School of Engineering and Science

Prof. Dr. Levent Onural
Director of the Institute

ABSTRACT

MOLTEN SALT ASSISTED SELF-ASSEMBLY (MASA):

SYNTHESIS OF MESOPOROUS SILICA-ZnO AND MESOPOROUS SILICA-CdO THIN FILMS

CÜNEYT KARAKAYA

M.S. in Chemistry

Supervisor: Prof. Dr. Ömer Dağ

January 2012

A series of mesostructured salt-silica-two surfactants (salt is $[Zn(H_2O)_6](NO_3)_2$, ZnX or $[Cd(H_2O)_4](NO_3)_2$, CdYand surfactants are cetyltrimethylammonium bromide (CTAB) and 10-lauryl ether, $C_{12}H_{25}(OCH_2CH_2)_{10}OH$, $C_{12}EO_{10}$) thin films were synthesized by changing the Zn(II) or Cd(II)/SiO_2 mole ratios. The films were prepared through spin coating of a clear solution of all the ingredients (salt, CTAB, $C_{12}E_{10}$, silica

source (tetramethyl orthosilicate,TMOS, and water) and denoted as meso-silica-ZnX-n and meso-silica-CdY-n, where n is Zn(II) or Cd(II)/SiO_2 mole ratios. The synthesis conditions were optimized by using the meso-silica-ZnX-1.14 and meso-silica-CdY-1.14 films and XRD, FT-IR spectroscopy, POM and SEM techniques. The stability of the films, especially in the high salt concentrations, was achieved above the melting point of salts. Slow calcination of the films, starting from the melting point of the salt to 450 ^oC has produced the mesoporous silica-metal oxide (ZnO and CdO) thin films, and denoted as meso-silica-ZnO-n and meso-silica-CdO-n, with n of 0.29, 0.57, 0.86, 1.14, and 1.43. The calcination process was monitored by measuring the FT-IR spectra and XRD patterns at different temperatures. Structural properties of the mesoporous films have been investigated using FT-IR spectroscopy, XRD, N_2 sorption measurements, UV-Vis spectroscopy, SEM, TEM and EDS techniques. It has been found that the meso-silica-ZnO-n and meso-silica-CdO-n films consist of nanocrystalline metal oxide nanoplates on the silica pore walls of the mesoporous framework. The formation of nanoplates of metal oxides was confirmed by etching the silica walls using diluted HF solution and by reacting with H_2S and H_2Se gases. The etching process produced CdO nanoplates without silica framework. The H_2S and H_2Se reactions with the CdO nanoplates or meso-silica-CdO have converted them to CdS and CdSe nanoplates or meso-silica-CdS and meso-silica-CdSe, respectively. Finally, a hypothetical surface coverage of metal oxide nanoplates has been calculated by combining the data of N_2 sorption measurements, UV-Vis spectroscopy and TEM images and found that there is a full coverage of CdO and partial coverage of ZnO over silica walls in the meso-silica-CdO-n and meso-silica-ZnO-n thin films, respectively.

Keywords: Mesoporous ZnO, Mesoporous CdO, Mesoporous silica, Thin Films, Lyotropic liquid crystals.

ÖZET

ERİYİK TUZ YARDIMLI KENDİLİĞİNDEN OLUŞMA (EYKO):

MEZOGÖZENEKLİ SİLİKA-ZnO VE MEZOGÖZENEKLİ SİLİKA-CdO İNCE FİLMLERİN SENTEZİ

CÜNEYT KARAKAYA

Kimya Bölümü Yüksek Lisans Tezi

Tez Yöneticisi : Prof. Dr. Ömer Dağ

Ocak 2012

Bu çalışmada, bir seri mezoyapılı tuz-silika yüzeyaktif içeren (tuz $[Zn(H_2O)_6](NO_3)_2$, ZnX veya $[Cd(H_2O)_4](NO_3)_2$, CdY dir ve yüzeyaktifler setiltirimethilamonyum bromür (CTAB) ve 10-löril eter, $C_{12}H_{25}(OCH_2CH_2)_{10}OH$, $C_{12}EO_{10}$ dur) ince film Zn(II)/SiO_2 veya Cd(II)/SiO_2 mol oranı değiştilerek sentezlendi. Filmler, spin kaplama yönetemi ile bütün girdileri (tuz, CTAB, $C_{12}E_{10}$, silika kaynağı (tetrametilortosilikat,TMOS, ve su) içeren şeffaf çözeltiler kullanılarak hazırlandı ve mezo-silika-ZnX-n ve mezo-silika-CdY-n (n Zn(II)/SiO_2 ve Cd(II)/SiO_2 mol oranıdır)

olarak isimlendirildi. Sentez koşulları, mezo-silika-ZnX-1.14 ve mezo-silika-CdY-1.14 filmleri kullanılarak ve XRD, FT-IR, POM ve SEM teknikleri ile detaylı bir şekilde incelenerek optimize edildi. Filmlerin kararlılığı, özellikle yüksek oranlarda, tuzların erime sıcaklığı üstünde tutulmasıyla sağlandı. Filmlerin yavaş ve tuzun erime noktasından 450 ^{o}C ye kadar ısıtılmaları mezogözenekli silika-metal oksit (ZnO ve CdO) ince filmlerini üretti ve elde edilen filmler mezo-silika-ZnO-n ve mezo-silika-CdO-n olarak adlandırıldı (n 0.29, 0.57, 0.86, 1.14, ve 1.43 olarak değiştirildi). Isıtma aşaması FT-IR tayfları ve XRD desenleri değişik sıcaklıklarda ölçülerek takip edildi. Elde edilen mezogözenekli filmlerin yapısal özellikleri detaylı olarak FT-IR spektroskopi, XRD, N_2 sorpsiyon ölçümleri, UV-Vis spektroskopi, SEM, TEM ve EDS teknikleri ile incelendi. Mezo-silika-ZnO-n ve mezo-silika-CdO-n filmlerinin silika duvar yüzeylerinin metal oksit nano-plakaları ile kaplandığı saptandı. Sentez esnasında metal oksit nano-plakaların oluşumu silika duvarların seyreltik HF çözeltisiyle aşındırılarak ve filmlerin H_2S ve H_2Se gazları ile tepkimeye sokularak doğrulandı. Kimyasal aşındırma sonucu metal oksit nano-plakalar elde edildi. Ayrıca, mezogözenekli yapıdaki bütün metal oksit nano-plakaların H_2S ve H_2Se ile tepkimeleri sonucu metal sülfür ve metal selenür dönüştürüldüğü gösterildi. Son olarak, metal oksit plakaların silika duvarlarını kaplama yüzdesi varsayımsal olarak hesaplandı. Hesaplar sonucu, ZnO'in yüzeyin yarısını CdO ise tüm yüzeyi kapladığı saptandı.

Anahtar Kelimeler: Mezogözenekli ZnO, Mezogözenekli CdO, Mezogözenekli silika, İnce Filmler, Liyotropik Sıvı Kristaller

ACKNOWLEDGEMENTS

I would like to express my gratitude to…

……My supervisor, Prof. Dr. Ömer Dağ for his guidance, encouragement, patience and supervision throughout my studies.

…….Yurdanur Türker and Cemal Albayrak for his contributions and scientific discussions.

…….Special thanks to my friends, Hacı, Çebi. Zafer, Fatih Abi, Emre, Hakan, Çebi, Sefa, Murat,Koray, Atıf and Tuğrul for his memorable helps and supports

….dear Professors in my thesis committee, Prof. Margarita Kantcheva, Prof. Erman Bengü, Prof. Saim Özkar and Prof. Emrah Özensoy

Finally, I am sincerely thankful to my family: my parents, Nuran Karakaya and Kamil Karakaya and my brother Furkan Karakaya for their continuous supports throughout during my life and to Şeyma Öztürk for her love and everlasting supports in my life.

Table of Contents

LIST OF FIGURES

TABLE OF CONTENT

1 INTRODUCTION

In the last few decades, chemists, material scientists and engineers have focused on developing new and functional inorganic materials for various applications. The motivation behind these studies is that most chemical reactions and charge transfer processes occur on the surface of the solid materials. The nanoscale materials are high surface area materials. One synthesis approach to obtain high surface area materials is the synthesis of porous materials that can be classified according to their pore size: microporous (≤ 2 nm), mesoporous (2-50 nm) and macroporous materials (≥50 nm) (*2*).

The most known examples of microporous materials are zeolites that have crystalline framework consisting of SiO_4 and AlO_4^- tetrahedral units, called aluminosilicates. (*3*) The tetrahedral arrangement of building units provides uniform and regular cages with small sized channels connecting each other. The cages generally have diameter of less than 14.2 Å and high surface area that makes them very important in many applications, such as chemical drying, shape selective separation,(*4*) shape selective heterogeneous catalysis,(*5*) and selective ion exchanger.(*6*) Despite usefulness in all of these applications, the microporosity in zeolites can have some drawbacks.(*7*) For example, the pores of zeolites are not accessible for the reactions if the reactants and products are larger than these pores. In addition, the pores of zeolites can be occluded by the products and this adversely affects the conversion efficiency of zeolitic catalysts. Therefore, in order to eliminate these kinds of drawbacks, materials having larger pores than traditional zeolites are needed.

1.1 The Inception of Mesoporous Materials

Mesoporous materials have pore size distributions between 2 nm and 50 nm that are suitable for attaining high surface area and eliminating the drawbacks of microporous materials. Silica is a good candidate as a framework for mesoporous materials due to its well-known chemistry, chemical stability, ability to be functionalized and biocompatibility. The first example of mesoporous silica materials were demonstrated by Japanese researchers in 1990.(*8*) Alkyltrimethylammonium–kanemite

complexes form three dimensional silica framework that resists to calcination process to remove the organic species, leading to mesoporous silica. Since the discovery of M41S family (MCM-41, MCM-48, and MCM-50)(*9*) that are synthesized using surfactants as a template, the templated siliceous periodic mesoporous materials have been extensively studied. Scientists had carried out comprehensive research to control the pore size, pore geometry, morphology and functionalization of pore walls of mesoporous silica powders. On the other hand, because of the limitations of use of mesoporous powders in many applications, many new synthesis protocols have been introduced to the literature to make mesoporous materials on a desired substrate as thin films.

1.1.1 Mesoporous Silica Powders

The general route to synthesize surfactant templated mesoporous silica powders is based on self-assembly of surfactant, above its critical micelle concentration (CMC), and silica precursors in an acidic or basic aqueous media. The type of surfactants (cationic, anionic or neutral), surfactant chain length and concentration, solvent and type of silica precursor are important in the control of morphology, pore size, surface area, pore volume and wall thickness of the mesoporous materials.

The first examples of mesoporous silica, known as M41S family were reported by Mobil scientists in 1992.(*9*) In the M41S family, the initial composition of charged cationic surfactant (cetyltrimetyl ammonium bromide (CTAB)) and tetraethylorthoslicate (TEOS) in optimized pH were altered in order to determine the structure of the final material such as hexagonal MCM-41, cubic MCM-48, lamellar MCM-50 as indicated in Figure 1.1.1.(*10*) Among the M41S family, the most popular one is the MCM-41 with a 2-D hexagonal structure with cylindrical 2-D pores through the particles, and belongs to *p6mm* space group.(*11*) The pore size distribution is in the range of 4 to 6 nm with about 1 nm wall thickness leading to higher than 1000 m^2g^{-1} surface area.

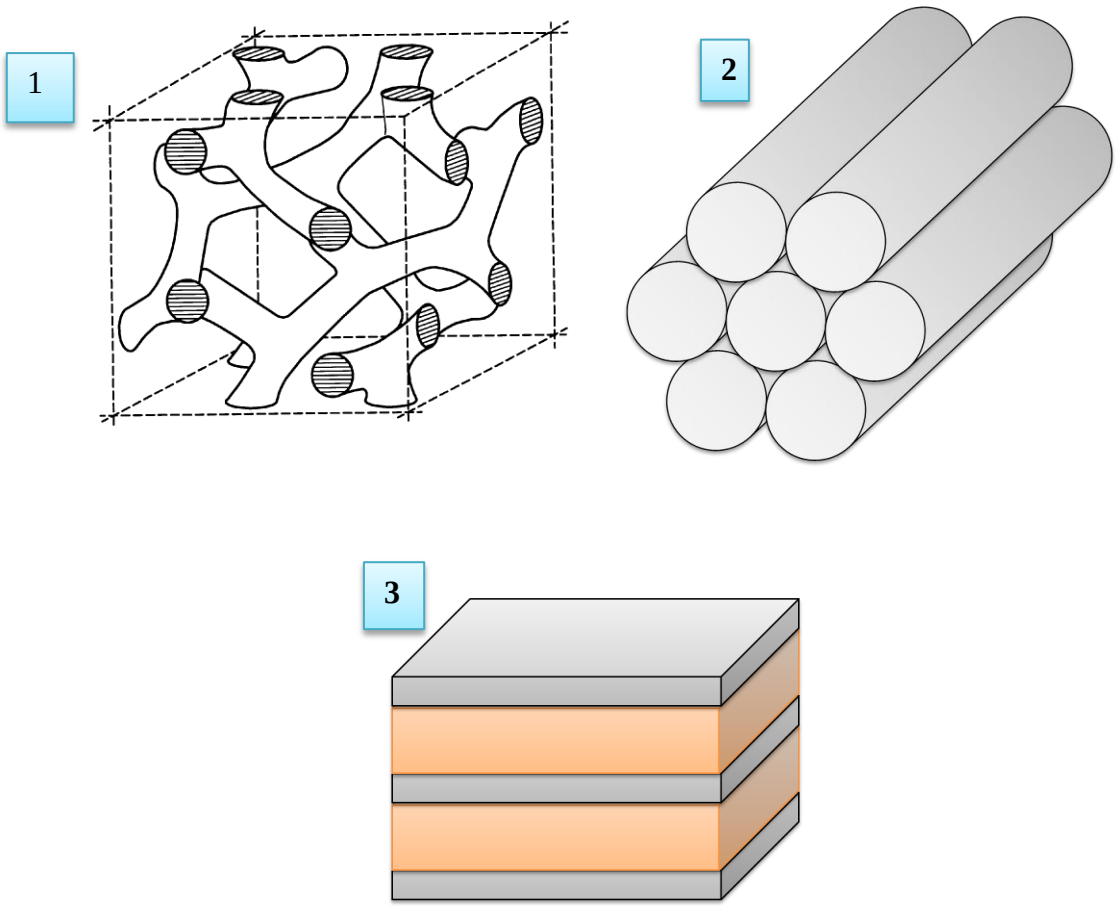

Figure 1.1.1 Schematic representation of M41S family with different structures 1) bicontinuous cubic, 2) 2D hexagonal, and 3) Lamellar. .

Other types of mesoporous ordered or disordered silica with different morphologies were further developed by changing surfactant type. SBA-n series were prepared by using cationic charged surfactant or nonionic surfactants in acidic media.(*12-15*) The SBA-15, which is the most important among the SBA-n family, has 2-D hexagonal arrangement of pores, prepared using a triblock copolymer ($EO_{20}PO_{70}EO_{20}$, P123).(*16*),(*17*) The pore size of SBA-15 is larger than that of MCM-41. In addition, the wall thickness is so thick (around 20 nm) that it provides extra thermal stability. Other members of SBA-n family, SBA-1 and SBA-6 have cubic, mesoporosity synthesized by using charged surfactants under acidic or basic conditions.(*18*, *19*)

1.2 True Liquid Crystal Templating (TLCT) Method

The mesoporous silica particles, like MCM-41 and SBA-15 are synthesized at surfactant concentrations above CMC. However, silica monolith with an ordered pore structure could not be synthesized in dilute conditions. Attard and coworkers introduced, for the first time, a novel method that uses liquid crystalline region of a surfactant and a silica precursor for the synthesis of silica monoliths.(*20*) They utilized the liquid crystalline phase of nonionic, oligo(ethylene oxide) surfactant of $C_{16}H_{33}(OCH_2CH_2)_8OH$, (represented as $C_{16}EO_8$) in the presence of a silica precursor. The hydrolyzed silica precursor (tetramethylorthosilicate, TMOS) by acid was impregnated into liquid crystalline phase. After polymerization of hydrolyzed silica precursor and removal of surfactant, a crack-free mesoporous silica monolith with a 2D hexagonal pore structure can be obtained: that is a negative copy of liquid crystalline phase. This method is known as true liquid crystal templating method (TLCT) and is illustrated in the Figure 1.2.1.

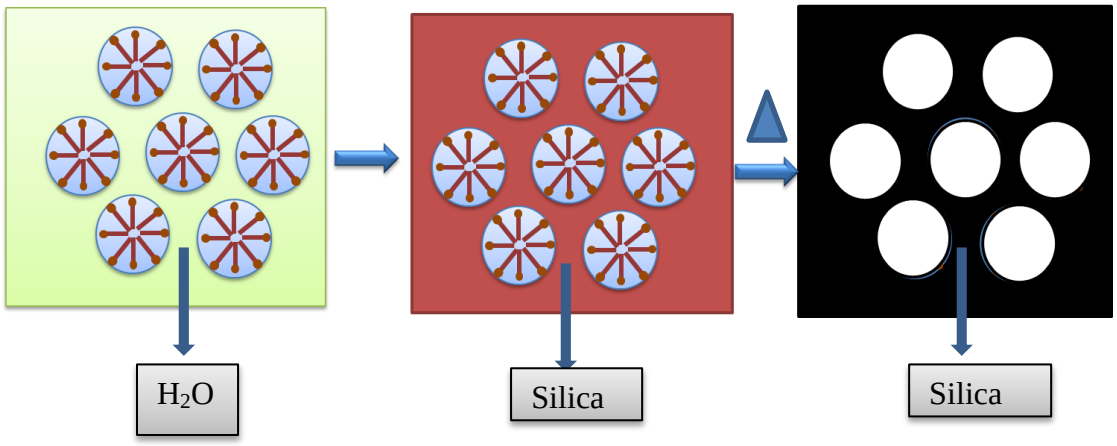

Figure 1.2.1: The illustration of true liquid crystalline templating method. The formation of liquid crystalline phase of surfactant (left), inclusion of inorganic precursor to liquid crystal phase (middle), and polymerization of inorganic precursor to solid matrix and removal of surfactant (right).

Mesoporous silica monoliths with various structures can be obtained via TLCT by altering the liquid crystalline phase with different surfactants, compositions and additives.(*21*, *22*) However, this method always produces thicker films or monoliths.

Therefore a new approach is necessary to investigate the thin film technologies of mesoporous materials. There are many publications on the synthesis of mesoporous silica thin films. (*23*),(*24*) The most attractive and widely investigated method is the evaporation induced self-assembly (EISA) that is also applicable to other mesostructured metal oxides.(*25*)

1.3 Evaporation Induced Self Assembly (EISA) Method

In order to overcome the drawbacks of TLCT method, as mentioned above, Brinker and coworkers have introduced, for the first time, the EISA method providing rapid formation of self-assembly of surfactant and inorganic moiety with a prefect, oriented replica of liquid crystal template.(*25*) The self-assembly of surfactant and inorganic moiety occurs at the same time and this provides a homogenous distribution of surfactant and inorganic precursors.

A typical phase diagram of a C_nEO_m-H_2O is showed in Figure 1.3.1. Notice that the surfactant molecules at low concentration form homogenous solution in an aqueous media. Above the CMC, they start to aggregate and to create micelles by the help of attractive (hydrophobic) and repulsive (hydrophilic) domains of surfactant and water. Furthermore, at higher concentration of surfactant and adequate temperature, the liquid crystalline phase with different structures can be formed according to surfactant percentage and temperature, such as cubic, hexagonal and lamellar. (*26*)

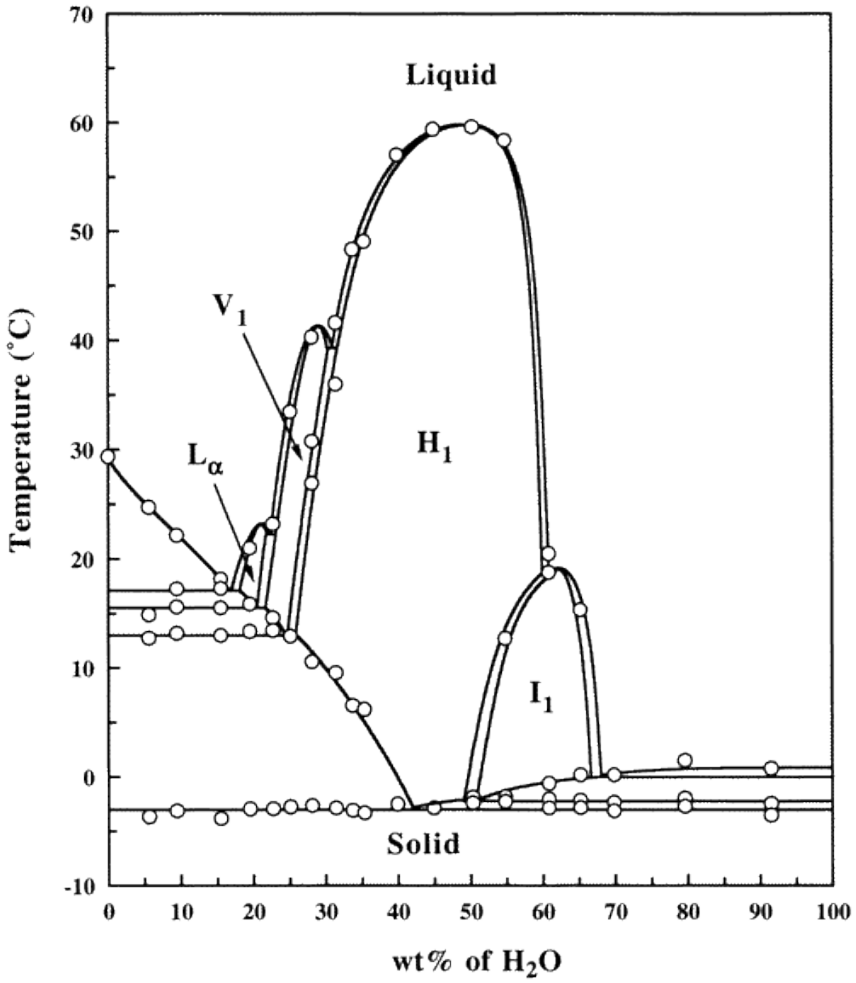

Figure 1.3.1: The phase diagram of $C_{12}EO_8$ and water: bicontinuous cubic (V_1), normal hexagonal (H_1), micelle cubic (I), micelle (L_1). (*27*)

The assembly process starts in a homogenous solution of surfactant and inorganic precursor with large amount of easily volatile solvent having low viscosity. Generally, dip coating of this solution over a substrate produces monoliths (*28*, *29*) or films.(*30*) The substrate, dipped into above solution is generally pulled upwards with constant rate; the evaporation of volatile solvent starts in the upper parts of substrate.(*31*) After evaporation of the solvent, a homogenous liquid crystalline phase starts forming on the surface of the substrate with the concentration of surfactant over time, as illustrated in Figure 1.3.2. The inorganic precursor in the LLC mesophase polymerizes and eventually solidifies the film into an ordered organic-inorganic mesostructures, in the aging step. The mesoorder of this liquid crystalline phase depends

on the dip coating rate and initial concentration of surfactant and inorganic precursor.(*25*) The surfactant molecules can be removed from the structure by either calcination or washing with a proper solvent. Moreover, the EISA process can also be operated by spin and spray coating methods.(*32*) In conclusion, the EISA process is a crucial and facile method for the synthesis of mesoporous silica, and also for some metal oxides thin films.

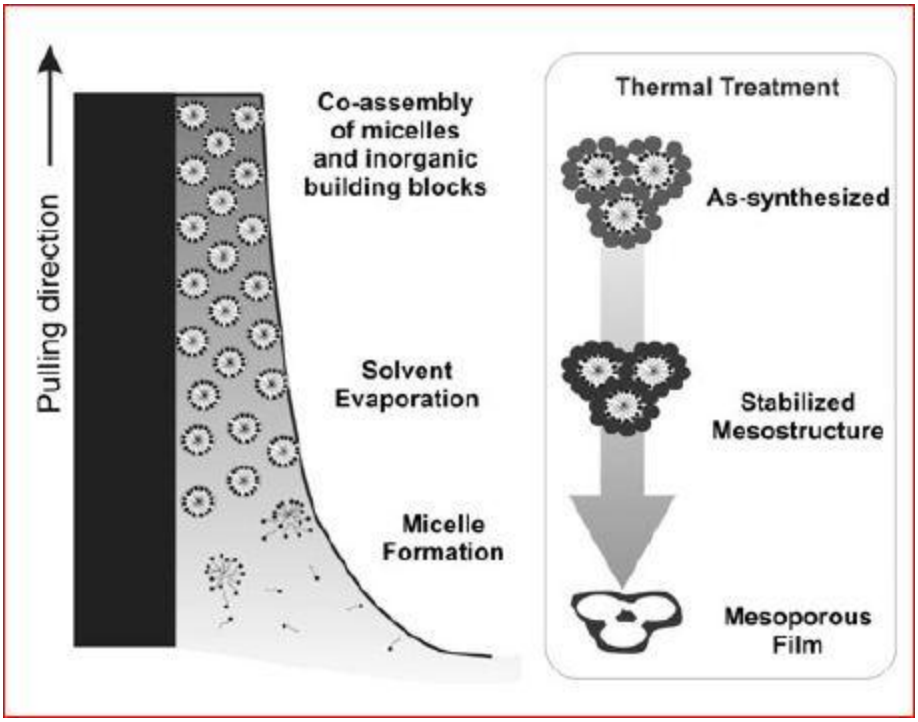

Figure 1.3.2: The schematic representation of Evoparation Induced Self Assemly (EISA) process.(*33*)

1.4 Mesoporous Transition Metal Oxides

Perhaps, the most studied and well-understood known mesoporous material is mesoporous silica owing to easy and well-known sol-gel chemistry of silica. However, mesoporous other metal oxides are more attractive than mesoporous silica because of great interest on their applications, as heterogeneous catalysts, photovoltaic devices, sensing, photocatalysts and biological applications.(*34-37*) Yet, the synthesis of mesoporous metal oxides is quite difficult compared to mesoporous silica. The first

difficulty is the reactivity of metal oxide precursor that makes the control of the polymerization step of metal oxide precursor more difficult.(*38*) In addition, during the calcination process, the pores may collapse due to redox reactions, phase transformation and crystallization. Despite those difficulties, chemists have developed some synthesis protocols to synthesize mesoporous metal oxides.

1.5 The EISA Process for Synthesis of Mesoporous Metal Oxides

The EISA process is also a powerful method for the synthesis of mesoporous films and monoliths. The first examples of mesoporous metal oxides, such as TiO_2, ZrO_2, Nb_2O_5, Ta_2O5, Al_2O_3, SnO_2, WO_3, HfO_2, and mixed oxides $SiAlO_y$, Al_2TiO_y, $ZrTiO_y$, $SiTiO_y$, and ZrW_2Oy via EISA process, were demonstrated by Stucky and coworkers.(*39*, *40*) Like the synthesis of mesoporous silica by EISA method, the mesoporous metal oxides were synthesized by using liquid crystalline templating from a dilute solution of surfactant and proper metal oxide precursor in a proper solvent. The EISA of surfactant and metal oxide precursor results a mesostructured solid upon evaporation of the solvent. Obtaining a stable metal oxide solution with a proper solvent is very important. The transition metal chlorides, MCl_4, are stable in ethanol in the presence of hydrochloric acid, due to the formation of stable chloroalkoxy complexes of metals. Fortunately, less reactive metal oxide precursors, like metal alkoxides ($M(OR_4)$), could be used to better control on the synthesis of mesoporous metal oxides.(*41*) Co-assembly of metal complexes using pluronics, such as P123 ($HO(CH_2CH_2O)_{26}$-$(CH(CH_3)CH_2O)_{70}$-$(CH_2CH_2O)_{26}H$, $EO_{26}PO_{70}EO_{26}$), and provides large pores with thicker metal oxide walls that can be crystallized upon calcination. Note that smaller surfactants cause the collapse ordered pore system upon calcination. The EISA process of mesoporous metal oxides is schematically represented in Figure 1.5.1.

Slow condensation of metal oxide precursor in the solution is very important to obtain a mesostructured framework. Metal alkoxides, such $Ti(OR)_4$, condenses itself into titania, TiO_2, in an acidic and humid environment. For a better controlled condensation of metal oxide precursor, bidentate ligands have been used. Bidente ligands such as carboxylate and nitrates are useful in the condensation and crystallization of the precursors owing to the formation of linkage among metal species.

a) Evaporation Induced Self-Assembly Process

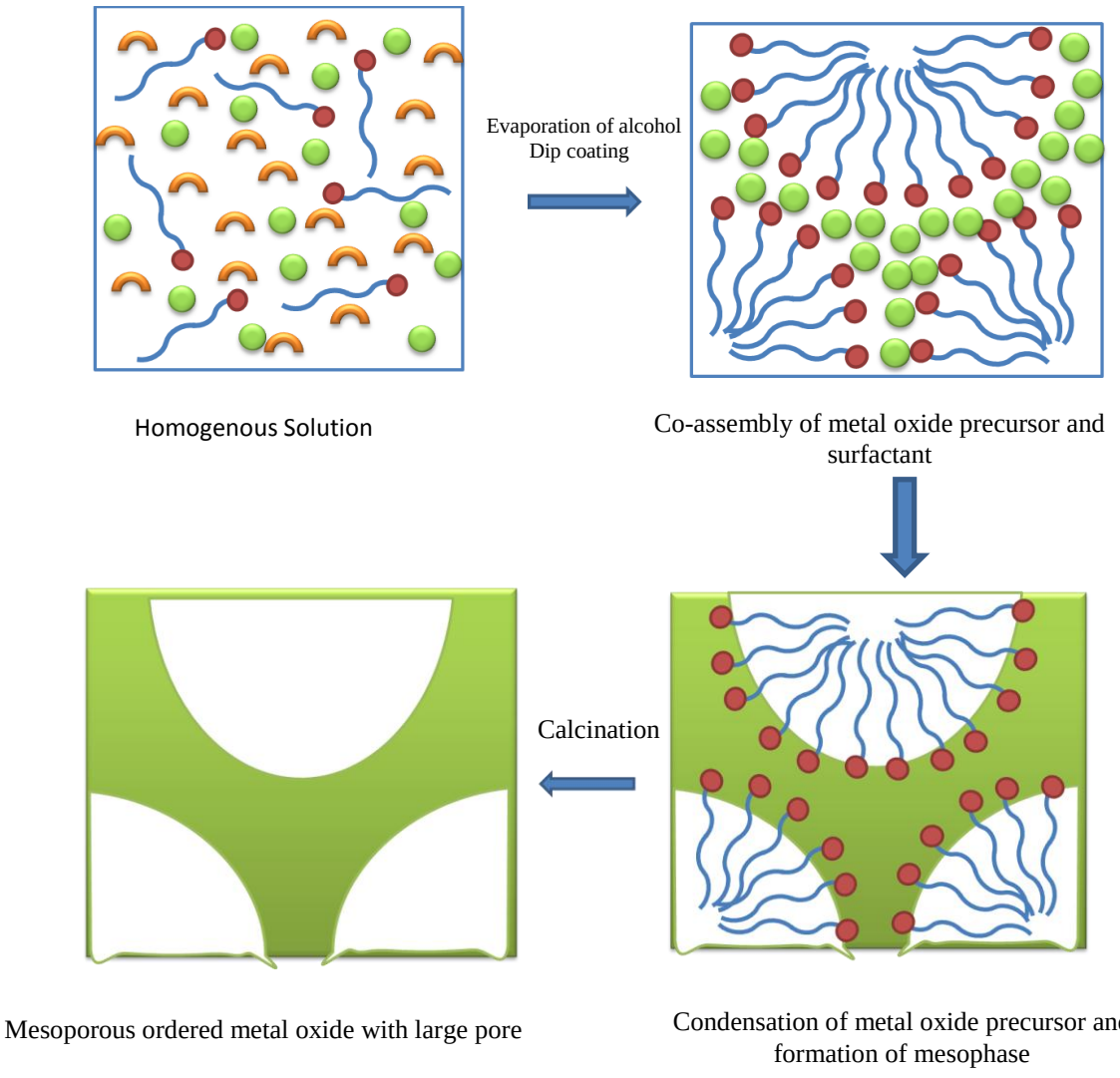

b) The Stabilization of Transition Metal Oxide Precursor (TMO) Condensation

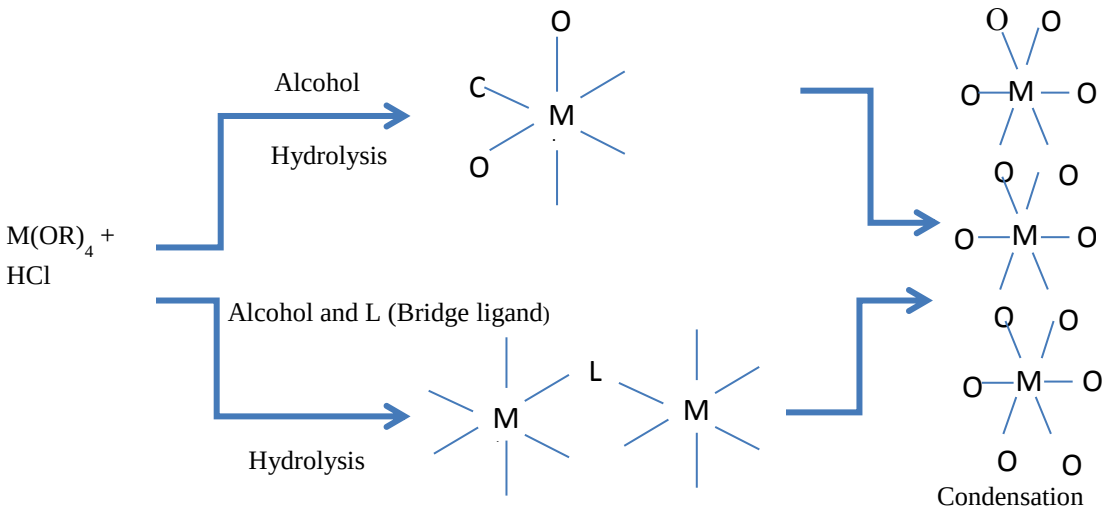

Figure 1.5.1: The schematic representation of EISA for the synthesis of Mesoporous metal oxides; a) the EISA process and b) the stabilization of metal oxide

The EISA method has been employed by several groups for the synthesis of various mesoporous metal oxides and mixed metal oxides.(*42-48*) Most of the synthesized mesoporous metal oxides and mixed metal oxides by EISA method are limited to early transition metals (Ti, Ta, Nb, Zr and etc.). Alkoxides of late transition metals (Fe, Ni, Co, Zn, Cd and etc.) with more d electrons are very reactive that makes the EISA method very difficult. The high reactivity results in an uncontrolled condensation and formation of bulk metal oxides. However, some transition metal oxides, such as Fe_2O_3 (*49*), CrO_x(*50*) and NiO (*51*) have been synthesized via EISA method. In the synthesis of mesoporous Fe_2O_3 and CrO_x , the metal precursors are their nitrate salts. The nitrate ion can coordinate to metal ion and also bridge two or more metal complexes in non-aqueous solution. This provides a slow condensation of metal precursor to metal oxide framework. However, the EISA method has some drawbacks in the synthesis of mesoporous transition metal oxides; i) since the gelation and

condensation step takes long such as 7- 14 days, it is not a facile method and ii) the crystalline walls are too thick (about 10 nm), causing a decrease in the surface area.

1.6 Nano-casting of Metal Oxides

Nano-casting method is a hard templating method, which is an alternative synthesis protocol for the synthesis of several mesoporous metal oxides with different pore topologies.(*52-57*) The nano-casting method has been applied for the synthesis of mesoporous metal oxides, as listed in Table 1.6.1.

The type of hard template and pore topology for nano-casting	**Mesoporous Metal Oxides**
SBA-15, 2-D hexagonal silica (p6mm)	CeO_2(*58-60*) Co_3O_4(*61-64*), Cr_2O_3(*58, 65-67*),Fe_2O_3(*58*), MnO_2(*68, 69*),NiO(*58*)
KIT-6, cubic (Ia3d) silica	CeO_2(*59*) (*70*), Cr_2O_3 (*71*) (*66*), Fe_3O_4 (*72*), In_2O_3 (*73*)
SBA-16 cubic (Im3;m) silica	Co_3O_4 (*74*) (*58*), In_2O_3 (*58*)
2D hexagonal (p6mm) carbon	CuO (*75*), MgO (*76*), ZnO (*77*)

Table 1.6-1: The summary of some mesoporous metal oxides via nano-casting

The nano-casting synthesis protocol involves three steps: i) inclusion of proper metal oxide precursor into the pores of hard templates, ii) conversion of metal oxide precursor in the mesopores to metal oxide upon calcination under ambient conditions, and iii) removal of the hard template. Common hard templates for the nano-casting route are mesoporous silica (SBA-15 and SBA-16) and mesoporous carbon. Nanocasting process, through using mesoporous silica for the synthesis mesoporous metal oxide, results in inverse replica of the mesoporous silica hard template. This means that the pores of the hard template are filled with the metal oxide during the calcination step and then the silica walls are removed to form mesoporous metal oxides. In SBA-15, the pore

structure is 2-D hexagonal and pores are connected to each other with micro channels. Therefore, even after the removal of silica walls, the metal oxide rods are connected to each other via micro rods leading to continuous, bridged metal oxide rods. The SBA-16 has a 3-D cubic pore topology that makes it more appropriate to obtain continuous mesoporous framework after removal of the silica template. Herein, the main trick for the synthesis of mesoporous metal oxide is the choice of mesoporous silica hard templates with thicker walls.

In order to obtain mesoporous metal oxide with true porous topology like in mesoporous silica, a better hard template is mesoporous carbon. The mesoporous carbon can be synthesized via nano-casting by using mesoporous silica (SBA-15). Therefore, the pores of mesoporous silica are filled with carbon, by decomposing carbon species in the pores, then the silica walls are etched out. This provides that the mesoporous metal oxides will have a true mesopore topology like in mesoporous silica after nano-casting step. These two path ways of nano-casting using mesoporous carbon and silica to create mesoporous metal oxides are schematically represented in Figure 1.6.1.

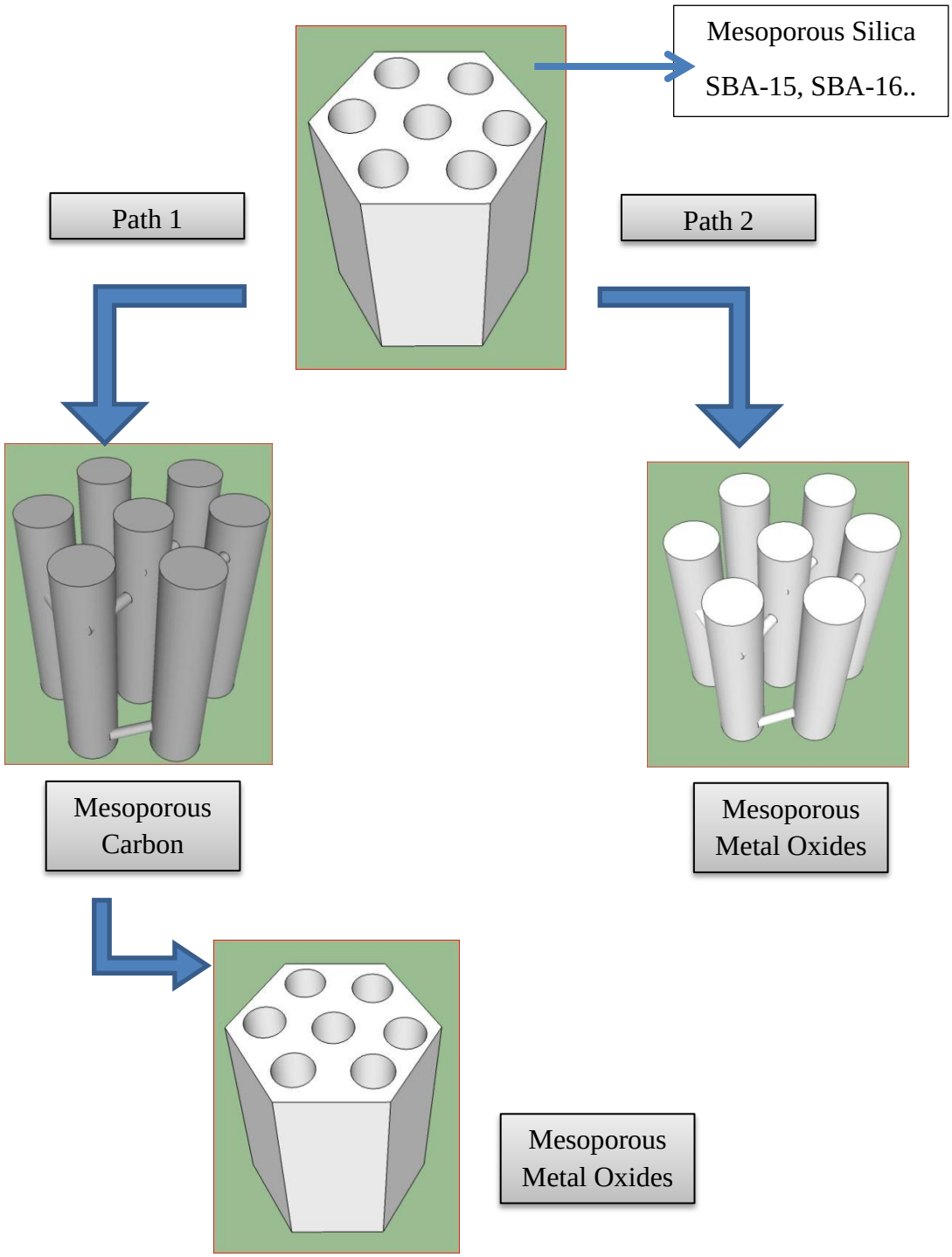

Figure 1.6.1: The schematic representation of two different paths of nano-casting for the synthesis of mesoporous metal oxides

A key factor in nano-casting method is impregnation of metal precursor into pores of mesoporous silica with an efficient filling. The metal nitrate salt in a proper

solvent is mixed well with mesoporous silica and then the solvent is evaporated. However, the impregnation method does not always provide efficient inclusion of metal nitrates into of the mesoporous silica. One strategy for an efficient pore filling uses mesoporous silica, in which the surfactant has been removed using microwaves.(*78*) The silanol groups on the surface of the pore can be kept during the calcination step and this enhances the filling rate of metal oxide precursor into pores in polar solvent. Another strategy for an efficient pore filling is functionalization of silanol groups with proper chelating ligands. Schüth and coworkers have used 2-dimensional hexagonal SBA-15 silica that is functionalized with vinyl groups for the synthesis of mesoporous Co_3O_4.(*79*) Vinyl groups can complex with Co^{2+} cations and facilitate the successful impregnation of metal salts into pores of SBA-15. An amino functionalized SBA-15 has also been used for the synthesis of mesoporous Cr_2O_3 and W_xO_y by using acidic solutions of $K_2Cr_2O_7$ and $H_3PW_{12}O_{40}$, respectively.(*65*, *66*, *80*) Another effective strategy in the literature is usage of molten metal salts without a solvent(*74*) (metal nitrates generally melt at low temperatures). In all of these strategies, the repetitive loadings is necessary in order to increase loading of metal oxide precursor in the mesopores, however, this may cause undesired formation of bulk metal oxide outside of mesoporous silica.

Despite the fact that a 100 % pore filling cannot be accomplished, after calcination process to convert metal oxide precursor to metal oxide, the metal oxides could not fill all the pores of mesoporous silica. There is a huge density difference between metal oxide precursors and metal oxides. This causes a large volume contraction. The general choice of metal oxide precursor for nanocasting method is metal nitrates. (*19*) that usually have low decomposition temperature. For example, the melting point of $[Zn(NO_3)_2].6H_2O$ is only 35.5 ^oC and its density is only 2.065 g/cm^3 but the density of ZnO is quite high, 5.606 g/cm^3. If one mole $[Zn(NO_3)_2].6H_2O$ is converted into one mole ZnO, the volume of zinc salt is decreased to its 10.1% . This means that the voids of mesoporous silica, totally filled with zinc nitrate hexahydrate, will only coat silica surface and only block 10.1% of the pore volume. Some other metal nitrates and their volume contraction are listed in Table 1.6.2. This enormous volume contraction of metal precursor is an important drawback for the synthesis of mesoporous metal oxides

through nanocasting method. Therefore, homogenous formation of mesoporous metal oxide over mesoporous silica may become impossible by using mesoporous silica or mesoporous carbon as a hard template. Furthermore, the multiple inclusions of metal oxide precursors into mesoporous silica to increase the degree of filling may not work well because of occlusion of the pores in the previous trials.

Precursor	**Target material**	**Percentage Of Volume Contraction (%)**
$Fe(NO_3)_3\ 9H_2O$	Fe_2O_3	93.66
$Cu(NO_3)_2\ 3H_2O$	CuO	87.91
$Zn(NO_3)_2\ 6H_2O$	ZnO	89.90
$Cd(NO_3)_2\ 6H_2O$	CdO	87.99
$Co(NO_3)_2\ 6H_2O$	Co_3O_4	93.46
$Mn(NO_3)_2\ 6H_2O$	MnO_2	89.23
$Cr(NO_3)_3\ 9H_2O$	Cr_2O_3	93.44

Table 1.6-2: The summary of some transition metal nitrates and their volume contraction

After the conversion of metal oxide precursor to metal oxide, the removal of hard template, mesoporous silica or mesoporous carbon, is necessary to obtain mesoporous metal oxides. The silica walls can be etched by NaOH or HF solutions.(*51, 53, 58, 72, 74*) If mesoporous carbon was used as a hard template, the carbon walls can be removed by calcination at 500-700 ^{o}C.(*75*) However, mesoporous carbon as a hard template may be an advantage for the synthesis of some mesoporous metal oxides, such ZnO(*77*) and MgO(*81*), compared to mesoporous silica. Because the HF or NaOH solution etches

these kinds of metal oxides due to their amphoteric character, and result a collapse of mesostructure.

In addition, nanocasting method is more applicable for the synthesis of mesoporous metal oxide powders rather than thin films. For the heterogeneous catalysis, it is important to produce large scale mesoporous catalyst with a high surface area.(*52, 55*) However, many applications, such photovoltaic applications, are based on thin film technologies.(*82, 83*)

1.7 Solid State Grinding Method

The nanocasting method for the synthesis of mesoporous metal oxides is quite time consuming and contains lots of steps (preparation of hard template, inclusion metal oxide precursor, condensation and template removal). Therefore, elimination of even one step, in nanocasting method, would be a great advantage for the synthesis of mesoporous metal oxides. In addition, the nanocasting method does not produce homogenous and continuous mesoporous frameworks. Wang and coworkers developed a novel method, in which a metal oxide precursor without a solvent is incorporated into the as-prepared mesoporous silica. Calcination results in a homogenous coating of pore surface with the metal oxides and removal of the surfactant.(*84*) This method has been employed to several metal oxides, such as MgO, CuO and ZnO. (*84-88*) In general, as-prepared mesoporous silica is grinded together with a metal nitrate salt without a solvent; the metal nitrate salt is incorporated into as-prepared mesoporous silica without any extra drawing force. Presence of surfactants inside the pores prevents the formation of nanorods ; instead formation of nanoparticles covering the surface of silica was enhanced. The schematic representation of solid state grinding method is shown in Figure 17.1.

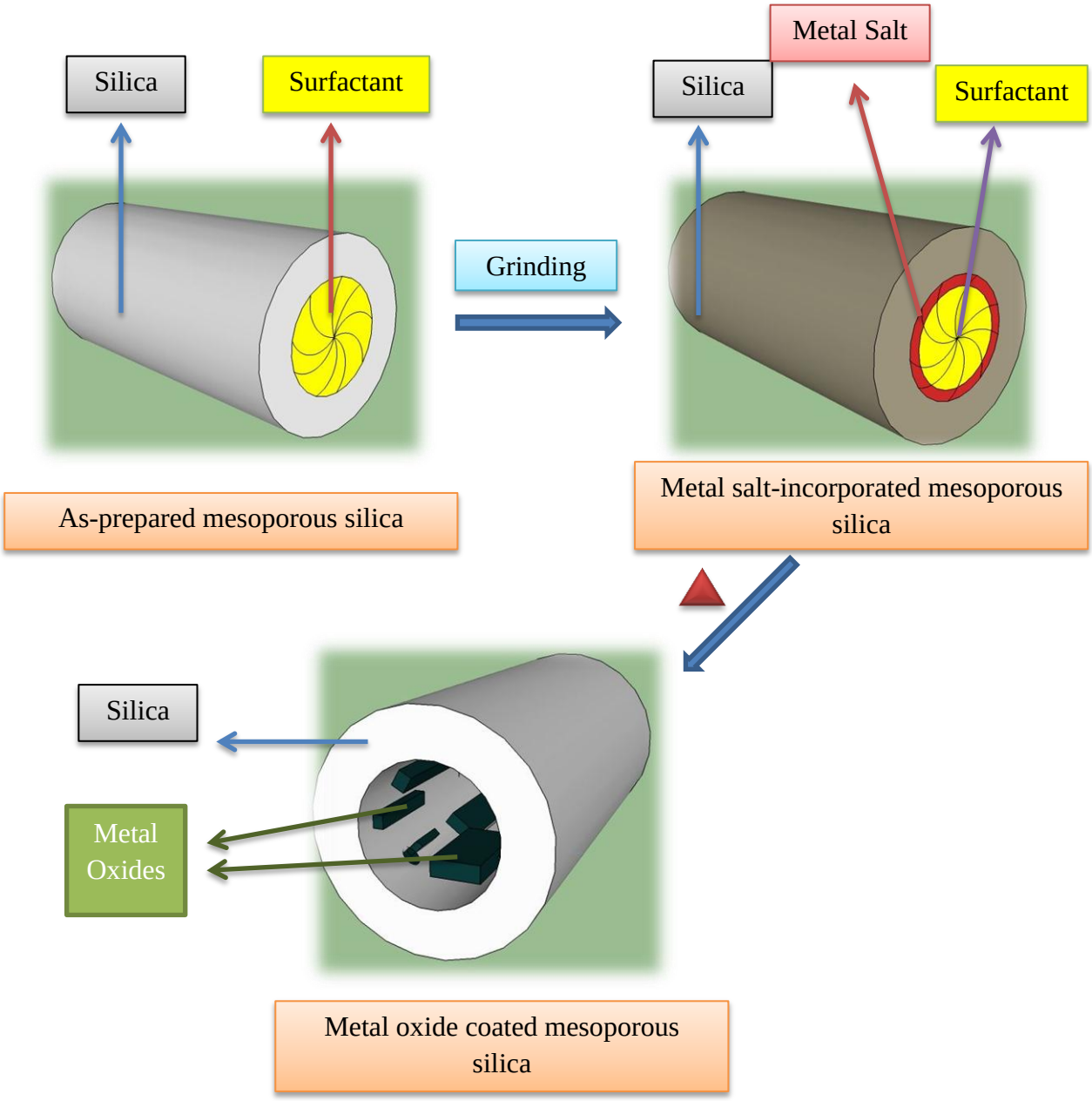

Figure 1.7.1: The schematic representation of solid state grinding method

The solid state grinding method is a less time consuming and a facile synthesis method compared to nanocasting method. However, the volume contraction problem still exists as in the nanocasting method and limits the surface coverage of the pores. In addition to this, loading of the metal oxide precursor, metal nitrate, is less than that in nanocasting method. To illustrate, this method has been employed to coat mesoporous SBA-15 with CuO with a coverage of only 15% of the surface of silica walls; authors of this work also mentioned that they observed pore blocking in some parts of mesoporous silica.(*84*) Therefore, a more efficient loading and conversion method is required to

enhance the metal oxide loading with a uniform distribution in the pores of mesoporous silica, specifically as thin films for advanced applications.

1.8 Lyotropic Liquid Crystalline (LLC) Mesophases of Transition Metal Salts

Liquid crystals are divided into two groups; thermotropic liquid crystals and lyotropic liquid crystals. While thermotropic liquid crystals are a kind of ordered assembly of molecules that shows a phase transformation with temperature change, the phase of lyotropic liquid crystals depends on a second component (solvent) and temperature. By using lyotropic liquid crystalline (LLC) templating method (know as true liquid crystalline templating, TLCT, method), different types of mesoporous materials have been synthesized as mentioned in the previous chapters.

Dag et al. have introduced a new type of LLC mesophase in which the transition metal aqua complexes act as a solvent and form the LLC mesophases with oligo(ethylene oxide) surfactants ($C_{12}H_{25}(CH_2CH_2O)_{10}OH$, $C_{12}E_{10}$).(*89*) Herein, they showed that the coordinated water molecules of the transition metal aqua complexes direct the self-assembly of surfactant molecules into hexagonal or cubic mesostructures with the help of hydrogen bonding (between ethylene oxide groups of the surfactant and coordinated water of aqua metal complex). The hexagonal LLC mesophase of $[Zn(H_2O)_6](NO_3)_2$ $-C_{12}EO_{10}$ is stable up to 70 w/w % (weight of salt over total weight percent) at RT. A schematic representation of this self-assembly in a hexagonal packing and its characteristic fan texture of hexagonal phase are shown in Figure 1.8.1.

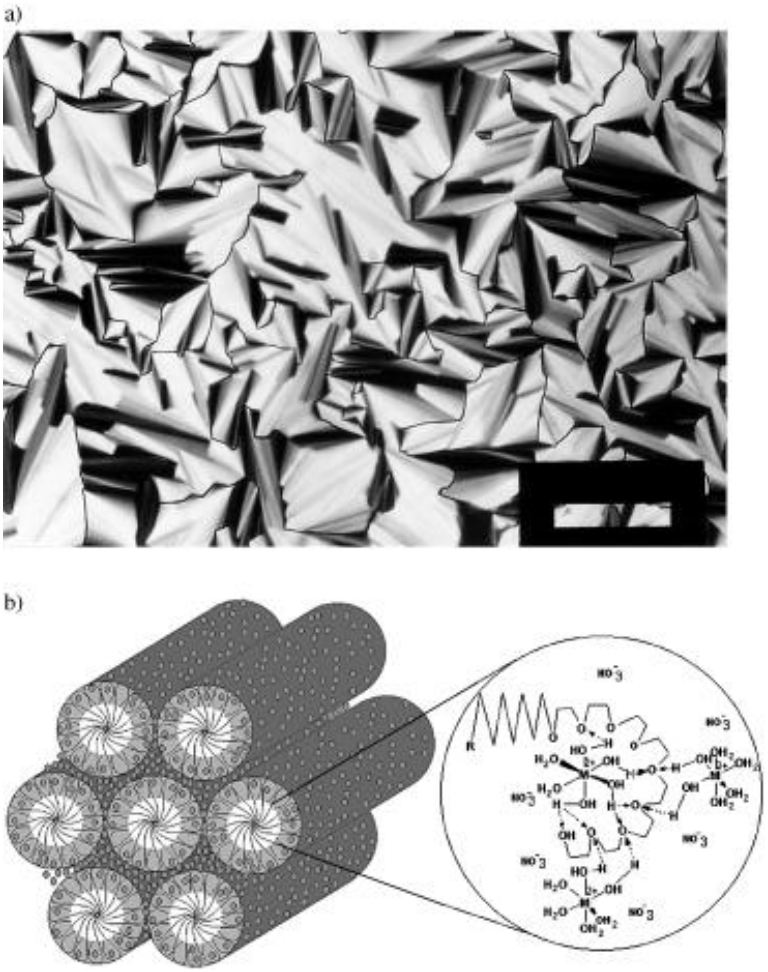

Figure 1.8.1: a) A POM image of $[Cd(H_2O)_4](NO_3)_2$ in $C_{12}H_{25}(CH_2CH_2O)_{10}OH$ and b) a schematic representation of a hexagonal LLC phase, the small circles represent metal complexes and NO_3^- ions.(*89*)

The thermal and structural properties and behaviors of this novel LLC phases have been investigated in detail using different surfactants and transition metal salts.(*90-94*) One of the important improvements in the salt-surfactant LLC mesophases is the addition of a charged surfactant, CTAB or SDS together with $C_{12}EO_{10}$. This resulted an increase in the metal salt, $[Zn(H_2O)_6](NO_3)_2$, content, up to 8 metal ion/$C_{12}EO_{10}$ mole ratio.(*94*) The charged surfactants balance the surface charge of the salt species in the hydrophilic domains; as a result, stabilize the mesophase at very high metal ion/$C_{12}EO_{10}$ mole ratios. The first phase diagram of $[Zn(H_2O)_6](NO_3)_2$ and $C_{12}EO_{10}$ system is shown

in Figure 1.8.2.(*90*) The new mesophase is stable below 0 ^{o}C. Moreover, they concluded that the zinc nitrate hexahydrate salt is in the molten phase in confined hydrophilic domains of the LLC mesophase and organize the surfactant molecules into mesophase. This discovery is an important step for both understanding the origin of the salt:surfactant LLC mesophases and designing new materials by using these phases.

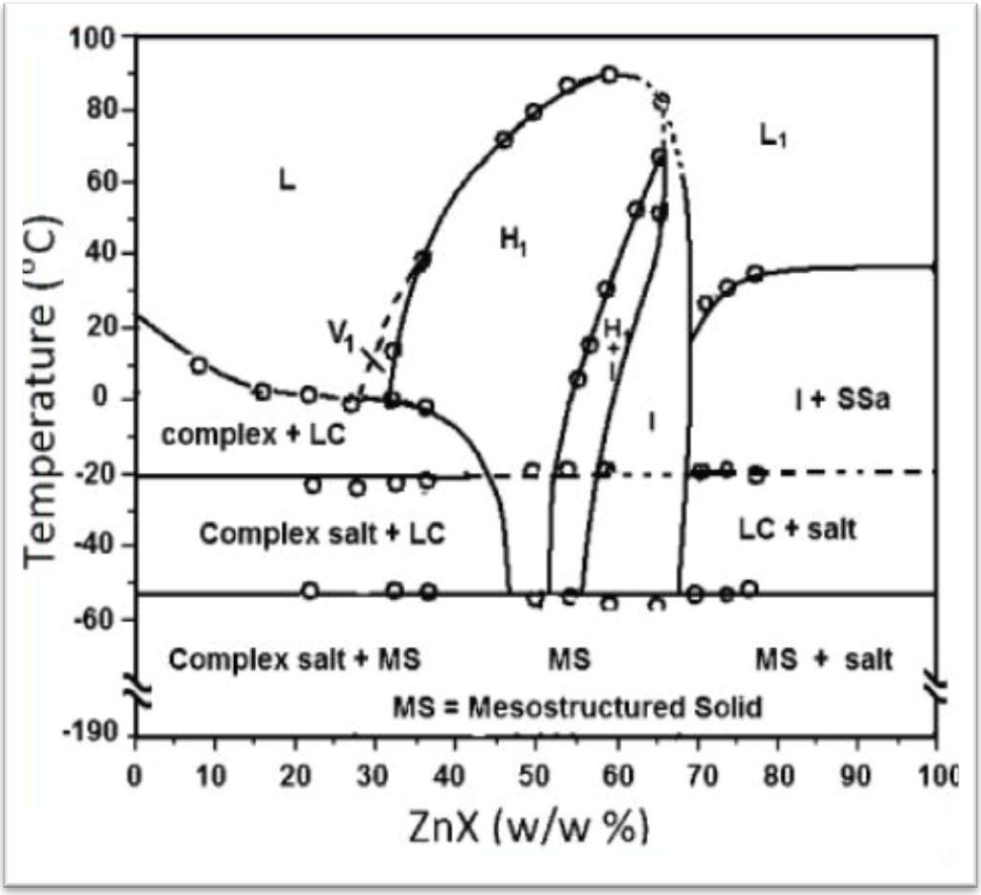

Figure 1.8.2: The phase diagram of $[Zn(H_2O)_6](NO_3)_2$ and $C_{12}EO_{10}$ system: bicontinuous cubic (V_1), normal hexagonal (H_1), micelle cubic (I), micelle (L_1).(*90*)

1.9 ZnO Nanoparticles and Mesoporous ZnO

ZnO is a n-type and wide band gap semiconductor with band gap of 3.37 eV and an exciton (e-h pair) binding energy of 60 meV. These properties make ZnO unique in many applications as a piezoelectric materials, UV light-emitting diodes, lasers, photovoltaic solar cells, UV-photodetectors, gas-sensors, and varistors.(*95-98*) For many applications of ZnO that require high surface area, the synthesis of mesoporous ZnO is

also very important.(*83, 99*) To the best of our knowledge, only one example of mesoporous ZnO prepared by EISA method was demonstrated by Schüth and coworkers.(*100, 101*) They have used a special organometallic single-source precursor for the controllable condensation of ZnO precursor. The mesoporous ZnO has also been prepared through nanocasting method.(*102*) Generally, ZnO nanoparticles were embedded into mesoporous silica to obtain high surface area ZnO without particle aggregation through solid state grinding method,(*103*) templating chelating ligand (*104*) and functionalization of silica walls (*105*). However, all these methods do not ensure high loading of zinc oxide into mesoporous silica.

In this thesis, we have developed a novel synthesis protocol for mesoporous silica–metal oxide (ZnO and CdO) thin films. In this method, two surfactants (a charged surfactant, CTAB and $C_{12}EO_{10}$) with a silica precursor, TMOS assemble together with an extensive amount of zinc nitrate hexahydrate, $[Zn(H_2O)_6](NO_3)_2$, or cadmium nitrate tetrahydrate, $[Cd(H_2O)_4](NO_3)_2$, into a liquid crystalline mesophase. The confinement of the metal salt in mesophase makes the metal salt transform into its molten phase that acts as a solvent and organizes two surfactants into a hexagonal liquid crystalline phase. Then, this mesophase can be converted into mesoporous silica-metal oxide thin films upon calcination. We named this novel synthesis protocol as molten salt assisted self-assembly (MASA) in which two solvents are used: a volatile solvent (water) which provides homogenous mixing of the ingredients into a clear solution and facilitate self-assembly and a non-volatile solvent (metal nitrate salts at molten state) that stabilizes and keeps the mesophase after water evaporation enables for the formation of metal oxide. The MASA synthesis protocol has been investigated by using x-ray diffraction (XRD), Fourier transform infrared (FT-IR) spectroscopy, UV-Visible absorption spectroscopy, Transmission electron microscopy (TEM), Energy dispersive x-ray spectroscopy (EDS), polarized optical microscopy (POM) and N_2 sorption surface area analysis.

2 EXPERIMENTAL

2.1 MATERIALS

The chemicals which are used throughout this investigation are: zinc nitrate hexahydrate $[Zn(H_2O)_6](NO_3)_2$ (%98 Aldrich) represented as ZnX, cadmium nitrate tetrahydrate $[Cd(H_2O)_4](NO_3)_2$ (%98 Aldrich) represented as CdY, tetramethylorthosilicate (TMOS) (%98 Aldrich), cetyltrimethylammonium bromide CTAB, 10-lauryl ether, $C_{12}H_{25}(OCH_2CH_2)_{10}OH$, ($C_{12}EO_{10}$), and deionized water.

2.2 SYNTHESIS

2.2.1 Synthesis of Mesostructured- ZnX Salt-Silica Thin Films

Dissolve a desired amount of ZnX (see Table 2.2.1), 0.291 g CTAB, and 0.500 g $C_{12}EO_{10}$ in 4.5 ml deionized water in a 25 ml vial by stirring on a magnetic stirrer for 1 day. Then add 0.050 g concentrated HNO_3 acid and 0.850 g TMOS to the above mixture and gently stir the mixture for another 5 min. A solution of 8.0 $ZnX/C_{12}EO_{10}$ or 1.14 $Zn(II)/SiO_2$ mole ratio contains 1.900 g ZnX, 0.291 g CTAB, 0.500 g $C_{12}EO_{10}$, 4.500 g H_2O, 0.050g HNO_3, and 0.850 g TMOS. Other compositions are given in Table 2.2.1.

Put 1.0 ml of the above solution on a substrate (glass, silicon wafer and/or quartz) over a spin coater and spin it at 1200 rpm for 1.0 min. Make sure the solution completely covers the substrate to ensure full coverage after coating. Put the film sample immediately into an oven at 55 ^oC for aging 5 minutes.

2.2.2 Fabrication of meso-silica-ZnO-n Thin films

Calcine above thin film from 55 to 450 ^oC by 1 ^oC/min increments in a temperature controlled furnace. Remove the film from the furnace prior to slowly cooling the furnace. The film is abbreviated as meso-silica-CdO-n, where n is Zn/Si mole ratio.

Sample name	The amounts of Chemicals (g)					
	ZnX	**$C_{12}EO_{10}$**	**CTAB**	**TMOS**	**HNO_3**	**H_2O**
meso-silica-ZnO-0.29	0.475	0.500	0.291	1.900	0.050	4.500
meso-silica-ZnO-0.57	0.950	0.500	0.291	1.900	0.050	4.500
meso-silica-ZnO-0.86	1.425	0.500	0.291	1.900	0.050	4.500
meso-silica-ZnO-1.14	1.900	0.500	0.291	1.900	0.050	4.500
meso-silica-ZnO-1.43	2.375	0.500	0.291	1.900	0.050	4.500
meso-silica-ZnO-1.71	2.850	0.500	0.291	1.900	0.050	4.500

Table 2.2-1: The amounts of chemicals used in the preparation of meso-silica-ZnO-n

2.2.3 Synthesis of meso-silica-CdO-n Thin Films

Dissolve a desired amount of $[Cd(H_2O)_4](NO_3)_2$ (see Table 2.2.2), 0.291 g CTAB, and 0.500 g $C_{12}EO_{10}$ in 4.5 ml deionized water in a 25 ml vial by stirring on a magnetic stirrer for 1 day. Then add 0.050 g concentrated HNO_3 acid and 0.850 g TMOS to the above mixture and gently stir the mixture for another 5 min. The sample with 8 $CdY/C_{12}EO_{10}$ or 1.14 $Cd(II)/SiO_2$ mole ratio contains 1.970 g CdY, 0.291 g CTAB, 0.500 g $C_{12}EO_{10}$, 4.500 g H_2O, 0.050g HNO_3, and 0.850 g TMOS. Other compositions are given in the Table 2.3.1.

Put 1.0 ml of the above solution on a substrate (glass, silicon wafer and/or quartz) over a spin coater and spin the sample at 1200 rpm for 1.0 min. Make sure the solution completely covers the substrate to ensure full coverage after coating. Put the film sample immediately into an oven at 65 ^oC for aging.

2.2.4 Fabrication of meso-silica-CdO-n Thin films

Calcine above thin film from 65 to 450 ^oC by 1 ^oC/min increments in a temperature controlled furnace. Remove the film from the furnace prior to slowly cooling the furnace. The film is abbreviated as meso-silica-CdO-n, where n is Cd/Si mole ratio.

2.2.5 Etching of meso-silica-CdO-n Thin Films

The calcined films or the powders, scraped from the substrates, were etched in a 4% HF solution in plastic vials. Centrifuge the solution to collect powder by decanting the liquid part into waste bottle. Add distilled water over the precipitate to wash out any remaining fluoride species. Centrifuge the mixture and remove the liquor and repeat the washing step 2 to 3 times. Then dry the powder in an oven.

Sample name	The amounts of Chemicals (g)					
	CdY	**$C_{12}EO_{10}$**	**CTAB**	**TMOS**	**HNO_3**	**H_2O**
meso-silica-CdO-0.29	0.492	0.500	0.291	1.900	0.050	4.500
meso-silica-CdO-0.57	0.985	0.500	0.291	1.900	0.050	4.500
meso-silica-CdO-0.86	1.478	0.500	0.291	1.900	0.050	4.500
meso-silica-CdO-1.14	1.970	0.500	0.291	1.900	0.050	4.500
meso-silica-CdO-1.43	2.460	0.500	0.291	1.900	0.050	4.500
meso-silica-CdO-1.71	2.956 g	0.500 g	0.291 g	1.900 g	0.050 g	4.500 g

Table 2.2-2: The amounts of chemicals used in the preparation of meso-silica-CdO-n

2.2.6 Synthesis of meso-silica-CdS-n Thin Films

Place the calcined meso-silica-CdO-n thin film in a vacuum chamber and evacuate the chamber for 2 min. Put 300 torr H_2S gas over the meso-silica-CdO-n thin films for 100 min at room temperature. Then pump out the unreacted excess H_2S gas from the reaction media for 5 min before removing the sample from the reaction chamber. The samples are labelled as meso-silica-CdS-n.

2.2.7 Synthesis of meso-silica-CdSe-n Thin Films

Place the calcined meso-silica-CdO-n thin film in a vacuum chamber and evacuate the chamber for 2 min. Put 300 torr of 5 % H_2Se gas (diluted with pure N_2 gas) over the sample for 15 min at RT to obtain meso-TiO_2-CdSe thin film. Then transfer the excess H_2Se gas in the reaction chamber over a CuO loaded mesoporous silica for 2 min to convert the excess H_2Se into CuSe nanoparticles. Then, evacuate the unreacted gas by using a rotary pump for 5 min before removing the sample. The samples are labelled as meso-silica-CdSe-n.

2.3 CHARACTERIZATION

2.3.1 X-Ray Diffraction (XRD)

The XRD patterns of the films of meso-SiO_2-ZnX and meso-SiO_2-CdY films on glass microscope slides were recorded by using Rigaku Miniflex diffractometer with a Cu K_α (1.5405 A°) x-rays source operating at 30 kV/15 mA. The fresh samples of meso-SiO_2-ZnX or CdY were monitored at small angles between 1 and 5^o, 2θ, with 1^o/ min scan rate for the investigation of mesostructure. For the high angle measurements approximately 20 films over glass slides were scraped and collected on a XRD sample holder. The high angle XRD patterns were recorded between 10 and 80^o, 2θ by using Pananalytical Multi-purpose x-ray diffractometer, equiped with a Cu K_α (1.5405 À) x-rays source operating at 45 kV/40 mA.

2.3.2 FT-IR Spectroscopy

FT-IR spectra of the meso-SiO_2-ZnX and meso-SiO_2-CdY films, coated over single crystal Si(100) wafers, were recorded by using Bruker Tensor 27 model FTIR spectrometer. The spectra were collected in the range of 400 and 4000 cm^{-1} with a resolution of 4 cm^{-1} and by collecting 128 scans. The calcination process of the meso-SiO_2-ZnX was monitored using homemade temperature controlled (Digi-Sense Cole Parlmer) sample holder. The calcined samples were diluted using KBr and pressed into KBr pellets for the FT-IR measurements.

2.3.3 UV-Vis Absorption Spectroscopy

The UV-Vis absorption spectra of meso-SiO_2-ZnO-n and meso-SiO_2-CdO-n thin films, coated on quartz substrates were collected by using Thermo Scientific Evolution 300/600 UV-Visible spectrometer. The spectra were obtained in the range of 200 and 800 nm with a resolution of 2 nm and 100 nm/min scan rate.

2.3.4 Polarized Electron Microscopy (POM) Images

The POM images of the films, coated on microscope glass substrate were recorded by using ZEISS Axio Scope A1 Polarizing Optical Microscope in transmittance mode with 20X optic lens, between crossed polarizers.

2.3.5 The N_2 (77.4 K) Sorption Measurements

The N_2 (77.4 K) sorption measurements were carried by using a TriStar 3000 automated gas adsorption analyzer (Micrometrics) in the relative pressure range, P/P_0, from 0.01 to 0.99. The samples of meso-SiO_2-ZnO-n and meso-SiO_2-CdO-n were collected from 15-25 films coated on glass microscope slides by scraping with razor blade and the amount of sample were ranged from 10 mg to 20 mg. Surface areas were calculated in the range from 0.05 to 0.3 relative pressure with 5 points. The powder samples were degassed under (~10^{-2} torr) vacuum for 3 hours at 300 ^oC in order to remove adsorbed water and volatile species in the pores prior to measurements.

2.3.6 Transmission Electron Microscopy (TEM) Images

The high resolution transmission electron microscope (HRTEM) images were collected by using a FEI Technai G2 F30 at an operating voltage of 200 kV. The

calcined films were scraped and ground in a mortar using 5 ml of ethanol for 10 min and dispersed using a sonication for 5 min. One drop of the dispersed ethanol solution was put on a TEM lacey grid and dried over a hot-plate. Then, for further comprehensive analysis of the crystal structure of ZnO and CdO nanoparticles, the images were analyzed by using the software of Digital Micrograph 3.6.5.

2.3.7 Scanning Electron Microscopy (SEM)

Nano-SEM images were recorded using Hitachi HD-2000 STEM in SEM mode. The samples were prepared by dispersing powders over the TEM grids. The SEM images were also recorded by using ZEISS EVOS-40, operated at 15 kV. The samples were prepared on silicon wafers that were attached to aluminum sample holders using conductive carbon adhesive tabs.

3 RESULT AND DISCUSSION

3.1 Optimization of the meso-silica-ZnX-n Films

In this thesis, mesostructured salted (ZnX or CdY) silica films were prepared and investigated to synthesize desired mesoporous silica-ZnO or CdO thin films. The meso-silica-ZnX-n films were prepared by spin coating a clear aqueous solution of CTAB, $C_{12}EO_{10}$, ZnX, HNO_3, and TMOS. To obtain the clear aqueous solutions, the mixture should be vigorously stirred for 1 day. Note that the surfactants, CTAB and $C_{12}EO_{10}$, which have long hydrophobic tails, are not easy to dissolve (it may take about 1 day) in an aqueous media. After dissolving the surfactants in water, HNO_3 and TMOS are added into the solution (TMOS hydrolyzes to $Si(OH)_4$ by an acid catalyzed hydrolysis reaction, Equation 3.1.1 and 3.1.2). Note that after addition of TMOS to above acidic solution; the solution warms up, indicating the hydrolysis of TMOS. The hydrolysis follows a condensation step with a pH dependent rate. The condensation of silica precursor in the reaction condition is so moderately high, (Equation 3.1.3) that after 2 hrs from the addition of TMOS and HNO_3, the SiO_2 nanoparticles are formed. The solution that is aged for more than 15 min is not good for the synthesis of meso-silica-ZnX-n thin films. Therefore, ideally in 5 min after the addition of TMOS, the solution should be spin coated over a substrate.

$Si(OCH_3)_4 + H_2O \rightarrow HO\text{-}\ Si(OCH_3)_3 + CH_3OH$ Hydrolysis (Eq 3.1.1)

$Si(OCH_3)_4 + 4\ H_2O \rightarrow Si(OH)_4 + 4\ CH_3OH$ Acid Catalyst Hydrolysis(Eq 3.1.2)

$Si(OH)_4 \rightarrow SiO_2 + H_2O$ Condensation (Eq 3.1.3)

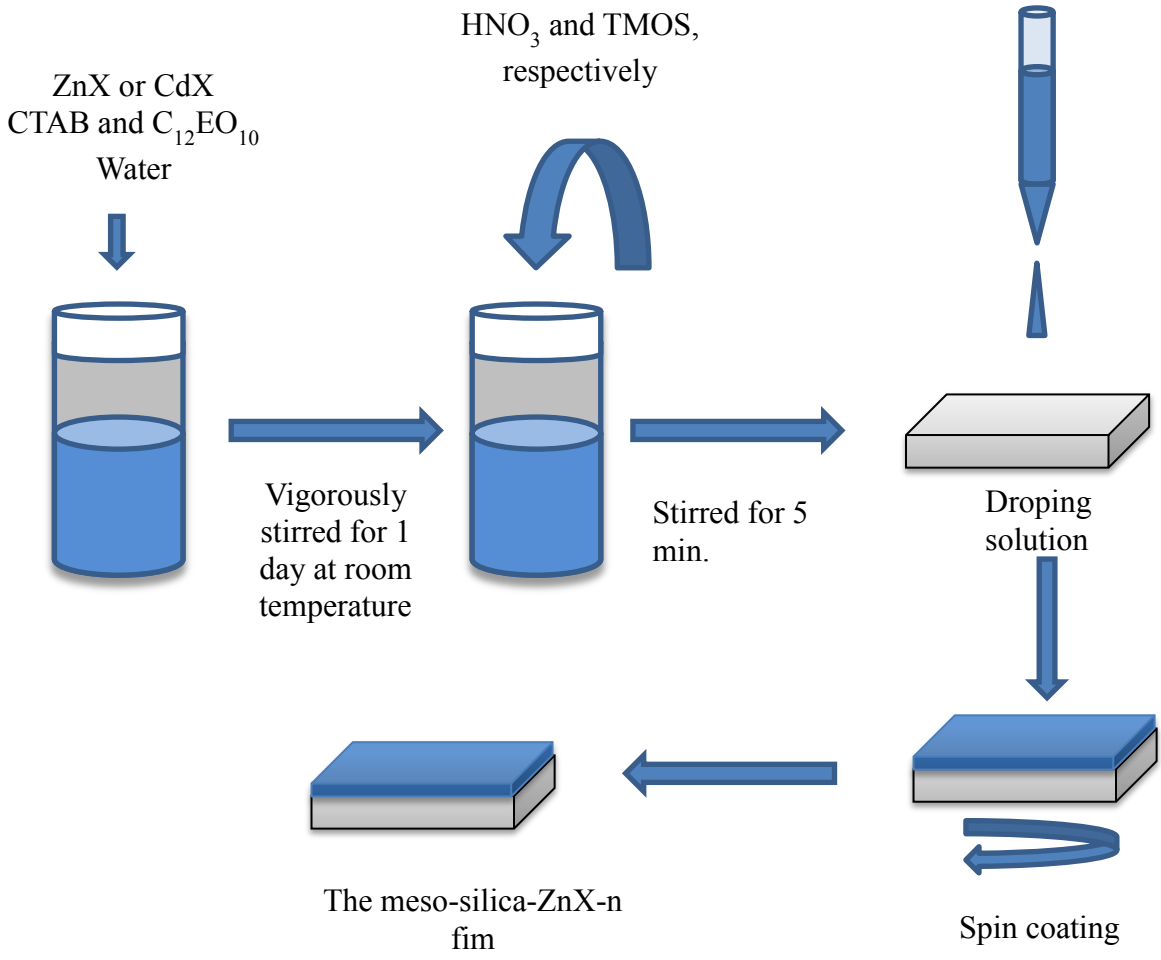

Figure 3.1.1: The representative preparation of the meso-silica-ZnX-n film by spin coating.

In order to prepare the meso-silica-ZnX-n films, the solution of CTAB, $C_{12}EO_{10}$, ZnX, HNO_3, water, and TMOS is put over a substrate on spin coater and spanned as represented in Figure 3.1.1. The excess water evaporates during spinning. The film thickness can be adjusted by altering spin rate and time. The ideal spinning rate and time is optimized to be 1200 rpm and 1 min, respectively, for the ideal thickness of meso-silica-ZnX-n thin films. The sample thickness is about 1 μm after the evaporation of water and methanol (a side product).

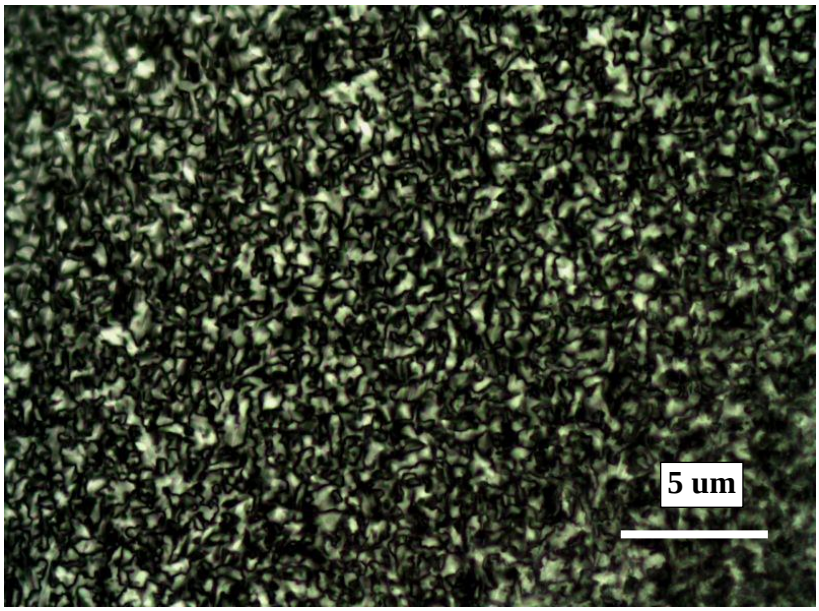

Figure 3.1.2: The POM image of an as-prepared meso-silica-ZnX-1.14 thin film.

The spin coated sample on a glass microscope slide has been characterized using XRD and POM techniques. The as-prepared meso-silica-ZnX-n films are likely in a liquid crystalline mesophase. POM is a useful technique for the determination of anisotropic mesostructures. A fan-like texture, observed from meso-silica-ZnX-1.14 film, under a polarized optical microscope (POM), is characteristic for this existence of 2-D hexagonal mesostructure, see Figure 3.1.2. The observed birefringence in the POM image is characteristic for anisotropic 2-D hexagonal mesophase.

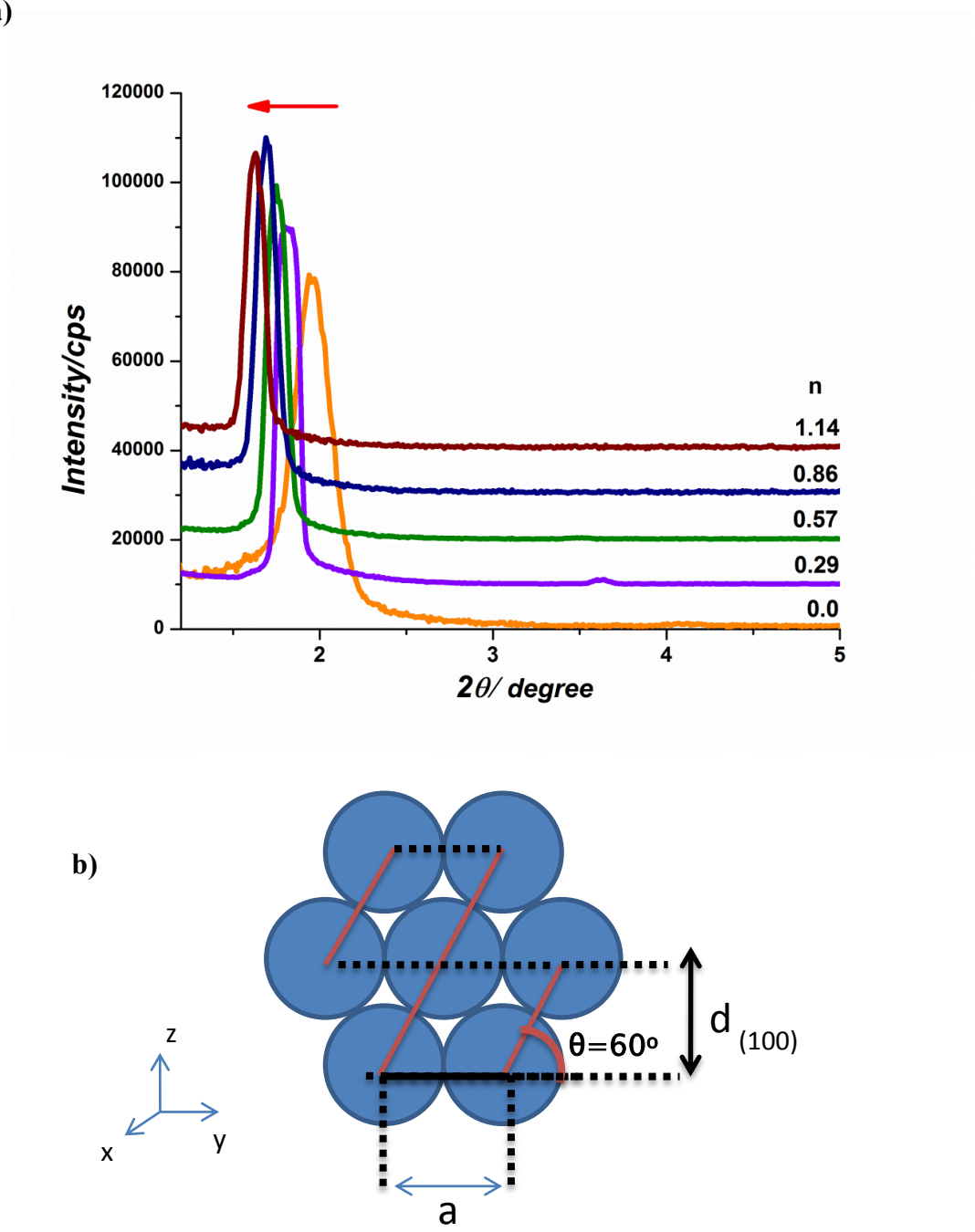

Figure 3.1.3 a) Small-angle XRD patterns of the as prepared meso-silica-ZnX-n thin films where n is Zn(II)/SiO_2 mole ratio(*1*). b) The schematic representation of $d_{(100)}$ planes in

The small angle diffraction lines observed from all compositions of meso-silica-ZnX-n (n is 0.29, 0.57, 0.86, 1.14, 1.43, and 1.71) belong to (100) and (200) planes of 2D hexagonal mesostructure, Figure 3.1.3.a. The d-spacing of the (100) planes, $d_{(100)}$,

can be calculated by utilizing the Bragg's law, $n\lambda = 2d\sin\theta$. For example, $d_{(100)}$ for the meso-silica-ZnX-0.29 is found to be about 4.8 nm, where 2θ is 1.84^o. The unit cell parameter, a, is calculated from $a = d_{(100)}/\sin(60^o)$ ($a = 4.8/0.866 = 5.5$ nm). The second line at 3.58^o, 2θ, corresponds to the (200) planes of 2D-hexagonal structure. The diffraction lines of meso-silica-ZnX-n, gradually shifts to smaller angles with increasing the ZnX content of the sample. It is reasonable that increase in the salt content in mesostructure increases the unit cell parameter, expands the hydrophilic domains in the mesostructure.

First, for the synthesis of ordered mesoporous silica-ZnO thin film, meso-silica-ZnX-n samples are aged at room temperature for the condensation of silica domains, which eventually provides a rigid 2-D hexagonal and ordered mesostructure. Then, by a controlled calcination under an air atmosphere, the ZnX salt is converted to ZnO and the surfactants are removed. As a consequence, the ordered mesoporous silica-ZnO thin films with 2-D hexagonal structure may be obtained upon calcination.

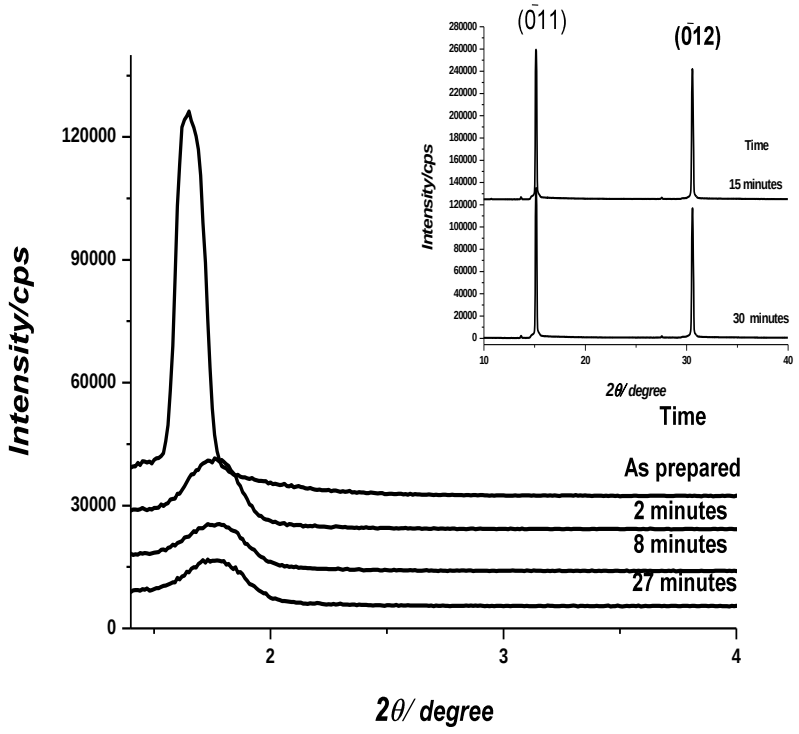

Figure 3.1.4: Small-angle and wide angle (inset) XRD patterns of the meso-silica-ZnX-1.14 thin films with different aging times where time is shown on the patterns

To elucidate and understand the underlying mechanism for the formation of meso-silica-ZnX-n, the stability of the mesostructure of as prepared meso-silica-ZnX-1.14 thin film was monitored by recording small angle and high angle diffraction patterns at different aging time. The highly intense diffraction line at around 1.4^{o}, 2θ shifts to around 1.8^{o}, 2θ and its intensity decreases after about 2 min, Figure 3.1.4. The diffraction lines at wide angle XRD pattern belong to ZnX salt, Figure 3.1.4 (PDF card number: 00-046-0595). This means that most of the ZnX salt leaches out from the mesostructure and crystalizes out of the 2D hexagonally oriented mesostructure. The shift from 1.4^{o}, 2θ to 1.8^{o}, 2θ, in the low angle diffraction line indicates that domains of the mesophase shrink more than 30%, and likely indication of leaching salt out of the mesostructure.

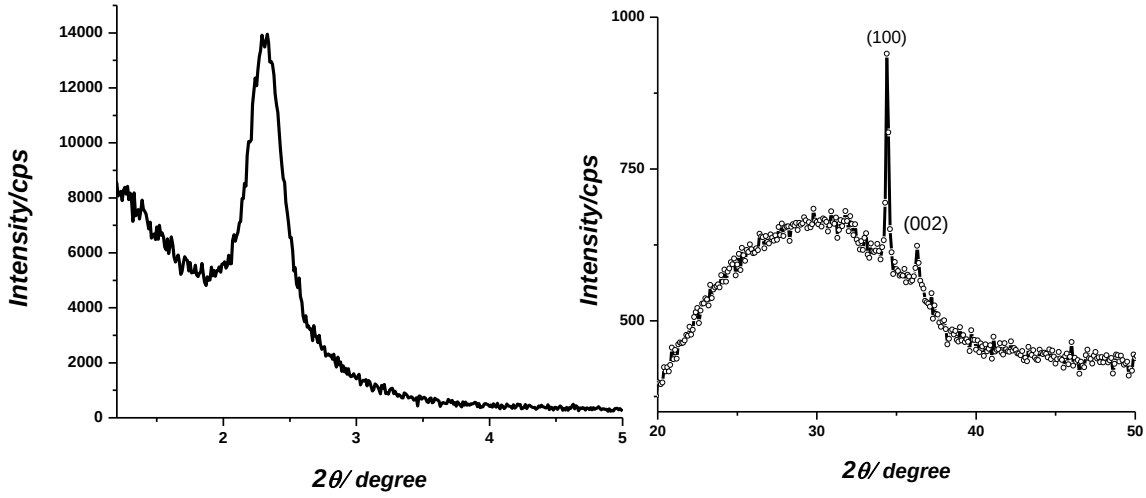

Figure 3.1.5: Small (top) and wide (bottom) angle XRD patterns of the calcined meso-silica-ZnX-1.14 thin film

If the films, in which ZnX salt leached out from the mesophase, are heated from room temperature (RT) to 450 ^{o}C with 1^{o}C /min intervals, the formation of bulk wurtzite ZnO is observed. The diffraction lines in wide-angle XRD pattern of the calcined sample of meso-silica-ZnX-1.14 belong to (100) and (002) planes of wurtzite ZnO (d_{100} = 2.8141 Å and d_{002} = 2.6027 Å), Figure 3.1.5. Interestingly, ordered 2-D hexagonal mesoporous silica-ZnO thin films and bulk ZnO form together. The diffraction line at around 2.4^{o}, 2θ in small-angle diffraction patterns of the calcined

sample of meso-silica-ZnX-1.14 originates from the (100) plane of 2-D hexagonal structure (d_{100} = 3.7 nm), see Figure 3.1.5. Because, all salt species does not leach out from the mesostructure, remaining ZnX in the mesophase with silica precursor forms the mesoporous ordered structure. As shown in the SEM image of this sample in Figure 3.1.6, after calcination, cracks and round hollows about 1 µm size are formed throughout the film. It is likely that the ZnX salt crystals leached out from the mesophase, formed bulk ZnO crystals. These crystals cover the surface of ordered mesoporous silica-ZnO in which less amount of ZnO than initial salt composition exists in the mesoporous domains of the film.

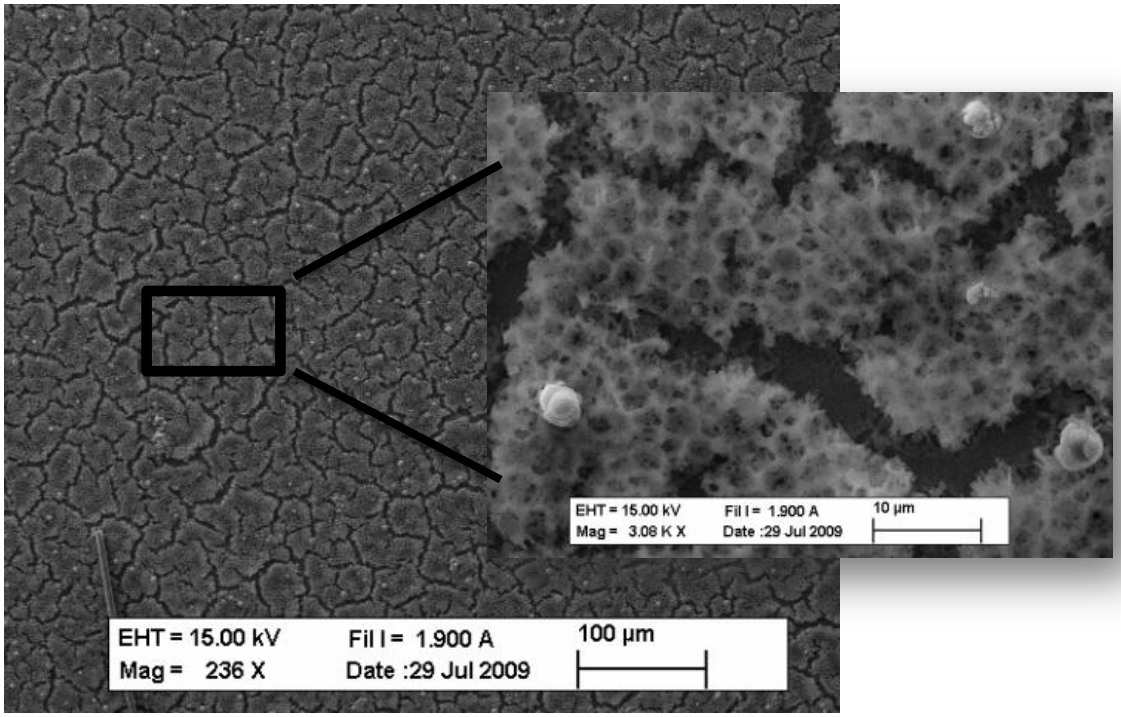

Figure 3.1.6: The SEM images of calcined the meso-silica-ZnX-1.14 thin film. Inset shows higher resolution SEM image of square.

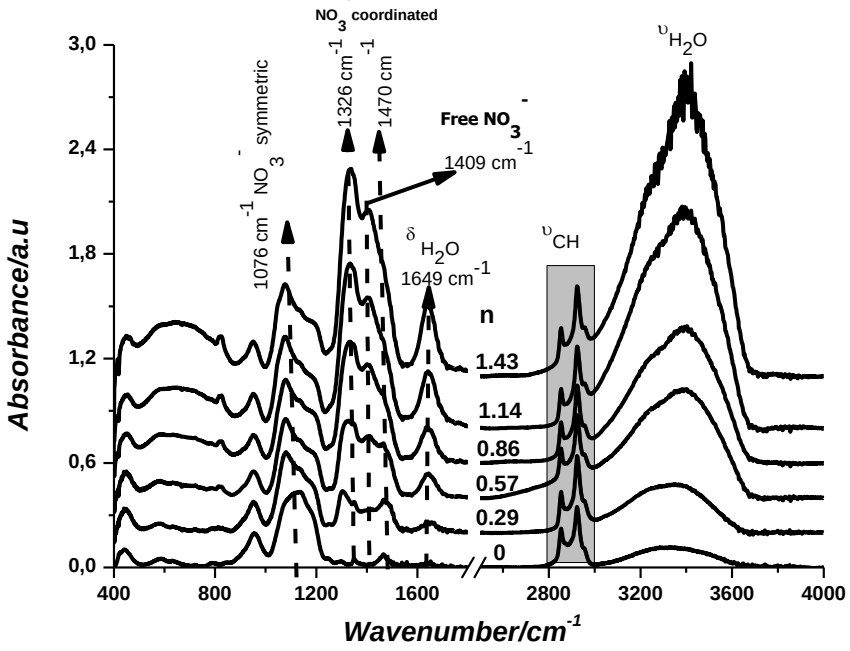

Figure 3.1.5: The FTIR spectra of meso-silica-ZnX-n (n is shown on the spectra) (*1*)

To understand and elucidate the stability issues of the meso-SiO_2-ZnX-n thin films, the FTIR spectra of meso-silica-ZnX-n films (where n is 0.29, 0.57, 0.86, 1.14, and 1.43) are analyzed. The peaks, at around 1326 and 1470 cm^{-1} in the FTIR spectra of meso-silica-ZnX-n, are assigned to antisymmetric stretching modes of nitrate ions that are coordinated to Zn(II) ion, see Figure 3.1.5. The intensity of these peaks increases with increasing salt content in the samples. At high salt content, the nitrate peaks are very similar to the peaks in molten ZnX salt.(*90*) Evaporation of water and methanol during spin coating transforms ZnX salt to its molten phase that is confined between the silica clusters and hexagonally organized surfactant domains at high ZnX concentrations. In the as-prepared thin films, the molten ZnX salt acts as a solvent and organizes the surfactant molecules and silica species into mesostructures.

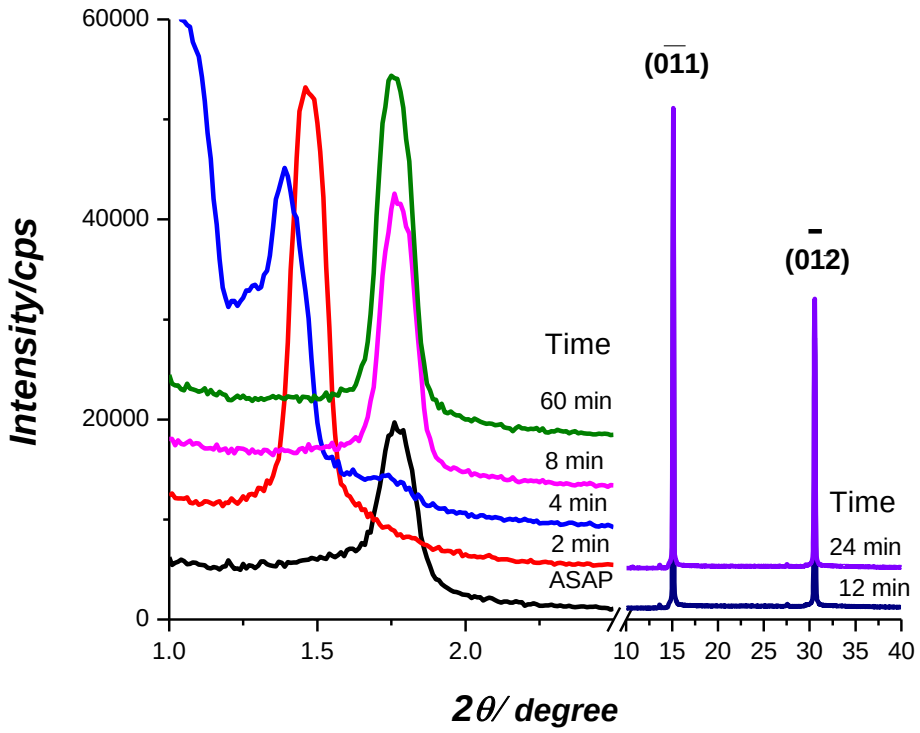

Figure 3.1.6: The small-angle and wide-angle XRD patterns of the as prepared meso-silica-ZnX-n thin film aged for 5 minutes at 55 ^{0}C and in time at room temperature where time is shown on the patterns

The meso-SiO_2-ZnX-n samples at high ZnX concentrations, above 0.57 Zn(II)/Silica mole ratio, can form the mesostructure by keeping ZnX salt in its molten phase. The mesostructure is stable if the samples are kept above melting point of ZnX salt. Notice that the melting point of $[Zn(H_2O)_6](NO_3)_2$ is only 36.5 ^{0}C. To understand the role of temperature above the melting point of salt species, small and wide angle XRD patterns of meso-SiO_2-ZnX-1.14 film sample were recorded over time after aging the samples at 55 ^{0}C. However the diffraction patterns were recorded at RT; the temperature of the samples reaches to RT in 2 min. The diffraction line at around 1.7^o, 2θ, of the sample aged for 5 min at 55 ^{0}C shifts to around 1.4^o in 2 min, and its intensity increases, see Figure 3.1.6. This means that when the sample film reaches RT, the volume of mesophase expands by absorbing ambient water and the mesophase becomes

better ordered. However, after 8 min of aging at RT, the diffraction line, at around 1.4^{o} shifts back to 1.7^{o} and the diffraction lines of ZnX salt in the wide angle appear (PDF card number: 00-046-0595). This is a characteristic behavior when the sample leaches out salt.

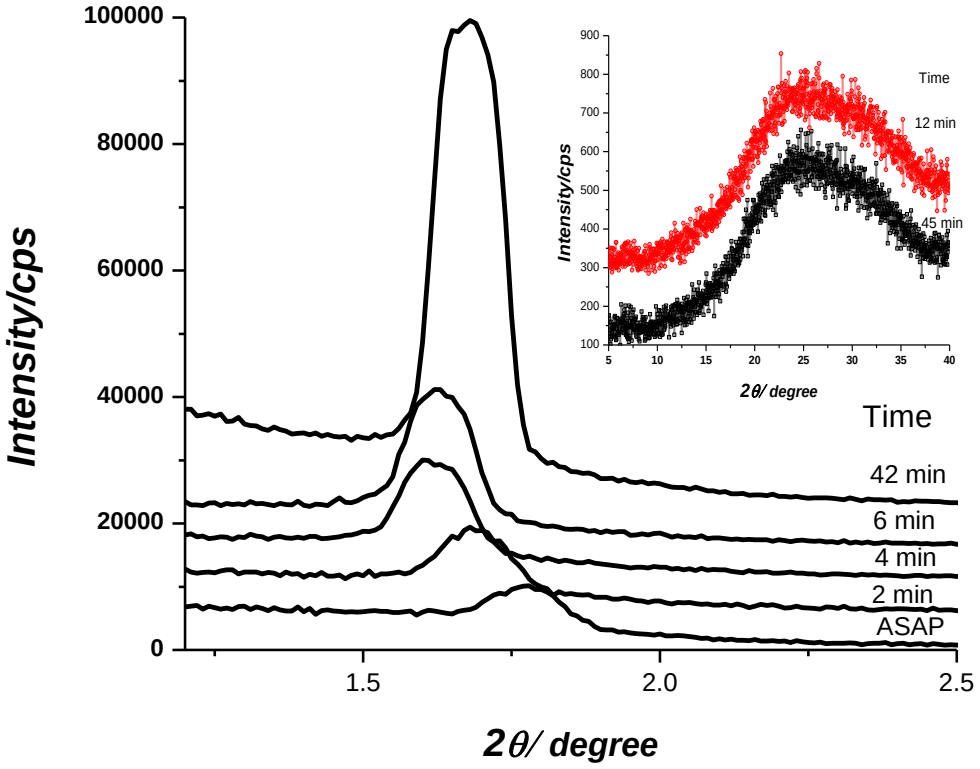

Figure 3.1.7: The small-angle and high angle XRD patterns of the as prepared meso-silica-ZnX-n thin film aged for 2 hours at 55 ^{0}C in time where time is shown on the patterns

This behavior shows that the structure of the meso-silica-ZnX-1.14 film is not stable at RT for a long time and some of the salt species leach out from the mesostructure. The aged sample at 55 ^{0}C for 2 hrs also shows a similar behavior, see Figure 3.1.7. However this sample is stable at RT over 1h. Notice also that there is no diffraction line at wide-angle region due to ZnX crystals, showing that the salt species are confined and likely in its molten phase between the silica and hexagonal organized

surfactant domains. This can be explained by the melting point depression due to confinement effect. Otherwise, high amount of salt has to crystallize during self-assembly. Therefore, longer aging, at 55 ^{o}C, stabilize the samples for a longer time at RT.

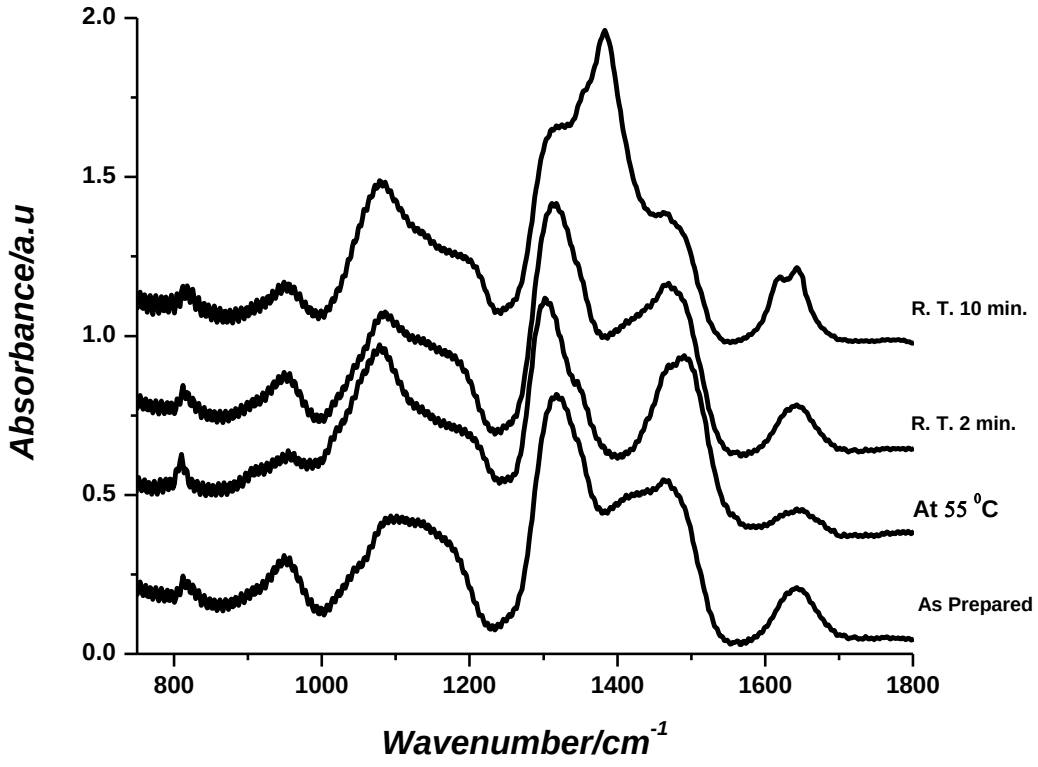

Figure 3.1.8: The FTIR spectra of as-prepared meso-silica-ZnX-1.14 at different temperature with time (Temperatures is shown on the spectra)

In order to understand the behavior of as-prepared meso-silica-ZnX-n at high salt concentrations, against aging, the FT-IR spectra of as-prepared meso-silica-ZnX-1.14 were also recorded during aging at 55 ^{o}C. The bottom spectrum in Figure 3.1.8 is the spectrum of the as-prepared sample. Then, the film sample was heated to 55 ^{o}C on a homemade IR heating stage, and its spectrum was recorded at 55 ^{o}C. Finally, the sample was cooled to RT and two more spectra were recorded 2 and 10 min later. The peaks between 1250 and 1480 cm^{-1}, due to asymmetric stretching modes of nitrate ions,

and at 1630 cm $^{-1}$, due to bending mode of water molecules show changes with temperature and time, Figure 3.1.8. By heating the sample to 55 ^{o}C, the coordination of nitrate ions to Zn (II) ion is enhanced due to enlarging the splitting of coordinated nitrate peak position and the intensity of the water peak at 1630 cm $^{-1}$ is decreased. However, cooling the sample to RT for 2 min, the peaks, due to coordinated nitrates, increased and the intensity of the water peak at 1630 cm $^{-1}$ increased, similar to the initial spectrum of as prepared sample, see Figure 3.1.8. This means that the coordinated water molecules evaporate at 55 ^{o}C (dehydration), and the ZnX salt species reabsorb the water molecules (hydration) at RT. This also explains the expansion of the mesophase, observed in the small angle XRD patterns, since the volume of ZnX salt species expands by the hydration. However, if the sample is kept at RT long enough, most of salt species leached out from the mesophase. This can also be observed in the FTIR spectrum (see top spectrum in Figure 3.1.8). The sharp peak at around 1400 cm^{-1} is due to ZnX crystals.

The mesostructure, at high salt concentration is only stable above the melting point of the salt. It means that the molten ZnX salt can organize the surfactants (CTAB and $C_{12}E_{10}$) and silica species into a 2-D hexagonal mesostructure. In conclusion, keeping samples above the melting point immediately after spin coating is prerequisite for the synthesis mesostructured silica-ZnX films.

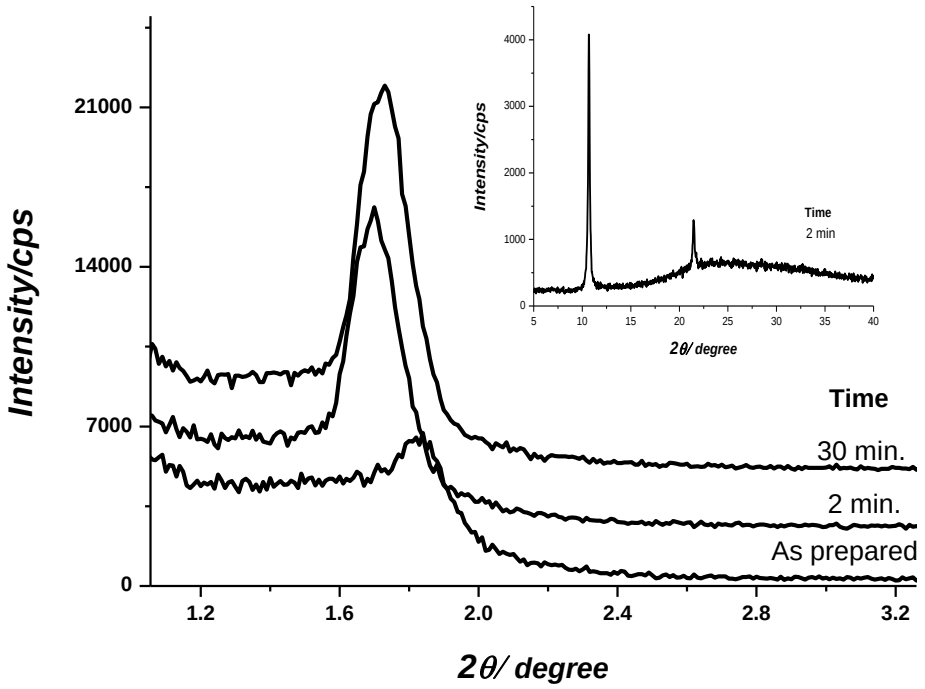

Figure 3.1.9: The small-angle and high angle (inset) XRD patterns of the as prepared meso-silica-ZnX-n thin film aged for 1 day at 55 ^{0}C in time where time is shown on the patterns

To further understand the effect of aging, the as-prepared meso-silica-ZnX-1.14 was aged at 55 ^{o}C for 1 day. The mesostructure still responses to the adsorption of water, such that, the diffraction line in the small angle XRD pattern shifts to lower angle, see Figure 3.1.9. However, the diffraction lines due to ZnX crystals appear in 2 min at RT, indicating that most of the salt species are not inside the mesophase despite aging the sample for one day. The calcination of this sample also produced bulk ZnO crystals.

In summary, the samples should be kept above the melting point of ZnX salt immediately after the assembly of mesophase through spin coating in order to keep the mesostructure stable. The aging temperature, 55 ^{o}C, is ideal for meso-silica-ZnX-n films. The samples are not stable at RT because of leaching out of the salt. The salt species, which are out of the mesostructure crystalize and form bulk metal oxide upon

calcination. Aging step should not be longer than 2 hrs because further aging step also causes leaching of salt species from the mesostructure.

3.2 Optimization of Synthesis Conditions for the meso-silica-CdY-n Films

The knowledge and experience that were gained from the optimization of the meso-silica-ZnX-n films can be applied to other salt – surfactant systems to show the generality of the synthesis method, developed in this thesis. Therefore, the meso-silica-CdY-n samples(where CdY is $[Cd(H2O)_4](NO_3)_2$) were prepared by spin coating a clear solution of CTAB, $C_{12}EO_{10}$, CdY, HNO_3, water, and TMOS as described in the preparation of the meso-silica-ZnX-n film samples.

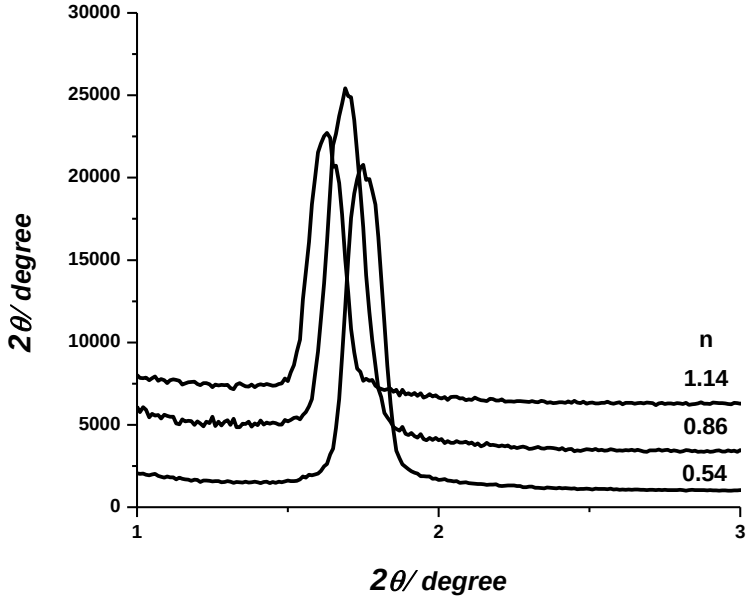

Figure 3.2.1: The small-angle diffraction patterns of as prepared meso-silica-CdY-n (n is 0.57, 0.86, and 1.14 and n is shown on the spectra

The small-angle diffraction lines observed from the as prepared meso-silica-CdY-n (n is Cd(II)/SiO_2 mole ratio and 0.57, 0.86, and 1.14) prove the formation of a 2D hexagonal mesostructure and they belong to (100) plane of the hexagonal mesostructure, Figure 3.2.1. As in the meso-silica-ZnX-n samples, increasing the salt content shifts the

diffraction line to smaller angles, indicating that the distance between surfactant domains increases with increasing salt content.

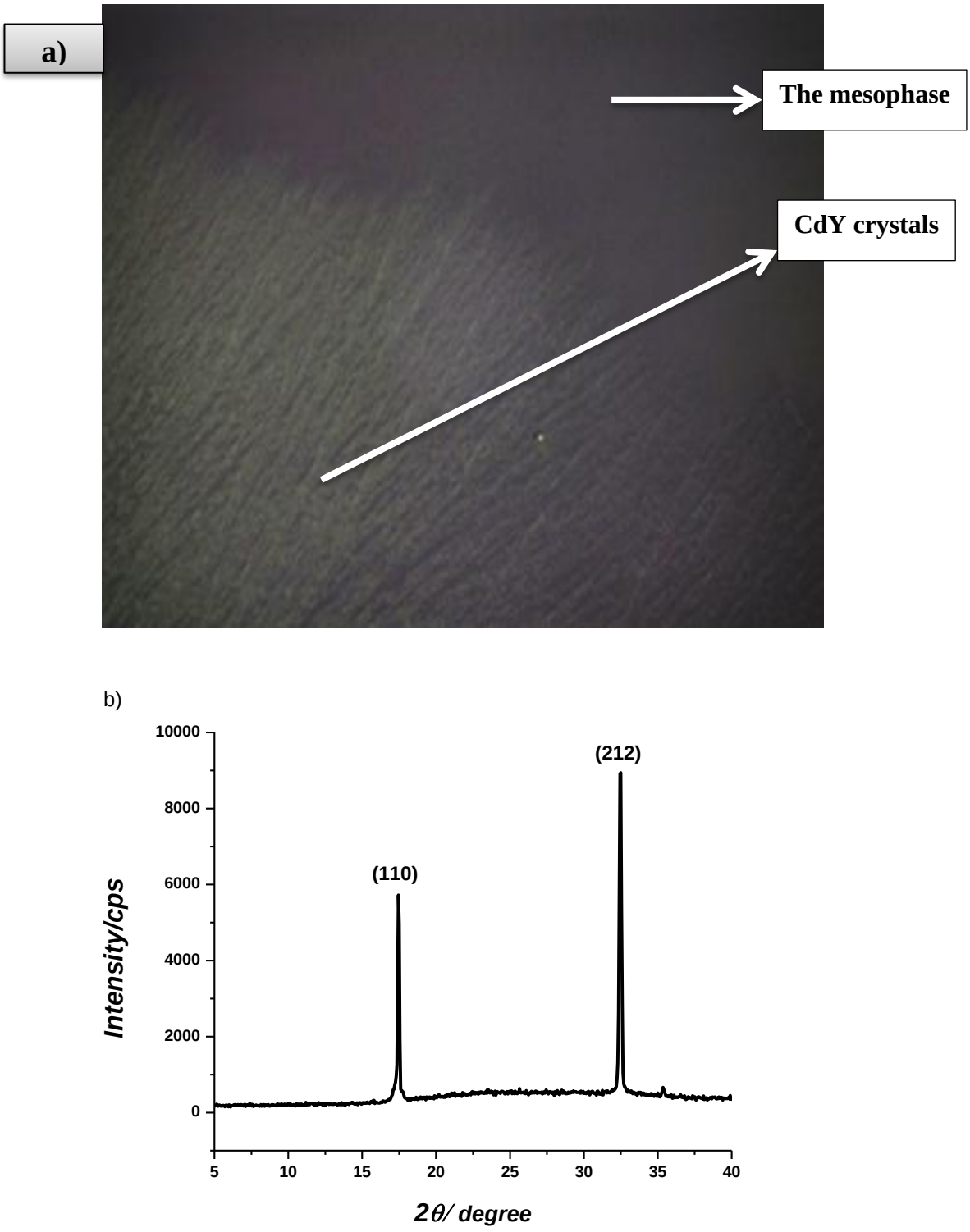

Figure 3.2.2: The POM image (a) and the high-angle diffraction patterns (b) of meso-silica-CdY-1.14, 5 minutes after preparation at RT.

To check the stability of meso-silica-CdY-n film samples at high salt concentrations, the POM image and the high-angle diffraction patterns of meso-silica-CdY-1.14 have been recorded after 5 min aging at RT, Figure 3.2.2. Since the films are too thin, a fan texture characteristic of 2D hexagonal mesostructure is difficult to observe. However, formation and growth of the CdY crystals can be monitored using the POM and thin films. The crystals cover the surface of the film and appear as sharp texture under the POM. Most salt species leached out from the mesostructure in 5 min. The wide-angle diffraction lines, in the XRD pattern of the samples, due to CdY salt crystals also appear upon crystallization of the films (PDF card number:04-011-2154).

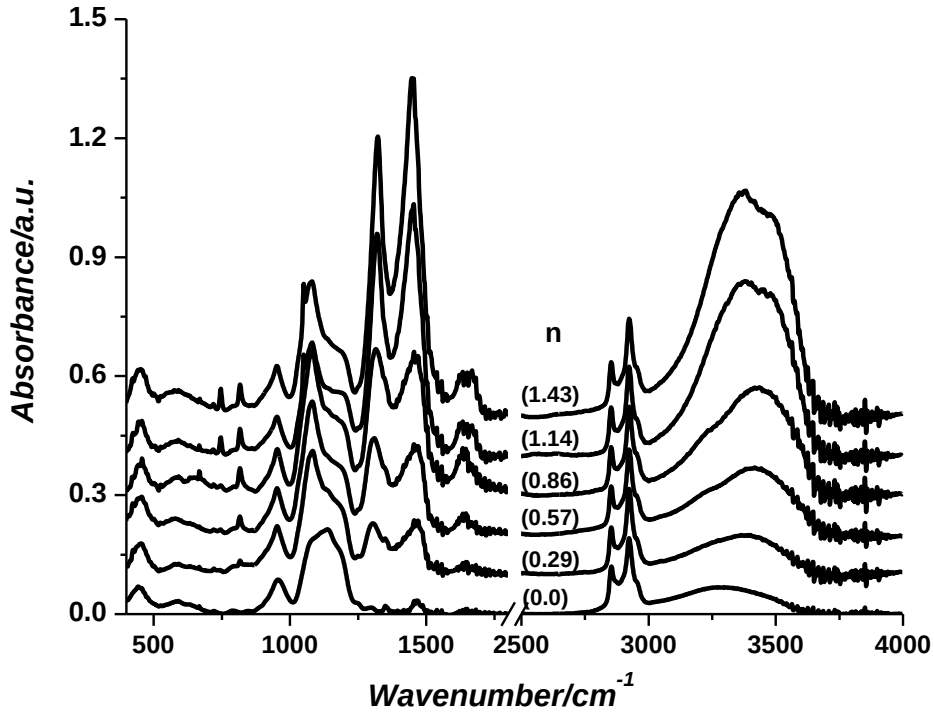

Figure 3.2.3: The FTIR spectra of meso-silica-CdY-n (n is shown on the spectra***) (1)***

FTIR spectroscopy is also a useful tool to follow the changes in the samples during aging at RT and high temperatures. The sharp peaks between 1250 and 1500 cm^{-1} in the FTIR spectra of meso-silica-CdY-n belong to asymmetric stretching mode of nitrate ions that are coordinated to Cd(II) ion, see Figure 3.2.3. Intensity of these peaks

increases with increasing salt content in the samples, Figure 3.2.3. At high salt content, the nitrate peaks are very similar to the peaks in the molten CdY salt. Therefore, by keeping the samples above the melting point of CdY salt, the mesostructure can be stabilized for the synthesis of mesoporous silica-CdO films as in the preparation of meso-silica-ZnX films.

3.3 Synthesis of the meso-silica-ZnO-n and meso-silica-CdO-n Thin Films

It is known from the optimization studies of the meso-silica-ZnX-n films in which the mesostructure, at high salt concentrations, can be stabilized after spin coating above the melting point of the salt. Interestingly, a slow calcination of the meso-silica-ZnX-n starting from 55 ^{o}C with an interval of 1^{o}C/min up to 450^{o}C, immediately after spin coating, forms transparent mesoporous films, denoted as meso-silica-ZnO-n (where n is the Zn/Si mole ratio).

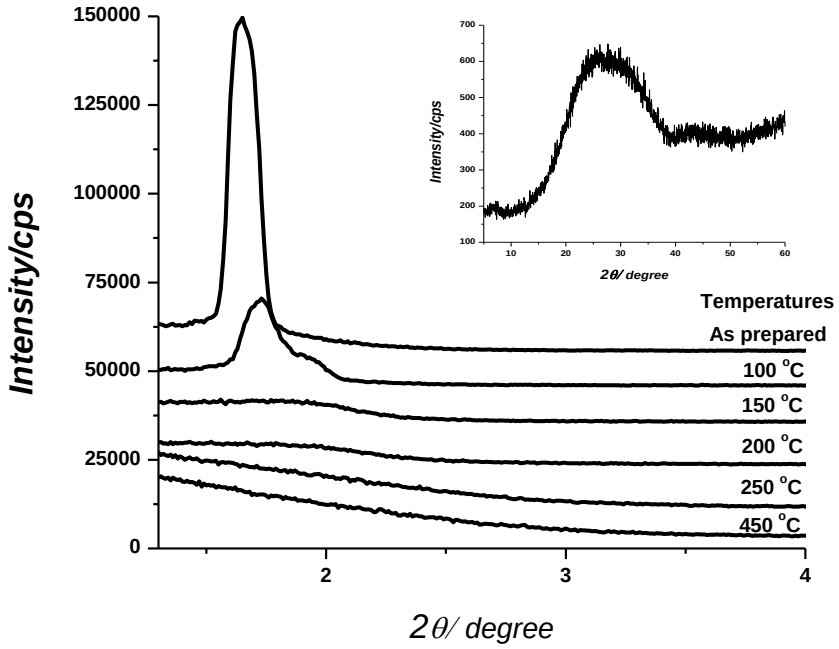

Figure 3.3.1: The small-angle XRD patterns of the meso-silica-ZnX-1.14 thin film during calcination where temperature is shown on the patterns and the high angle XRD patterns of the meso-silica-ZnO-1.14 (inset)

The small angle diffraction line loses its intensity at around 100-150 ^{o}C and it completely vanishes at around 250 ^{o}C during the calcination step, see Figure 3.3.1. This means that the calcination yields a completely disordered structure. More importantly, there is no diffraction line due to ZnO crystals, indicating that bulk ZnO does not form in the films during the calcination process, see Figure 3.3.1 (inset). It means that all salt species decompose into ZnO on the silica pore-walls, where it cannot grow into bulk large ZnO crystals.

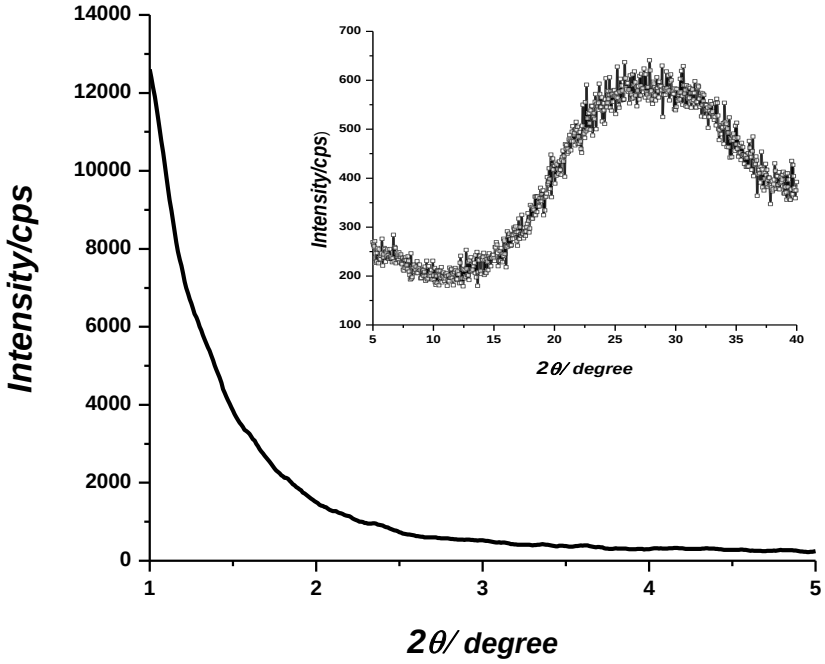

Figure 3.3.2: The small-angle XRD patterns of the meso-silica-CdO-1.14 thin film and the high angle XRD patterns of the meso-silica-CdO-1.14 (inset)

The slow calcination of the meso-silica-CdY-n films starting from 65 ^{o}C with an interval of 1^{o}C/min up to 450 ^{o}C, immediately after spin coating, forms transparent mesoporous films denoted as meso-silica-CdO-n (where n is the Cd/Si mole ratio). Like in the synthesis of the meso-silica-ZnO-n films, the calcination process causes loss of meso-order in the films, as it is shown in the small angle diffraction pattern of the meso-silica-CdO-1.14; see Figure 3.3.2. Also, there is no diffraction line due to bulk CdO in the high angle XRD pattern. All salt species decompose into CdO on the silica pore-walls and cannot grow into bulk CdO crystals. On the other hand, despite all,

above the salt/silica mole ratio of 1.43, the film samples leach out some of the salt species and form bulk oxide upon calcination step in addition to meso-silica-CdO-x (where x is Cd/Si mole ratio and in unknown).

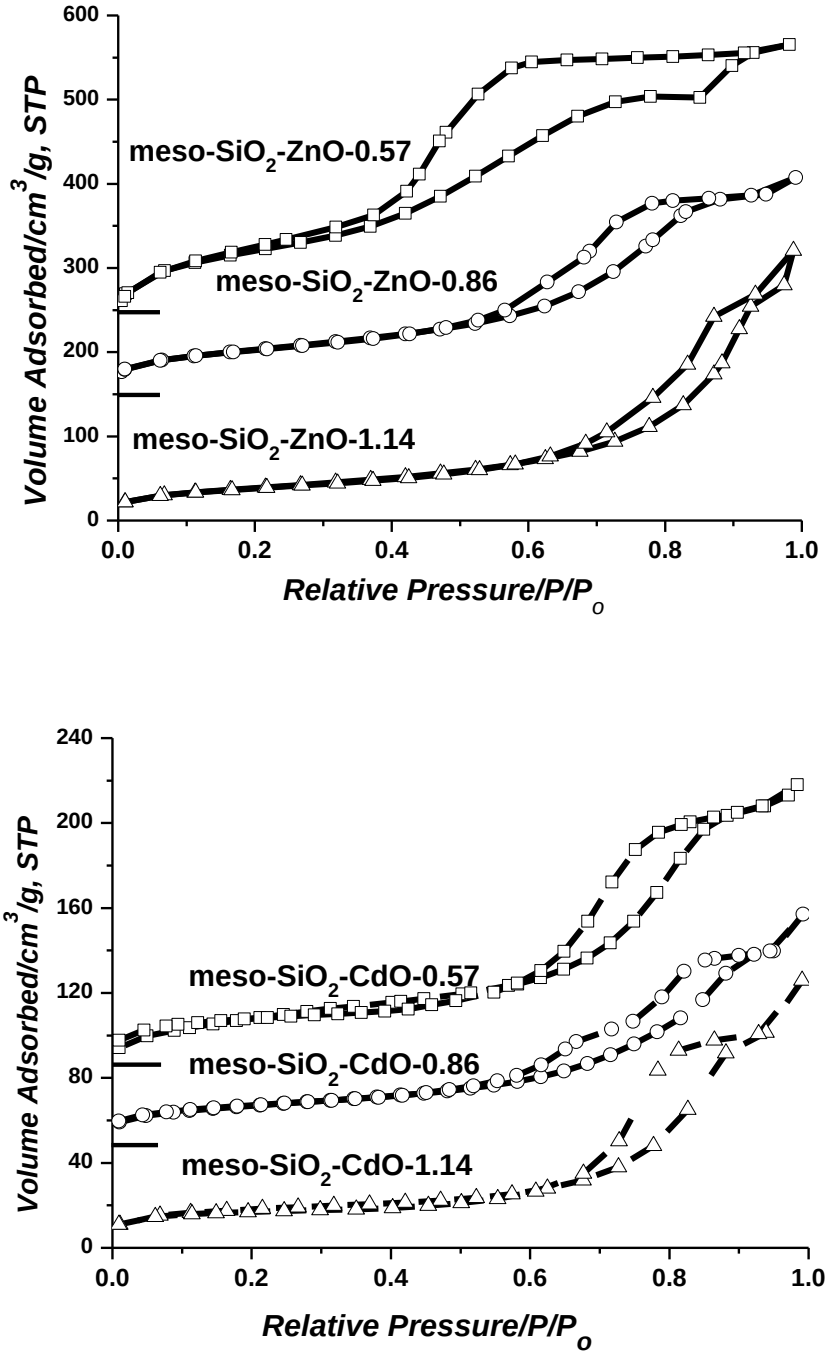

Figure 3.3.3: The N_2 sorption isortherms of the meso-silica-ZnO-n (up) and the meso-silica-CdO-n (down) samples where n values are shown on each plot(*1*)

To prove above proposal, whether the meso-silica-ZnO-n and mesoporous-silica-CdO-n films have mesoporosity or not, the films were recording N_2 adsorption-desorption isotherms. At least 20 mg powder sample is needed for an accurate N_2 adsorption-desorption measurements. Therefore, tens of meso-silica-ZnO-n and mesoporous-silica-CdO-n film samples, which were coated over the glass slides, were scraped to obtain needed amount of sample (one film coated on a glass slide is about 1 mg). Scraping the samples from the meso-silica-ZnO-0.29 and meso-SiO_2-CdO-0.29 samples is very difficult. Therefore, N_2 adsorption-desorption measurements are done for only the meso-silica-ZnO-n and mesoporous-silica-CdO-n (where n is 0.57, 0.86, and 1.14) samples, see Figure 3.3.3. In all the N_2 sorption isotherms, the hysteresis on the adsorption and desorption branches shows that the meso-silica-ZnO-n and mesoporous-silica-CdO-n (where n is 0.57, 0.86, and 1.14) samples have mesoporosity. These isotherms are type IV isotherms and characteristic of the mesoporous materials.

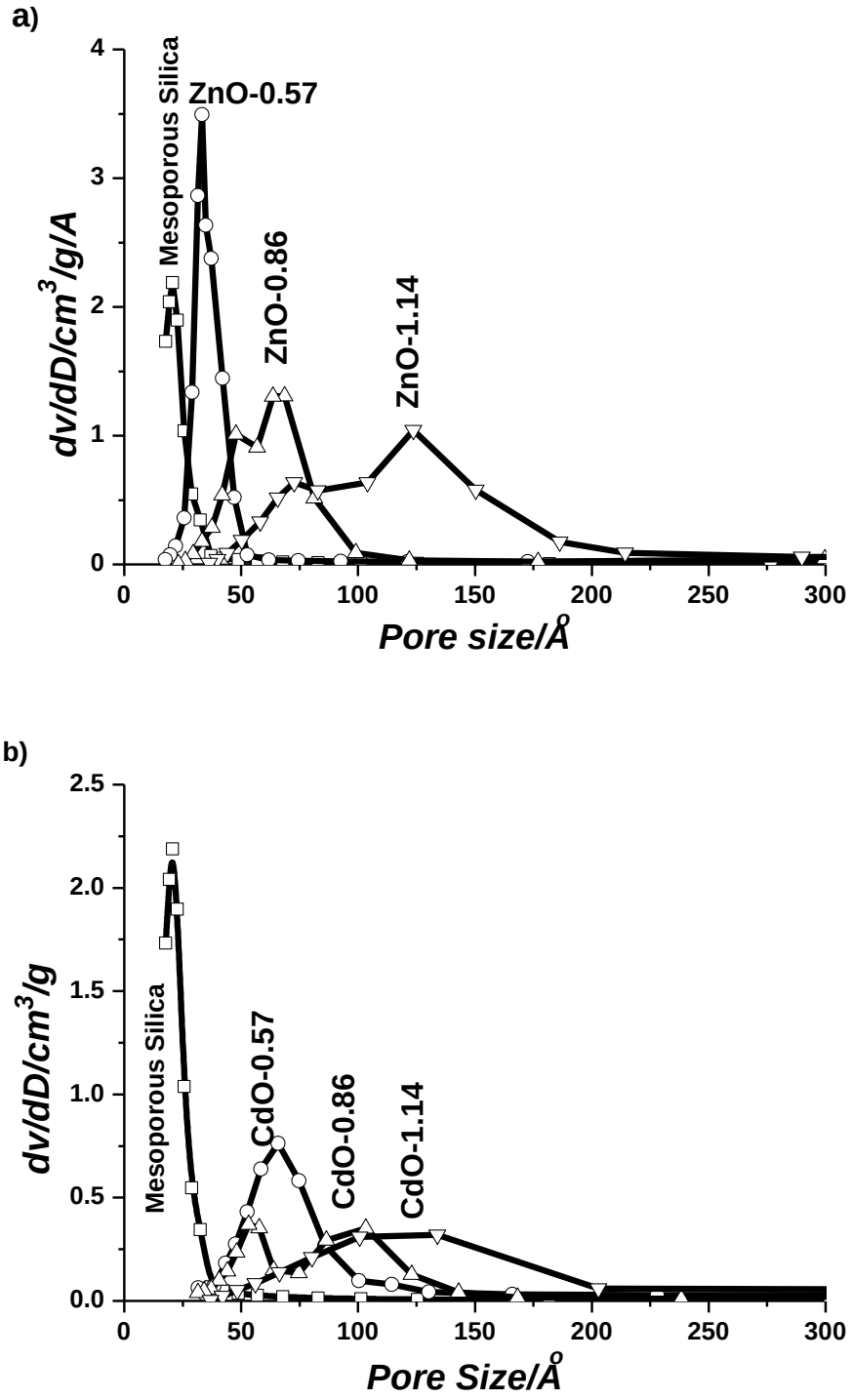

Figure 3.3.4: The pore size distribution of the mesoporous-silica-ZnO-n (a) and mesoporous-silica-CdO-n (b)where n values are shown on each plot(*1*)

The Brunauer-Emmett-Teller (BET) surface areas that are 430, 175, and 130 m^2/g in the meso-silica-ZnO-n samples, where n is 0.57, 0.86, and 1.14, respectively, decreases with increasing the ZnO content in the meso-silica-ZnO-n samples. The BET surface areas of the mesoporous-silica-CdO-n, where n is 0.57, 0.86, and 1.14 are 85, 55, and 50 m^2/g , respectively. The same trend as in the meso-silica-ZnO-n samples is observed in the meso-silica-CdO-n; increase in the metal oxide content decreases the surface area. Note also that a calcined salt-free mesoporous silica film has a surface area of 950 m^2/g with a relatively narrow pore-size distribution centered at 2.1 nm, see Figure 3.3.4. The Barrett-Joyner-Halenda (BJH) pore-size distribution curves of the mesoporous-silica-ZnO-n and mesoporous-silica-CdO-n samples become broader and shift to higher values with increasing metal oxide content in the samples. For example, the pore size distribution of the meso-silica-ZnO-1.14 is centered at 12.4 nm and starts from 5 nm and tails up to 20 nm. The mesostructure, in the fresh sample, is distorted and expanded during calcination process. During the calcination, above 150 ^oC, the order of hexagonal mesostructure goes to a disordered mesostructure, and at the end of calcination, completely disordered mesoporous silica-metal oxide samples having expanded pores, especially in the high ZnO and CdO amounts, are formed. The decrease in the surface area and increase in pore size distribution with increasing ZnO or CdO content clearly show that the silica-ZnO or CdO walls of the mesoporous structure becomes thicker in the samples .

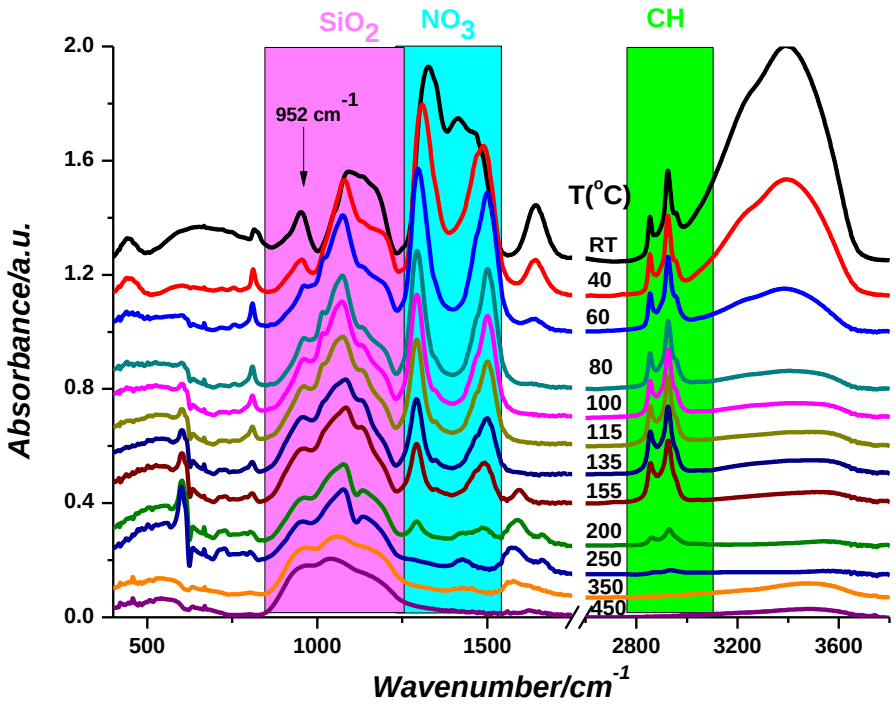

Figure 3.3.5: The meso-silica-ZnX-1.14 during calcination at different temperature (temperature is shown on the spectra) (*1*)

In order to elucidate the structural properties of the mesoporous silica-ZnO film samples, the calcination step was monitored by recording the FT-IR absorption spectra of meso-silica-ZnX-1.14 at different temperatures, see Figure 3.3.5. The intensity of nitrate peaks starts gradually to decrease on heating the films at around 100 ^{o}C and the peaks completely disappear at around 250 ^{o}C. This means that all nitrates are decomposed at around 250 ^{o}C. The peaks due to symmetric and antisymmetric stretching modes of the surfactants are observed at around 2820 and 2920 cm^{-1} and their intensities decline at around 200 ^{o}C and completely disappear at 250 ^{o}C. The peaks between 1100 and 1220 cm^{-1} are assigned to the υ-SiO symmetric and antisymmetric stretching modes and the peaks at around 952 cm^{-1} is due to silanol groups (SiO-H) of silica framework. (*106*) The calcination causes changes on the υ-SiO and υ-SiO-H stretching modes. The peak due to the υ-SiO-H stretching mode disappeared at 100 ^{o}C and the peaks due to υ-SiO symmetric and antisymmetric stretching mode gradually shifted to lower frequencies at higher temperatures. These changes are most probably

due to reaction between silanol groups and Zn(II) to form Si-O-Zn linkages. As discussed previously, the nitrate ions are coordinated to Zn (II) ions and upon calcination, they decompose. In addition to this, above 100 ^{o}C, there is no water molecule, coordinated to Zn (II) ions. Furthermore, the silanol groups are very reactive with transition metal ions. Therefore, the Zn(II) species react with silanol groups and cause changes on the υ-SiO symmetric and asymmetric stretching frequencies, while the υ-SiO-H stretching mode disappears. The FT-IR spectral changes are consistent with the changes in the XRD patterns of meso-silica-ZnX-1.14 during calcination. The decomposition of nitrates causes reaction between Zn(II) ions and silica framework and a distortion on the silica-metal oxide framework. Fortunately, due to stability of the surfactants up to 200 ^{o}C and solidification of the mesostructure by the polymerization of the silica species together with Zn(II) ions, mesoporous thin film can be obtained upon calcination. Yet, the calcined samples have disordered and non-uniform pore size distribution.

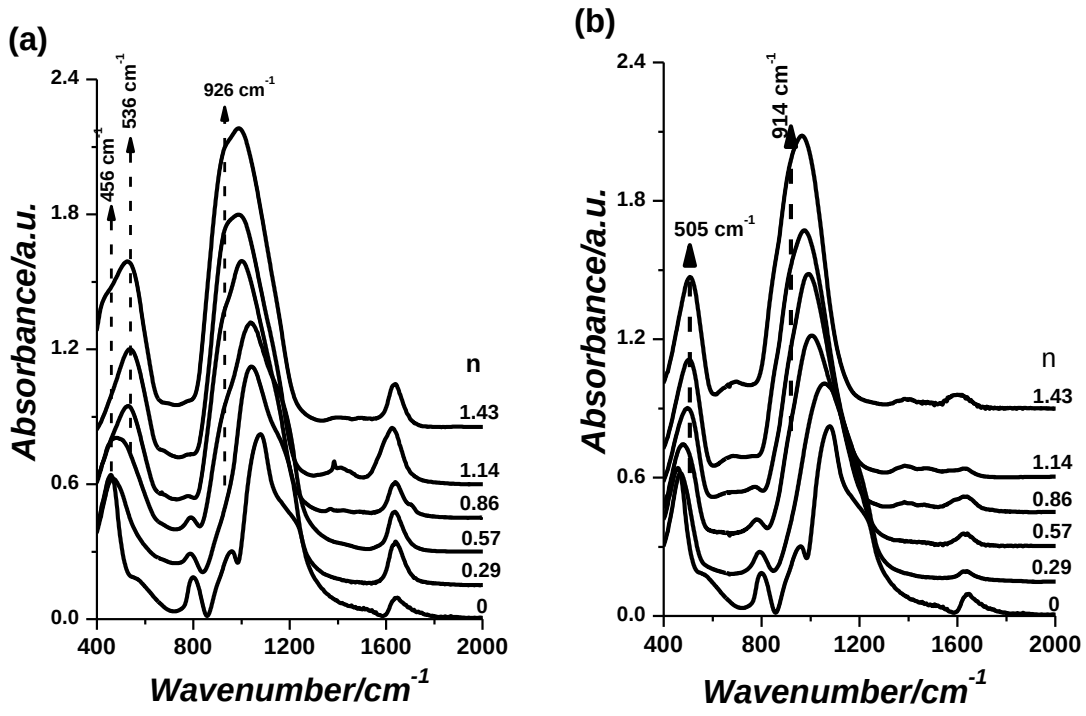

Figure 3.3.6: FTIR spectra of (a) meso-silica-ZnO-n, (b) meso-silica-CdO-n (n is Zn or Cd/SiO_2 mole ratio) (*1*)

To further understand the calcination process, the FTIR spectra of the meso-silica-ZnO-n and the meso-silica-CdO-n (n is 0, 29, 0.57, 0.86, 1.14, and 1, 43) were recorded for all compositions and shown in Figure 3.3.6. Intensity of the peaks at around 926 cm^{-1} in the meso-silica-ZnO-n samples and at 914 and 864 cm^{-1} in the meso-silica-CdO-n samples gradually increase with increasing metal oxide component of the samples up to metal oxide/silica mole ratio of 1.14. The meso-silica-ZnO-1.43 and the meso-silica-CdO-1.43 samples always formed bulk ZnO and CdO, respectively, together with mesoporous framework that contains relatively low metal oxide. Therefore, the peak due to υ-SiO stretching mode of the silica-metal oxide interface, Si-O-Zn and Si-O-Cd, loses its intensity compared to its metal oxide content.

The peak of the mesoporous silica at 1080 cm^{-1} gradually shifts to lower frequencies with increasing metal oxide content in the samples of meso-silica-ZnO-n and meso-silica-CdO-n up to 1.14 mole ratio. A similar trend is also observed in the peak at around 456 cm^{-1} due to bending mode of SiO_2. The peaks at 538 and 505 cm^{-1} in the spectra of meso-silica-ZnO-n and and meso-silica-CdO-n, respectively, gradually increase in intensity with increasing metal oxide content. If some of ZnO or CdO form bulk oxides, the shift is profoundly less. Therefore, the FT-IR spectroscopy and XRD techniques can be complementarly used to better chracterize the samples.

Moreover, to the best of our knowledge, the mixed oxides, like MSi_xO_y do not exist. Therefore, the Si-O-M bond (M is Zn or Cd) should be in the interface between the metal oxide nanoplates (see latter) and mesoporous silica framework.

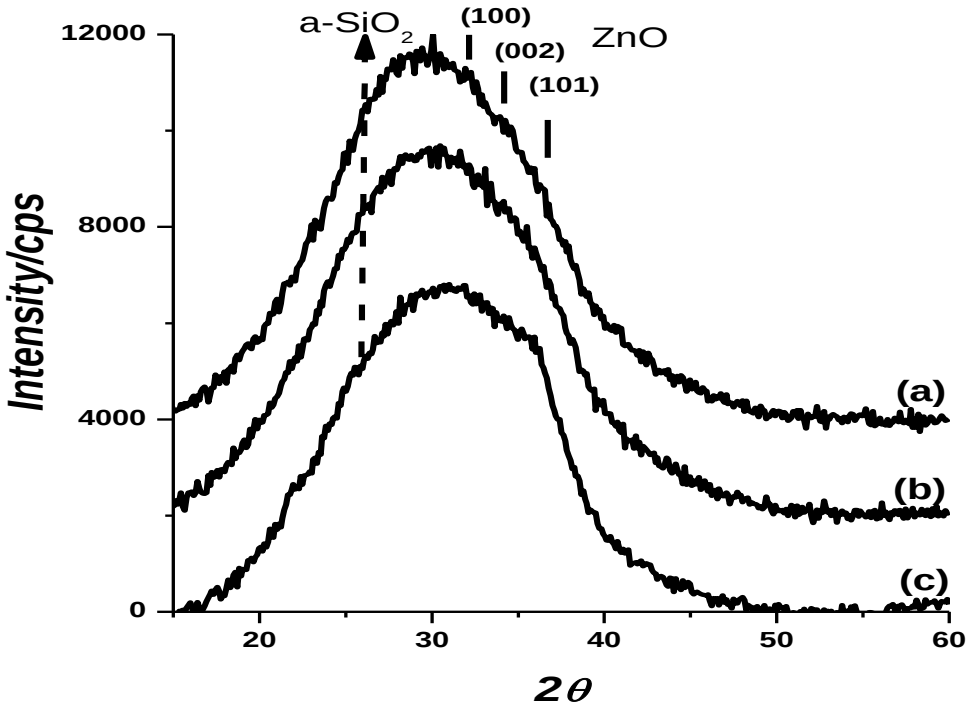

Figure 3.3.7: The XRD pattern of meso-silica-ZnO-0.86 at (a) 450^{o}C, (b) 550^{o}C, and (c) 650^{o}C. The common diffraction lines of ZnO are marked on the patterns(*1*)

Up to now, from the comprehensive analysis of the meso-silica-ZnO-n and meso-silica-Cd-n samples using FTIR and N_2 adsorption-desorption measurements, the samples are mesoporous and contains silica-ZnO and silica-CdO pore-walls, respectively. However, there is no information about the crystal structure of metal oxides in the mesoporous structure because the wide-angle XRD patterns of the films, obtained from the samples coated on the glass slides, are very broad with no definite diffraction line. The XRD patterns of the samples require large amount of powder samples. So, around 30 films coated on the glass slides were scraped to fill the XRD powder sample holder. Figure 3.3.7 shows the XRD pattern of meso-silica-ZnO-0.86 at 450, 550, and 650 ^{o}C. The common diffraction lines correspond to (100), (002), and (101) planes of wurtzite structure of ZnO are marked on the patterns. However, the wide angle diffraction lines are so broad that they cannot be resolved due to being amorphous or ultra-small nanocrystallites. The diffraction lines due to ZnO domains cannot be resolved even by heating the samples at 550 and 650 ^{o}C, see Figure 3.3.7. Therefore, a

more sophisticated characterization tool is needed to determine the crystal structures of ZnO or CdO in the samples.

The UV-Vis absorption spectra of both meso-silica-ZnO-n and meso-SiO_2-CdO-n samples were recorded using the films coated over quartz slides, see Figure 3.3.8. The samples only absorb in the UV region. Note that, the films are crack-free and transparent. The intensity of absorption band gradually increases with increasing ZnO content in the films.

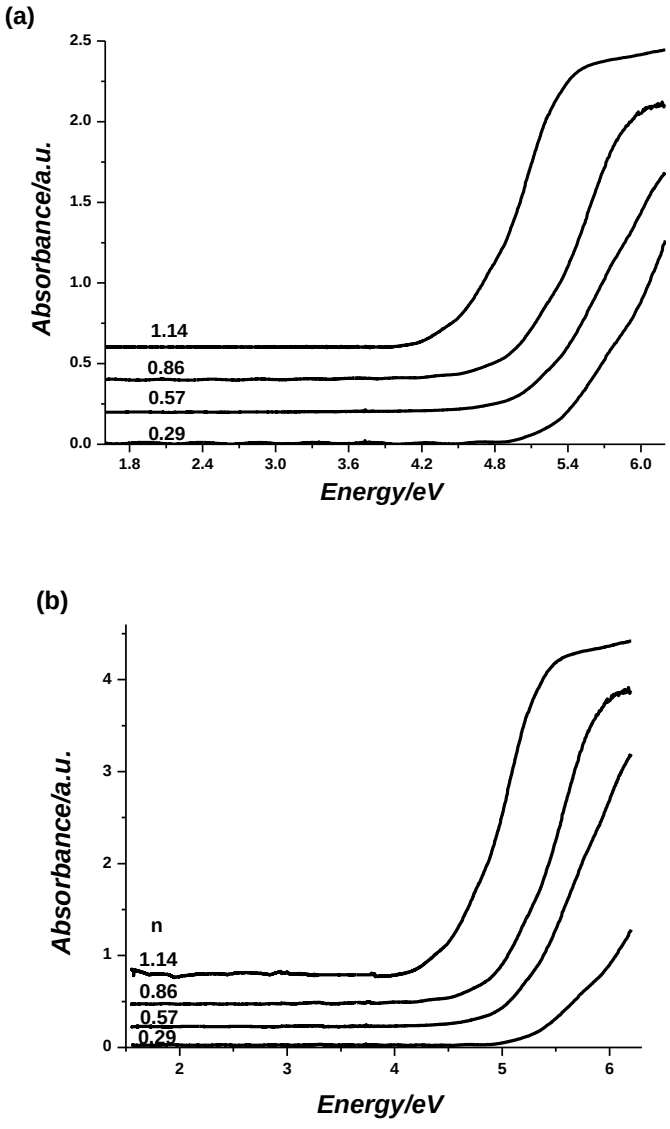

Figure 3.3.8: (a) UV-Vis absorption spectra of meso-silica-ZnO-n (*1*) (b) of meso-silica-CdO-n (n is shown on the spectra)

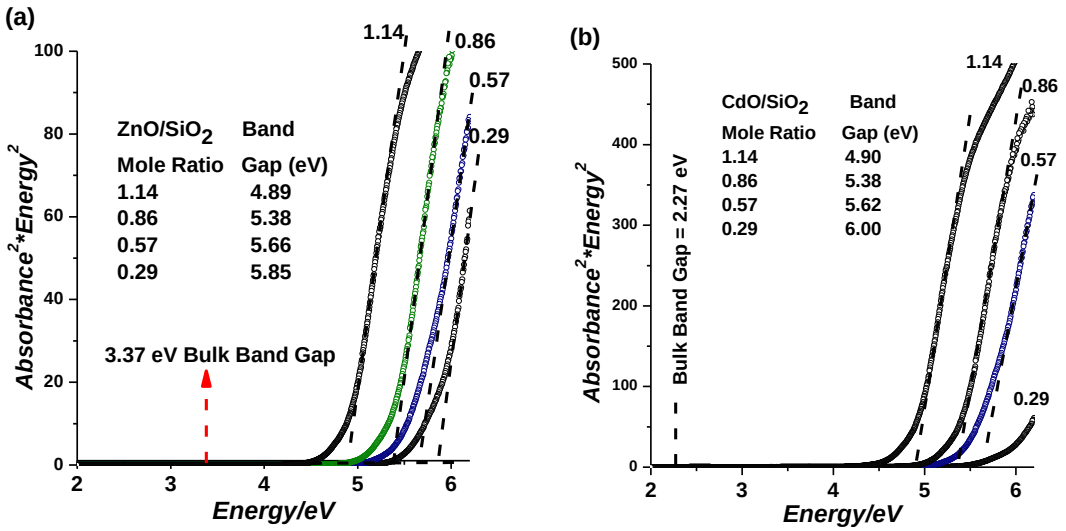

Figure 3.3.9: Direct gap fitting of UV-Vis absorption spectra of (a) meso-silica-ZnO-n (n is the ZnO/SiO_2 mole ratio, inset is a table of composition (ZnO/SiO_2 mole ratio) and band-gap values (eV)) and (b) meso-silica-CdO-n (n is the CdO/SiO_2 mole ratio, inset is a table of composition (CdO/SiO_2 mole ratio) and band-gap values (eV)). (*1*)

In order to find the band gap and also calculate the particle size, the UV-Vis absorption spectra of films were re-plotted using direct gap relationship in which, the y-axis is the square of absorbance times energy and x-axis is the energy, see Figure 3.3.8. The bulk band gap of ZnO is 3.37 eV. (*107*) Compared to bulk oxide, the highest blue shift is 2.48 eV for the meso-silica-ZnO-0.29 film and lowest blue shift is 1.52 eV from the meso-silica-ZnO-1.14. The bulk band gap of CdO is 2.84 eV. The highest blue shift is 3.77 eV from the meso-silica-CdO-0.29 film and lowest blue shift is 2.63 eV for the meso-silica-CdO-1.14. The band gaps of both meso-silica-ZnO-n and meso-silica-CdO-n are listed in the insets of Figure 3.3.8. The blue-shift, observed in both meso-silica-ZnO-n and meso-silica-CdO-n films are due to the quantum confinement effect. It is well known that a decrease in particle size of a semiconductor increases the band gap. The particle size of both CdO and ZnO in the mesostructure can be calculated using an effective mass model (EMM). (*108*) This model is formulated in equation 3.3.1;

$$\mathbf{E(R) = E_g + \hbar^2 \pi^2 / 2R^2 \; x \; (1/m_e + 1/m_h) - 1.8e^2 / 4\pi\epsilon_0\epsilon R} \qquad \textbf{Eq 3.3.1.}$$

where E_g is the bulk band gap (eV), r is particle size (Å), h ($\hbar = h/2\pi$) is the Planck` s constant, m_e is the effective mass of electron, m_h is the effective mass of hole, m_0 is the free electron mass (9.110×10^{-31} kg), ϵ_0 is the permittivity of free space ($8.85418782 \times 10^{-12}$ $C^2N^{-1}m^{-2}$), ϵ is the dielectric constant, e is the charge on the electron (1.602176×10^{-19} C).

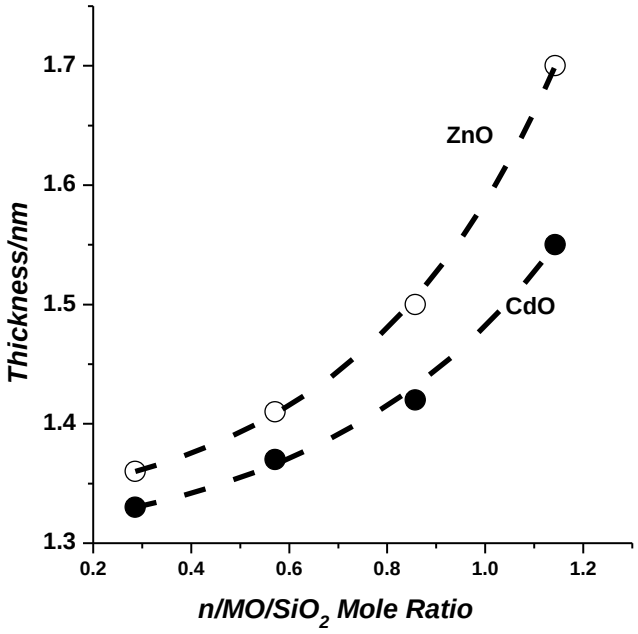

Figure 3.3.10: The plots of the thickness of ZnO and CdO in the meso-silica-MO-n versus n(*1*)

The thickness of ZnO and CdO, calculated using effective-mass model, in the meso-silica-ZnO-n and meso-silica-CdO-n films versus n are plotted in Figure 3.3.10. Thickness of the ZnO or CdO increases with increasing metal content of the samples, Figure 3.3.10. The particle size of ZnO for meso-silica-ZnO-n films alters between 1.4 and 1.7 nm. This means that the ZnO nanoparticles are very small and have a few layer of zinc oxide in the silica framework or over silica-walls. The particle size of CdO domains are calculated to be in the range between 1.3 and 1.6 nm.

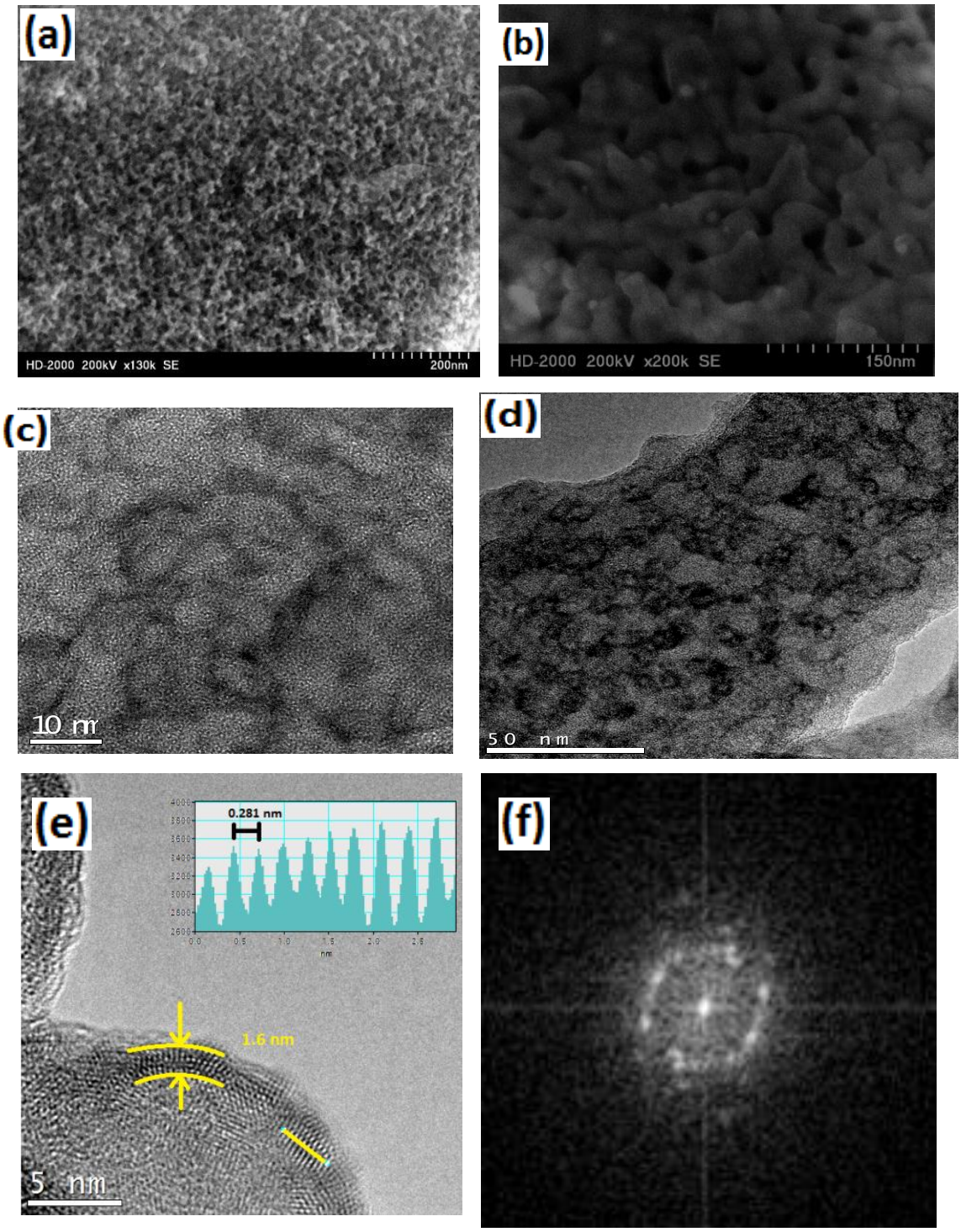

Figure 3.3.11: The SEM images of meso-silica-ZnO-1.14 (a, b), TEM images of meso-silica-ZnO-n, n is (c) 0.86, (d)1.14, and (e) 0.57 (inset is the yellow line showing the spacings between the lines), and (f) FFT of a crystalline domain(*1*).

To further understand the structural details of the films, a series of TEM and SEM images have also been collected and analyzed from some of the meso-silica-ZnO-n and meso-silica-CdO-n samples. The samples for TEM imaging were well grinded in a mortar and diluted in ethanol and dispersed by sonication to get very small particles on a TEM grid. The SEM images of the meso-silica-ZnO-1.14 sample, in Figure 3.3.10 (a) and (b), clearly show that the sample has sponge like mesoporosity. The pores are disordered and have relatively large pore size distribution. The TEM images of the meso-silica-ZnO-n, n is 0.86, 1.14, and 0.57 are shown in Figure 3.3.10 (b), (c) and (d), respectively. Due to contrast difference between silica and ZnO domains, ZnO domains are darker than silica domains. In the high resolution TEM images, Figure 3.3.10 (e), lattice fringes of ZnO crystals can be observed. By taking the Fast Fourier Transform (FFT) of a selected ZnO nanocrystal in the image, the lattice spacing are calculated, see Figure 3.3.10 (f). The observed lattice spacings of 0.281, 0.260, and 0.162 nm are due to the (100), (002), and (110) lattice planes of the ZnO nanocrystallites in wurtzite structure, where the unit cell parameters, a and c are 0.325 and 0.520 nm, respectively, and consistent with bulk ZnO values. In addition, the particle size range between 1.4 and 1.7 nm, calculated from the UV-Vis spectra data is also consistent with the size of these domains, observed in the TEM images. Figure 3.3.10 (e) clearly shows that the particle size is around 1.6 nm for the meso-silica-ZnO-0.57 sample.

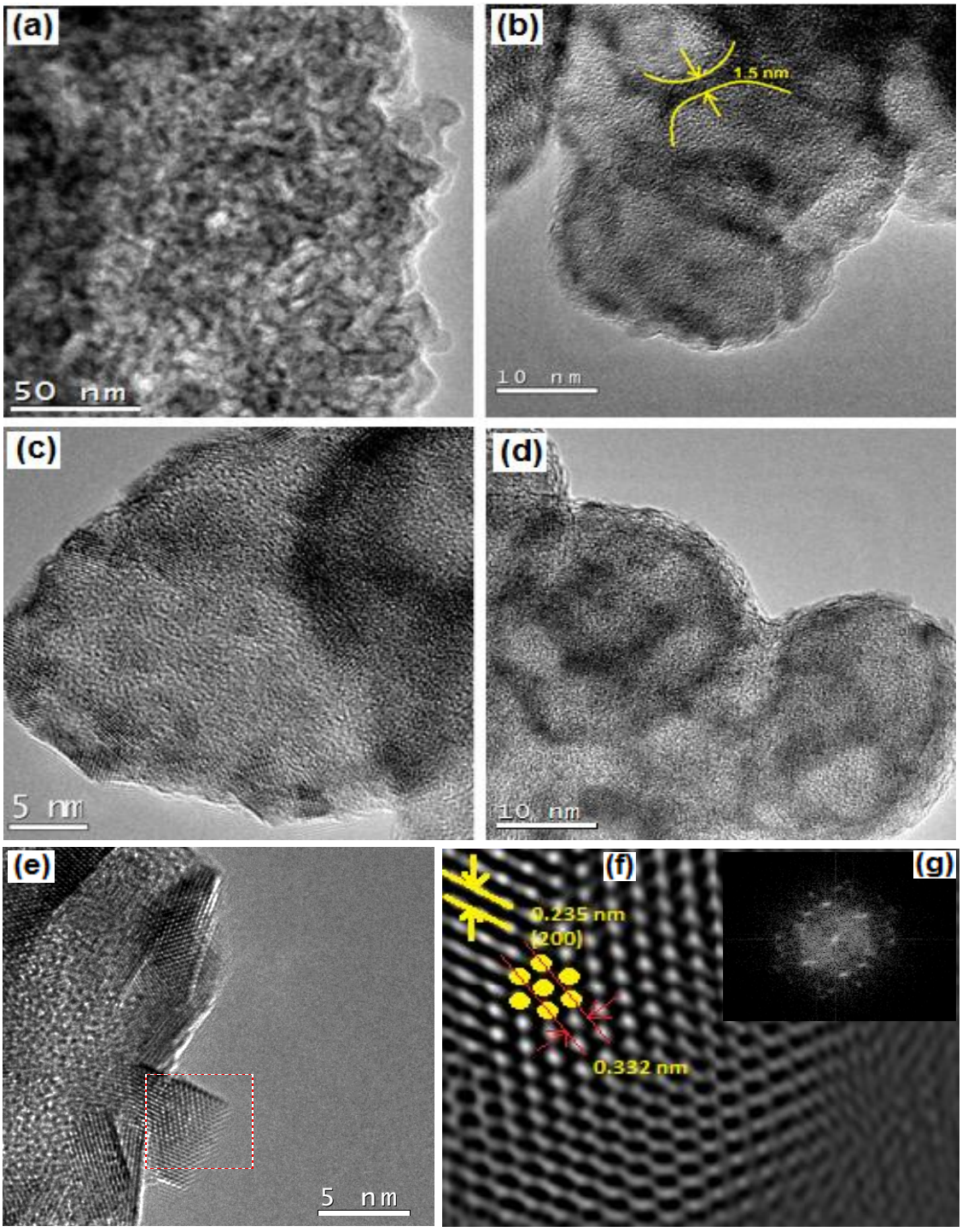

Figure 3.3.12:The TEM images of the meso-silica-CdO-n, n is (a, b) 0.57, (c) 0.86 and (d) 1.14.(e) HRTEM image of the meso-silica-CdO-0.86 and the FFT (f) and inverse FFT (g) of the marked region of (e). (*1*)

Figure 3.3.12 shows the TEM images of the meso-silica-CdO-n smaples, where n is 0.57, 0.86, and 1.14. The TEM images show that the samples are sponge-like mesoporous. Like in the meso-silica-ZnO-n samples, darker domains are due to crystalline CdO particles, see Figure 3.3.11 (b), (c) and (d). In the high resolution TEM images, Figure 3.3.11 (e), the CdO domains are nanocrystalline, and display lattice fringes. The FFT and its inverse FFT of the selected region in the TEM image display lattice spots, corresponding to lattice planes with 0.332, 0.271, and 0.235 nm spacings. They are due to (110), (111), and (200) planes, respectively, of cubic CdO, where the unit cell constant, a, is 0.469 nm.

The high resolution TEM images of the meso-silica-CdO-1.14 sample also show 15 nm nanocrystalline domains, see Figure 3.3.11 (e). However, Figure 3.3.12 (b) shows CdO nanocrystals with a 1.6 nm thicknesses, which is more consistent with the UV-Vis data. If the CdO nanocrystals have confinement at least in one-dimension like in nanoplates, the QCE is observed only on thickness axis of the CdO nanoparticles. Therefore, CdO particles are like nanoflakes (or nanoplates), and the blue shift in the UV-Vis spectra caused by the quantum confinement effect in one-dimension.

Furthermore, in both TEM images of the meso-silica-CdO-n and the meso-silica-ZnO-n, the location of the CdO and ZnO domains, respectively, are not well understood. The darker domains, corresponding to metal oxide, exist as rings and follow each other. However, it is difficult to understand whether metal oxide nanoparticles coat the silica walls or are homogeneously embedded in the silica walls.

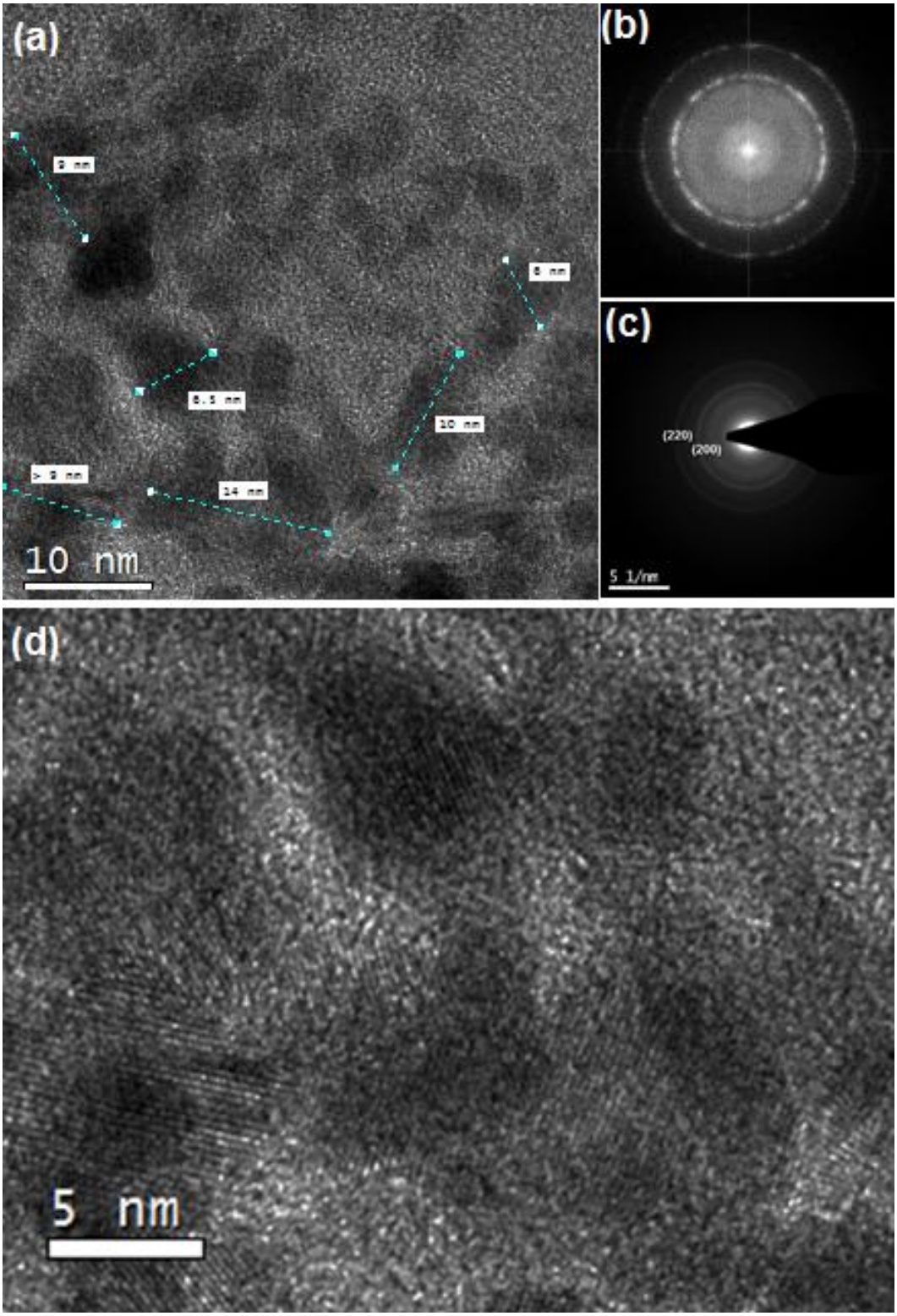

Figure 3.3.13: The meso-silica-CdO-0.86 film upon HF etching; (a) TEM image of (b) FFT of a large area, (c) SAED pattern, (d) magnified TEM image. (*1*)

In order to clear the ambiguity about the morphology of nanocrystals of ZnO and CdO in the mesostructure, the silica walls of the meso-silica-CdO-0.86 film is etched by using a 4% aqueous HF solution. The selected area diffraction pattern (SAED) of the etched samples prove that the CdO nanocrystals have a face centered cubic crystal structure, in which the intense diffraction rings are originating from the (200) and (220) planes of cubic CdO nanocrystallites, see Figure 3.3.13 (c). The FFT of a large area TEM image displays two rings, corresponding to the (200) and (220) planes of cubic CdO crystals. The particles after etching look like nanoflakes as large as 10 to 15 nm. It is difficult to observe the particle thickness. To be consistent and in not conflict with the UV-Vis data, the thickness of the particles must be around 1.6 nm. This can only be explained by the fact that the CdO particles are in the form of nanoplates. The quantum confinement effect is observed in just one dimension, along the thickness axis of the metal oxide nanoplates.

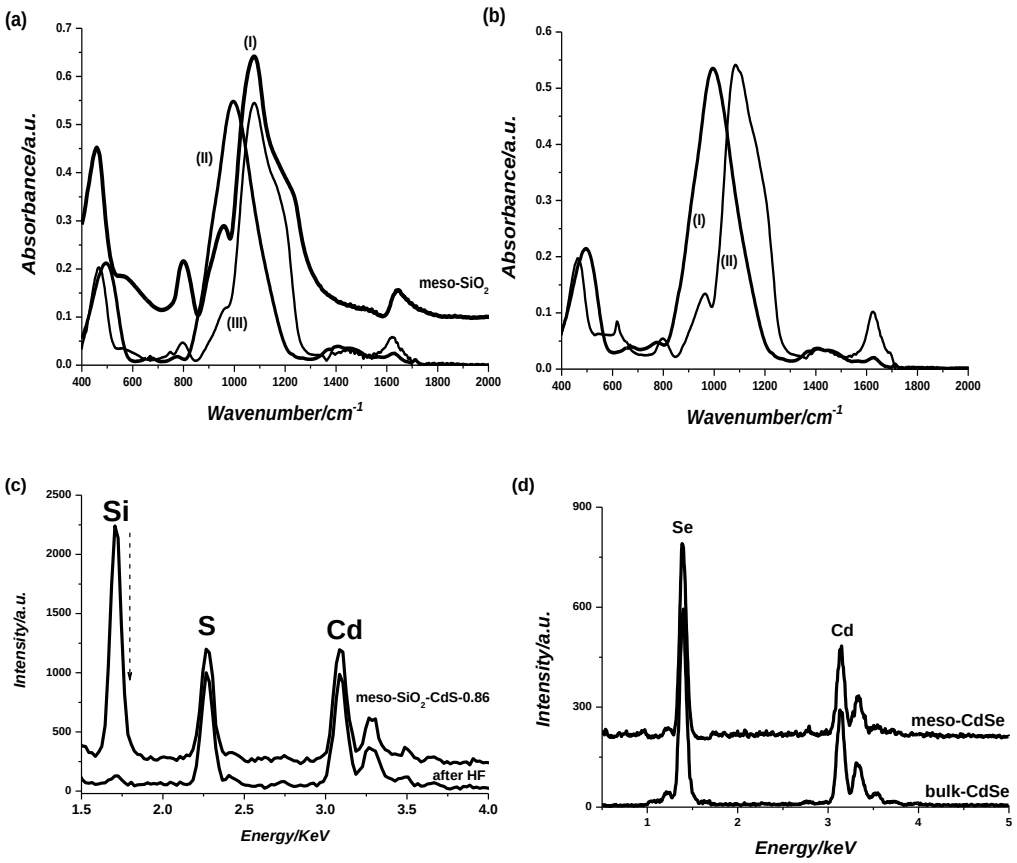

Figure 3.3.14 The FTIR spectra of (a) (I) pure meso-SiO_2 and before H_2Se reaction (II) and after H_2Se reaction of meso-silica-CdO-0.86, (b) before H_2S reaction (I) and after (II) H_2S reaction of meso-silica-CdO-0.86, The EDS spectra of (c) meso-silica-CdS-0.86 and (d) meso-silica-CdSe-0.86 thin films. (*1*)

In order to solve second ambiguity about the structural composition of silica-metal oxide walls, the meso-silica-CdO-0.86 is reacted with a H_2S or H_2Se gases at room temperature to convert CdO nanoplates into CdS or CdSe nanoplates. After reaction of meso-silica-CdO-0.86 with H_2S or H_2Se gas, the samples were denoted as meso-silica-CdS-0.86 and meso-silica-CdSe-0.86, respectively. The samples, before and after reactions, were analyzed by using FTIR spectroscopy, Figure 3.3.14 (a) and (b). The peaks at 914 cm $^{-1}$ corresponding to Si-O-Cd bonds in the FTIR spectrum of the

meso-silica-CdO-0.86 disappear after reactions under H_2S or H_2Se gases. Moreover, the spectra of the meso-silica-CdS-0.86 and the meso-silica-CdSe-0.86 are like pure mesoporous silica. This is due to the fact that all Si-O-Cd bonds break through H_2S or H_2Se reactions. The full conversion of the cadmium oxide to cadmium sulfide or to cadmium selenide was ensured using the EDS data, see Figure 3.3.12. The S/Cd and Se/Cd intensity ratios in the EDS data are the same as commercial bulk CdS and CdSe. In conclusion, the full conversion of the cadmium oxide nanoplates to cadmium sulfide or to cadmium selenide nanoplates proves that the metal oxide nanoplates coat the silica walls: they are not embedded in the silica walls.

meso-silica-CdO-n n (CdO/SiO_2 Mole Ratio)	**Surface Area meso-SiO_2-CdO-n (m^2/g)**	**Surface area for 1 g of CdO (m^2/g)**	**% Surface Coverage**
1.14	50	70	113
0.86	55	85	101
0.57	85	154	58
meso-silica-ZnO-n n (ZnO/SiO_2 Mole Ratio)	**Surface Area meso-SiO_2-CdO-n m^2/g)**	**Surface area for 1 g of CdO (m^2/g)**	**% Surface Coverage**
1.14	130	214	49
0.86	175	325	37
0.57	430	948	13

Table 3.3-1: Parameter for surface coverage calculated from measured data.

Therefore, the CdO and ZnO nanoplates coat the surface of silica walls in the films and the number of Si-O-M bond, where M is Zn or Cd increases by increasing metal oxide content in the samples. The surface coverage of silica wall with metal oxide nanoplates can be calculated hypothetically by using UV-Vis and the N_2 sorption data. The mass of metal oxide in 1 g sample can be calculated using the CdO/SiO_2 mole

ratios. Also, volumes of metal oxide nanoplates can be calculated using the densities of ZnO and CdO and their thickness. The thickness of metal oxide nanoplates is known from UV-Vis data for each sample. Therefore, the surface area of metal oxides nanoplates can easily be calculated by dividing a volume of metal oxide with a specific thickness. If the surface of silica walls is completely covered with metal oxide nanoplates, this hypothetically calculated surface should be the surface area measured by the N_2 sorption measurements. The percent coverage of silica walls can be calculated from the percentage ratios of measured and calculated surface areas. Table 3.3.1 shows the calculated and measured surface areas and also the coverage of silica surface with nanoplates of metal oxides for meso-silica-ZnO-n and meso-silica-CdO-n, where n is 1.14, 0.86, and 0.57. From these calculations, it is reasonable to conclude that a full coverage of the silica surface was achieved in the meso-SiO_2-CdO-0.86 sample, but even in meso-silica-ZnO-1.14, the surface coverage is about 50%,

4 CONCLUSION

The salt-surfactant LLC mesophase concept and the EISA method have been successfully combined to form the mesostructured silica-ZnX or CdY films up to a 1.14 salt/silica mole ratio. Herein, two solvent systems have been employed; the primary solvent is the molten salt that does not evaporate during spin coating and is converted to metal oxide nanoplates during calcination, the second solvent is water, which evaporates during spin coating. Two solvent systems provide our method distinguishes from the EISA method. Therefore, we called this novel method for the synthesis mesoporous silica-metal oxide films as **molten salt assisted self-assembly (MASA)**. In order to employ MASA successfully, there is one very critical prerequisite; the films should be kept above the melting point of salt after spin coating to get stable mesostructured films. Otherwise, most of salt species leach out from the mesostructure, giving bulk metal oxide upon calcination. Also, using transition metal salt having low melting point is very critical. Because of this, metal nitrate salts $[Zn(H_2O)_6](NO_3)_2$ and $[Cd(H_2O)_4](NO_3)_2$), which have melting points very close to RT, are chosen for this investigation. A slow calcination gives uniformly coated 1.4-1.7 nm thick crystalline metal oxide nanoplates on the pore walls of mesoporous silica films. By MASA method, the loading of metal oxide nanoplates in both the meso-silica-ZnO-n and the meso-silica-CdO-n films can be increased up to 1.14 Zn or Cd(II)/silica mole ratios. This leads to ~100 and ~50 % surface coverage of the silica walls in the meso-SiO_2-CdO-n and meso-SiO_2-ZnO-n thin films, respectively. Pure metal oxide nanoplates without silica framework can also be obtained by etching the silica walls using dilute HF solution. The meso-SiO_2-CdO-n films under a H_2S or H_2Se atmosphere can be converted to meso-SiO_2-CdS-n and meso-SiO_2-CdSe-n film, in which all CdO nanoplates are converted to CdS and CdSe nanoplates, respectively. The MASA method is not limited to the mesoporous silica-CdO and ZnO thin films, other transition metal salts or alkali earth metal salts can be used. Also, the MASA method is not limited to silica frameworks; for example, it can also be employed for the synthesis of mesoporous titania-metal oxide films (see future section).

The MASA method has many advantages compared to other methods such as nano-casting, solid-state grinding and EISA methods for the synthesis of mesoporous ZnO and CdO thin films. First advantage is that the MASA process is one-step and facile synthesis method for the preparation of mesoporous silica-metal oxide thin films. Nano-casting and solid-state grinding methods are time consuming due to several long steps. These methods are limited and only employed for the synthesis of powders. Second advantage is that no extra conditions such as humidity, aging, etc., are required in the MASA method. Third advantage is the uniform distribution of metal oxide nanoparticles inside the pores without pore blocking. Final advantage is that the maximum loading can be increased up to 61 and 71 w/w% in the meso-SiO_2-ZnO-n and meso-SiO_2-CdO-n, respectively. The surface coverage can also be adjusted up to ~100 % and ~50 % of silica walls in the meso-SiO_2-CdO-n and meso-SiO_2-ZnO-n thin films, respectively.

Therefore, MASA is a new self-assembly process with many advantages and can be employed to produce mesoporous mixed oxide thin films for thin film applications.

5 FUTURE WORK

5.1 The Preparation of meso-titanina-ZnX-n Thin Films

To show the MASA method is not limited to silica, we have changed the silica with titania. In this work, mesostructured salted-titania films were prepared and investigated towards stable and desired mesoporous titania-ZnO. The films were prepared by spin coating a clear solution of CTAB, $C_{12}EO_{10}$, ZnX,, HNO_3, and $Ti(OBu)_4$ in ethanol. Compared to MASA method in the synthesis of meo-silica-ZnX-n thin films, ethanol has to be used instead of water with an adequate amount of HNO_3 acid, in order to prevent the uncontrolled condensation of titania precursor. Note that $Ti(OBu)_4$ is quite reactive to water. Therefore, MASA method has been modified by changing the polymerizing precursor, solvent and pH to prepare mesostructured ZnX-titania films. The experimental procedure of MASA process is the same with the protocol for the synthesis of meso-silica-ZnO-n films. As-prepared mesostructured ZnX-titania films are denoted as meso-titania-ZnX-n, where n is the Zn/Ti mole ratio. Three samples with n of 0.29, 0,57 and 0,86 has been prepared.

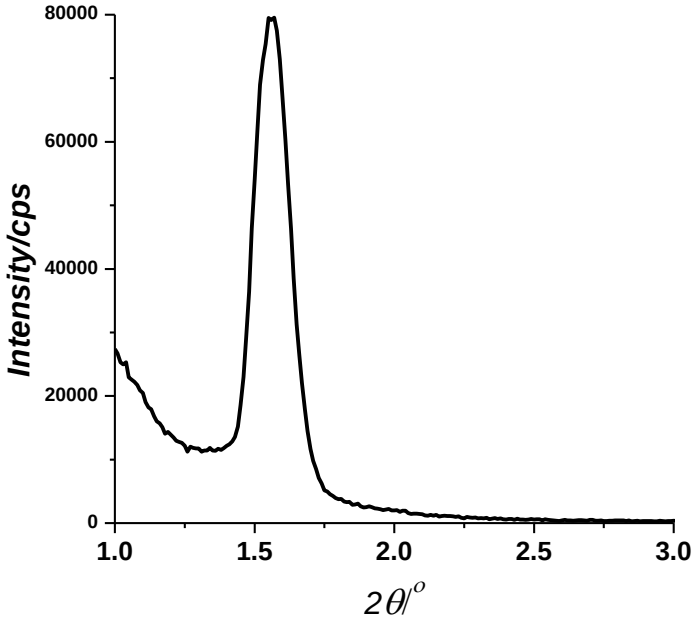

Figure 5.1.1 small-angle XRD pattern of as-prepared meso-titania-ZnX-0.86

Small-angle XRD pattern of the as-prepared meso-titania-ZnX-0.86 display a diffraction line at 1.56°, 2θ (5.6 nm, d-spacing) corresponds to (100) plane of 2D hexagonal mesostructure, Figure 5.1.1. This proves that the MASA method can be applied to synthesize mesoporous titania-ZnO films. Because, as in the synthesis of meso-silica-ZnO-n thin films, the molten ZnX salt can also be confined between the titania and surfactant domains. This is a perquisite to obtain a mesoporous materials upon calcination. Note that keeping the samples above the melting point of salt is very important for the MASA process. Therefore, the fresh as-prepared films have been kept in an oven above the melting point of salt before calcination.

5.2 The Synthesis of meso-titania-Zn_2TiO_4 Thin Films

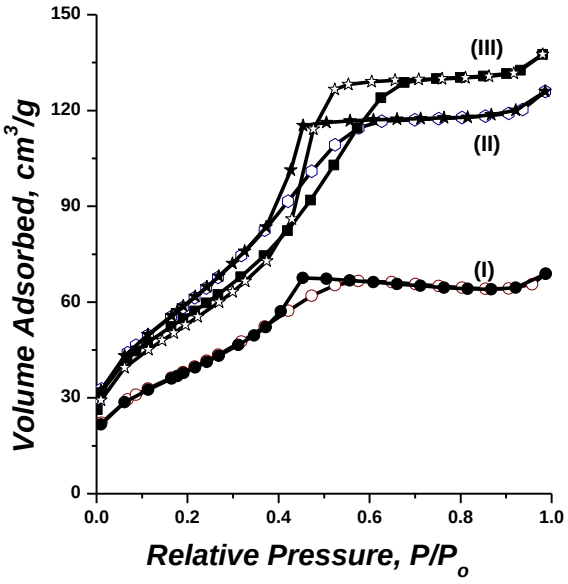

Figure 5.2.1 N_2 sorption isotherms of meso-titania-Zn_2TiO_4 with a Zn/Ti mole ratio of (I) 0.29, (II) 0.57, and (III) 0.89.

As-prepared meso-titania-ZnX-n thin films have been calcined from 60 to 450 °C with an interval of 1 °C/min, and the product is dumped as meso-titania-Zn_2TiO_4. The calcined films have been further characterized by using XRD and N_2 sorption measurements. The N_2 sorption data display type IV isotherms, characteristic of mesoporous materials, see Figure 5.2.1.

To find the structural detail of mesoporous calcined films, the XRD patterns of calcined meso-titania-ZnO-0.86 sample, which was heated at different temperatures, have been recorded, Figure 5.2.2. The wide angle XRD pattern of meso-titania-Zn_2TiO_4-0.86 powders, obtained by scraping around 20 thin films displays broad diffraction lines at 30.0, 34.7, 42.7, 53.5, 56.5, 62, and 72.4^o, 2θ, corresponding to the (220), (311), (400), (422), (511), (440), and (533) planes, respectively, of nanocrystalline Zn_2TiO_4. The particle size increases with heating samples, but the meso-Zn_2TiO_4 is stable up to 650 ^{o}C, see Figure 5.2.2. Note that the sharp diffraction lines corresponding to ZnO bulk oxide was not observed in the XRD pattern.

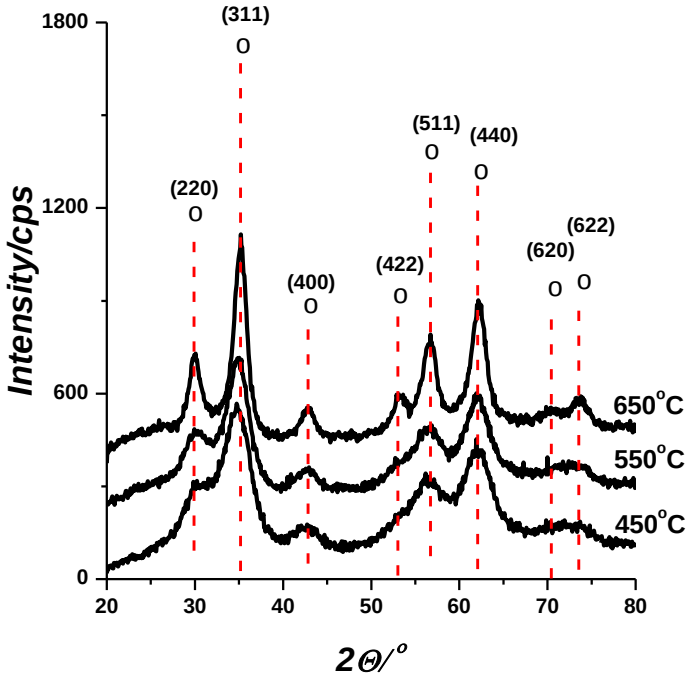

Figure 5.2.2 . The wide angle XRD pattern of meso-titania-Zn_2TiO_4-0.86 powders heated at different temperature (the temeperature are shown in the graph.)

The data of XRD and N_2 sorption measurements ensures that MASA method is applicable for the synthesis of mesoporous titania-metal oxide samples. Although the mesoporosity can successively be formed by the MASA method, the composition of the

pore-walls is quite different from that of silica. These two metals, titanium and zinc, form mixed oxide, zinc titanate, rather than titania-ZnO as in the silica system. The MASA method can be further adopted to obtain other metal titanates, possibly mixed metal titanates.

6 REFERENCES

1. C. Karakaya, Y. Turker, C. Albayrak, O. Dag, Assembly of Molten Transition Metal Salt–Surfactant in a Confined Space for the Synthesis of Mesoporous Metal Oxide-Rich Metal Oxide–Silica Thin Films. *Chemistry of Materials* 23, 3062 (2011/06/28, 2011).

2. L. B. McCusker, F. Liebau, G. Engelhardt, Nomenclature of structural and compositional characteristics of ordered microporous and mesoporous materials with inorganic hosts - (IUPAC recommendations 2001). *Pure Appl. Chem.* 73, 381 (Feb, 2001).

3. G. Schrimpf, M. Schlenkrich, J. Brickmann, P. Bopp, Molecular dynamics simulation of zeolite NaY: a study of structure, dynamics, and thermalization of sorbates. *The Journal of Physical Chemistry* 96, 7404 (1992/09/01, 1992).

4. T. T. Moore, W. J. Koros, Non-ideal effects in organic–inorganic materials for gas separation membranes. *Journal of Molecular Structure* 739, 87 (2005).

5. A. Corma, V. Fornes, S. B. Pergher, T. L. M. Maesen, J. G. Buglass, Delaminated zeolite precursors as selective acidic catalysts. *Nature* 396, 353 (Nov, 1998).

6. A. Farkas, M. Rozic, Z. Barbaric-Mikocevic, Ammonium exchange in leakage waters of waste dumps using natural zeolite from the Krapina region, Croatia. *J. Hazard. Mater.* 117, 25 (Jan, 2005).

7. K. Egeblad, C. H. Christensen, M. Kustova, C. H. Christensen, Templating Mesoporous Zeolites†. *Chemistry of Materials* 20, 946 (2008/02/01, 2007).

8. T. Yanagisawa, T. Shimizu, K. Kuroda, C. Kato, THE PREPARATION OF ALKYLTRIMETHYLAMMONIUM-KANEMITE COMPLEXES AND THEIR CONVERSION TO MICROPOROUS MATERIALS. *Bull. Chem. Soc. Jpn.* 63, 988 (Apr, 1990).

9. C. T. Kresge, M. E. Leonowicz, W. J. Roth, J. C. Vartuli, J. S. Beck, ORDERED MESOPOROUS MOLECULAR-SIEVES SYNTHESIZED BY A LIQUID-CRYSTAL TEMPLATE MECHANISM. *Nature* 359, 710 (Oct, 1992).

10. J. S. Beck *et al.*, A new family of mesoporous molecular sieves prepared with liquid crystal templates. *Journal of the American Chemical Society* 114, 10834 (1992/12/01, 1992).

11. P. Selvam, S. K. Bhatia, C. G. Sonwane, Recent Advances in Processing and Characterization of Periodic Mesoporous MCM-41 Silicate Molecular

Sieves. *Industrial & Engineering Chemistry Research* 40, 3237 (2001/07/01, 2001).

12. P. Feng, X. Bu, G. D. Stucky, D. J. Pine, Monolithic Mesoporous Silica Templated by Microemulsion Liquid Crystals. *Journal of the American Chemical Society* 122, 994 (2000/02/01, 1999).

13. Q. Huo *et al.*, Generalized synthesis of periodic surfactant/inorganic composite materials. *Nature* 368, 317 (1994).

14. D. Zhao *et al.*, Novel Mesoporous Silicates with Two-Dimensional Mesostructure Direction Using Rigid Bolaform Surfactants. *Chemistry of Materials* 11, 2668 (1999/10/01, 1999).

15. D. Zhao *et al.*, Continuous Mesoporous Silica Films with Highly Ordered Large Pore Structures. *Advanced Materials* 10, 1380 (1998).

16. D. Zhao *et al.*, Triblock Copolymer Syntheses of Mesoporous Silica with Periodic 50 to 300 Angstrom Pores. *Science* 279, 548 (January 23, 1998, 1998).

17. D. Zhao, Q. Huo, J. Feng, B. F. Chmelka, G. D. Stucky, Nonionic Triblock and Star Diblock Copolymer and Oligomeric Surfactant Syntheses of Highly Ordered, Hydrothermally Stable, Mesoporous Silica Structures. *Journal of the American Chemical Society* 120, 6024 (1998/06/01, 1998).

18. Q. Huo, D. I. Margolese, G. D. Stucky, Surfactant Control of Phases in the Synthesis of Mesoporous Silica-Based Materials. *Chemistry of Materials* 8, 1147 (1996/01/01, 1996).

19. Q. Huo *et al.*, Organization of Organic Molecules with Inorganic Molecular Species into Nanocomposite Biphase Arrays. *Chemistry of Materials* 6, 1176 (1994/08/01, 1994).

20. G. S. Attard, J. C. Glyde, C. G. Goltner, Liquid-crystalline phases as templates for the synthesis of mesoporous silica. *Nature* 378, 366 (1995).

21. K. J. Edler, P. A. Reynolds, A. S. Brown, T. M. Slawecki, J. W. White, Shear and salt effects on the structure of MCM-41 synthesis gels. *J. Chem. Soc.-Faraday Trans.* 94, 1287 (May, 1998).

22. A. Firouzi, D. J. Schaefer, S. H. Tolbert, G. D. Stucky, B. F. Chmelka, Magnetic-field-induced orientational ordering of alkaline lyotropic silicate - surfactant liquid crystals. *Journal of the American Chemical Society* 119, 9466 (Oct, 1997).

23. V. R. Tirumala *et al.*, Mesoporous Silica Films with Long-Range Order Prepared from Strongly Segregated Block Copolymer/Homopolymer Blend Templates. *Chemistry of Materials* 19, 5868 (2007/11/01, 2007).

24. N. Nishiyama, S. Tanaka, Y. Egashira, Y. Oku, K. Ueyama, Enhancement of Structural Stability of Mesoporous Silica Thin Films Prepared by Spin-Coating. *Chemistry of Materials* 14, 4229 (2002/10/01, 2002).

25. C. J. Brinker, Y. Lu, A. Sellinger, H. Fan, Evaporation-Induced Self-Assembly: Nanostructures Made Easy. *Advanced Materials* 11, 579 (1999).

26. D. Grosso *et al.*, Fundamentals of Mesostructuring Through Evaporation-Induced Self-Assembly. *Advanced Functional Materials* 14, 309 (2004).

27. Zheng, M. Suzuki, T. Inoue, Phase Behavior of an Aqueous Mixture of Octaethylene Glycol Dodecyl Ether Revealed by DSC, FT-IR, and 13C NMR Measurements. *Langmuir* 18, 1991 (2002/03/01, 2002).

28. N. A. Melosh, P. Davidson, B. F. Chmelka, Monolithic Mesophase Silica with Large Ordering Domains. *Journal of the American Chemical Society* 122, 823 (2000/02/01, 2000).

29. N. A. Melosh *et al.*, Molecular and Mesoscopic Structures of Transparent Block Copolymer−Silica Monoliths. *Macromolecules* 32, 4332 (1999/06/01, 1999).

30. D. Grosso *et al.*, Two-Dimensional Hexagonal Mesoporous Silica Thin Films Prepared from Block Copolymers: Detailed Characterization and Formation Mechanism. *Chemistry of Materials* 13, 1848 (2001/05/01, 2001).

31. A. Gibaud *et al.*, Evaporation-Controlled Self-Assembly of Silica Surfactant Mesophases. *The Journal of Physical Chemistry B* 107, 6114 (2003/06/01, 2003).

32. Y. Lu *et al.*, Aerosol-assisted self-assembly of mesostructured spherical nanoparticles. *Nature* 398, 223 (1999).

33. G. Soler-Illia *et al.*, Mesoporous hybrid and nanocomposite thin films. A sol–gel toolbox to create nanoconfined systems with localized chemical properties. *Journal of Sol-Gel Science and Technology* 57, 299 (2011).

34. A. Taguchi, F. Schüth, Ordered mesoporous materials in catalysis. *Microporous and Mesoporous Materials* 77, 1 (2005).

35. M. Hartmann, Ordered Mesoporous Materials for Bioadsorption and Biocatalysis. *Chemistry of Materials* 17, 4577 (2005/09/01, 2005).

36. M. A. Carreon, V. V. Guliants, Ordered Meso- and Macroporous Binary and Mixed Metal Oxides. *European Journal of Inorganic Chemistry* 2005, 27 (2005).

37. M. H. Bartl, S. W. Boettcher, E. L. Hu, G. D. Stucky, Dye-Activated Hybrid Organic/Inorganic Mesostructured Titania Waveguides. *Journal of the American Chemical Society* 126, 10826 (2004/09/01, 2004).

38. S. W. Boettcher, J. Fan, C.-K. Tsung, Q. Shi, G. D. Stucky, Harnessing the Sol–Gel Process for the Assembly of Non-Silicate Mesostructured Oxide Materials. *Accounts of Chemical Research* 40, 784 (2007/09/01, 2007).

39. P. Yang, D. Zhao, D. I. Margolese, B. F. Chmelka, G. D. Stucky, Generalized syntheses of large-pore mesoporous metal oxides with semicrystalline frameworks. *Nature* 396, 152 (1998).

40. P. Yang, D. Zhao, D. I. Margolese, B. F. Chmelka, G. D. Stucky, Block Copolymer Templating Syntheses of Mesoporous Metal Oxides with Large Ordering Lengths and Semicrystalline Framework. *Chemistry of Materials* 11, 2813 (1999/10/01, 1999).

41. P. C. A. Alberius *et al.*, General Predictive Syntheses of Cubic, Hexagonal, and Lamellar Silica and Titania Mesostructured Thin Films§. *Chemistry of Materials* 14, 3284 (2002/08/01, 2002).

42. J. Haetge, P. Hartmann, K. Brezesinski, J. Janek, T. Brezesinski, Ordered Large-Pore Mesoporous Li4Ti5O12 Spinel Thin Film Electrodes with Nanocrystalline Framework for High Rate Rechargeable Lithium Batteries: Relationships among Charge Storage, Electrical Conductivity, and Nanoscale Structure. *Chemistry of Materials* 23, 4384 (2011/10/11, 2011).

43. T. Brezesinski *et al.*, Self-Assembly and Crystallization Behavior of Mesoporous, Crystalline HfO2 Thin Films: A Model System for the Generation of Mesostructured Transition-Metal Oxides. *Small* 1, 889 (2005).

44. K. Cassiers *et al.*, Surfactant-Directed Synthesis of Mesoporous Titania with Nanocrystalline Anatase Walls and Remarkable Thermal Stability. *The Journal of Physical Chemistry B* 108, 3713 (2004/03/01, 2004).

45. P. C. Angelomé, G. J. d. A. A. Soler-Illia, Organically Modified Transition-Metal Oxide Mesoporous Thin Films and Xerogels. *Chemistry of Materials* 17, 322 (2005/01/01, 2004).

46. J. C. Yu, L. Zhang, Z. Zheng, J. Zhao, Synthesis and Characterization of Phosphated Mesoporous Titanium Dioxide with High Photocatalytic Activity. *Chemistry of Materials* 15, 2280 (2003/06/01, 2003).

47. Wu *et al.*, Hollow Spheres Based on Mesostructured Lead Titanate with Amorphous Framework. *Langmuir* 19, 1362 (2003/02/01, 2003).

48. M. Mamak, N. Coombs, G. Ozin, Self-Assembling Solid Oxide Fuel Cell Materials: Mesoporous Yttria-Zirconia and Metal-Yttria-Zirconia Solid Solutions. *Journal of the American Chemical Society* 122, 8932 (2000/09/01, 2000).

49. B. Sun *et al.*, Synthesis of Mesoporous α-Fe2O3 Nanostructures for Highly Sensitive Gas Sensors and High Capacity Anode Materials in Lithium Ion Batteries. *The Journal of Physical Chemistry C* 114, 18753 (2010/11/11, 2010).

50. A. K. Sinha, K. Suzuki, Three-Dimensional Mesoporous Chromium Oxide: A Highly Efficient Material for the Elimination of Volatile Organic Compounds. *Angewandte Chemie* 117, 275 (2005).

51. S. Banerjee, A. Santhanam, A. Dhathathreyan, P. M. Rao, Synthesis of Ordered Hexagonal Mesostructured Nickel Oxide. *Langmuir* 19, 5522 (2003/06/01, 2003).

52. J. Deng *et al.*, Ultrasound-Assisted Nanocasting Fabrication of Ordered Mesoporous MnO2 and Co3O4 with High Surface Areas and Polycrystalline Walls. *The Journal of Physical Chemistry C* 114, 2694 (2010/02/18, 2010).

53. G. S. Armatas, A. P. Katsoulidis, D. E. Petrakis, P. J. Pomonis, M. G. Kanatzidis, Nanocasting of Ordered Mesoporous Co3O4-Based Polyoxometalate Composite Frameworks. *Chemistry of Materials* 22, 5739 (2010/10/26, 2010).

54. C. West, R. Mokaya, Nanocasting of High Surface Area Mesoporous Ga2O3 and GaN Semiconductor Materials. *Chemistry of Materials* 21, 4080 (2009/09/08, 2009).

55. P. Ji, J. Zhang, F. Chen, M. Anpo, Ordered Mesoporous CeO2 Synthesized by Nanocasting from Cubic Ia3d Mesoporous MCM-48 Silica: Formation, Characterization and Photocatalytic Activity. *The Journal of Physical Chemistry C* 112, 17809 (2008/11/20, 2008).

56. M. Tiemann, Repeated Templating†. *Chemistry of Materials* 20, 961 (2008/02/01, 2007).

57. J.-H. Smått, C. Weidenthaler, J. B. Rosenholm, M. Lindén, Hierarchically Porous Metal Oxide Monoliths Prepared by the Nanocasting Route. *Chemistry of Materials* 18, 1443 (2006/03/01, 2006).

58. B. Tian *et al.*, General Synthesis of Ordered Crystallized Metal Oxide Nanoarrays Replicated by Microwave-Digested Mesoporous Silica. *Advanced Materials* 15, 1370 (2003).

59. W. Shen, X. Dong, Y. Zhu, H. Chen, J. Shi, Mesoporous CeO2 and CuO-loaded mesoporous CeO2: Synthesis, characterization, and CO catalytic oxidation property. *Microporous and Mesoporous Materials* 85, 157 (2005).

60. E. Rossinyol *et al.*, Nanostructured metal oxides synthesized by hard template method for gas sensing applications. *Sensors and Actuators B: Chemical* 109, 57 (2005).

61. T. Wagner, J. Roggenbuck, C.-D. Kohl, M. Fröba, M. Tiemann, in *Studies in Surface Science and Catalysis*, S. Q. Y. T. Dongyuan Zhao, Y. Chengzhong, Eds. (Elsevier, 2007), vol. Volume 165, pp. 347-350.

62. M. Tiemann, Porous Metal Oxides as Gas Sensors. *Chemistry – A European Journal* 13, 8376 (2007).

63. K. M. Shaju, F. Jiao, A. Debart, P. G. Bruce, Mesoporous and nanowire Co3O4 as negative electrodes for rechargeable lithium batteries. *Physical Chemistry Chemical Physics* 9, 1837 (2007).

64. A. Rumplecker, F. Kleitz, E.-L. Salabas, F. Schüth, Hard Templating Pathways for the Synthesis of Nanostructured Porous Co3O4. *Chemistry of Materials* 19, 485 (2007/02/01, 2007).

65. K. Zhu, B. Yue, W. Zhou, H. He, Preparation of three-dimensional chromium oxide porous single crystals templated by SBA-15. *Chemical Communications*, 98 (2003).

66. C. Dickinson *et al.*, Formation Mechanism of Porous Single-Crystal Cr2O3 and Co3O4 Templated by Mesoporous Silica. *Chemistry of Materials* 18, 3088 (2006/06/01, 2006).

67. W. Zhou, K. Zhu, B. Yue, H. He, C. Dickinson, in *Studies in Surface Science and Catalysis*, I. M. C. E. van Steen, L. H. Callanan, Eds. (Elsevier, 2004), vol. Volume 154, Part A, pp. 924-930.

68. M. Imperor-Clerc, D. Bazin, M.-D. Appay, P. Beaunier, A. Davidson, Crystallization of β-MnO2 Nanowires in the Pores of SBA-15 Silicas: In Situ Investigation Using Synchrotron Radiation. *Chemistry of Materials* 16, 1813 (2004/05/01, 2004).

69. S. Zhu, Z. Zhou, D. Zhang, H. Wang, Synthesis of mesoporous amorphous MnO2 from SBA-15 via surface modification and ultrasonic waves. *Microporous and Mesoporous Materials* 95, 257 (2006).

70. S. C. Laha, R. Ryoo, Synthesis of thermally stable mesoporous cerium oxide with nanocrystalline frameworks using mesoporous silica templates. *Chemical Communications*, 2138 (2003).

71. K. Jiao *et al.*, Growth of porous single-crystal Cr2O3 in a 3-D mesopore system. *Chemical Communications*, 5618 (2005).

72. F. Jiao *et al.*, Ordered Mesoporous Fe2O3 with Crystalline Walls. *Journal of the American Chemical Society* 128, 5468 (2006/04/01, 2006).

73. B. Tian *et al.*, Facile Synthesis and Characterization of Novel Mesoporous and Mesorelief Oxides with Gyroidal Structures. *Journal of the American Chemical Society* 126, 865 (2004/01/01, 2003).

74. W. Yue, A. H. Hill, A. Harrison, W. Zhou, Mesoporous single-crystal Co3O4 templated by cage-containing mesoporous silica. *Chemical Communications*, 2518 (2007).

75. X. Lai *et al.*, Ordered Mesoporous Copper Oxide with Crystalline Walls. *Angewandte Chemie International Edition* 46, 738 (2007).

76. J. Roggenbuck, M. Tiemann, Ordered Mesoporous Magnesium Oxide with High Thermal Stability Synthesized by Exotemplating Using CMK-3 Carbon. *Journal of the American Chemical Society* 127, 1096 (2005/02/01, 2005).

77. T. Waitz *et al.*, Crystalline ZnO with an enhanced surface area obtained by nanocasting. *Applied Physics Letters* 90, 123108 (2007).

78. B. Tian *et al.*, Microwave assisted template removal of siliceous porous materials. *Chemical Communications*, 1186 (2002).

79. Y. Q. Wang *et al.*, Directing the Formation of Vinyl-Functionalized Silica to the Hexagonal SBA-15 or Large-Pore Ia3d Structure. *Chemistry of Materials* 15, 5029 (2003/12/01, 2003).

80. B. Yue *et al.*, Preparation and characterization of three-dimensional mesoporous crystals of tungsten oxide. *Chemical Physics Letters* 407, 83 (2005).

81. J. Roggenbuck, G. Koch, M. Tiemann, Synthesis of Mesoporous Magnesium Oxide by CMK-3 Carbon Structure Replication. *Chemistry of Materials* 18, 4151 (2006/08/01, 2006).

82. R. Zhang, S. Kumar, S. Zou, L. L. Kerr, High-Density Vertically Aligned ZnO Rods with a Multistage Terrace Structure and Their Improved Solar Cell Efficiency. *Crystal Growth & Design* 8, 381 (2008/02/01, 2007).

83. Y.-Z. Zheng *et al.*, Novel ZnO-Based Film with Double Light-Scattering Layers as Photoelectrodes for Enhanced Efficiency in Dye-Sensitized Solar Cells†. *Chemistry of Materials* 22, 928 (2010/02/09, 2009).

84. Y. M. Wang, Z. Y. Wu, L. Y. Shi, J. H. Zhu, Rapid Functionalization of Mesoporous Materials: Directly Dispersing Metal Oxides into As-Prepared SBA-15 Occluded with Template. *Advanced Materials* 17, 323 (2005).

85. W.-H. Tian *et al.*, Adsorptive Desulfurization by Copper Species within Confined Space. *Langmuir* 26, 17398 (2010/11/16, 2010).

86. E. Li, V. Rudolph, Transesterification of Vegetable Oil to Biodiesel over MgO-Functionalized Mesoporous Catalysts†. *Energy & Fuels* 22, 145 (2008/01/01, 2007).

87. Z. Y. Wu *et al.*, Generating Superbasic Sites on Mesoporous Silica SBA-15. *Chemistry of Materials* 18, 4600 (2006/09/01, 2006).

88. Y. M. Wang, Z. Y. Wu, H. J. Wang, J. H. Zhu, Fabrication of Metal Oxides Occluded in Ordered Mesoporous Hosts via a Solid-State Grinding Route: The Influence of Host–Guest Interactions. *Advanced Functional Materials* 16, 2374 (2006).

89. Ö. Çelik, Ö. Dag, A New Lyotropic Liquid Crystalline System: Oligo(ethylene oxide) Surfactants with $[M(H_2O)_n]X_m$ Transition Metal Complexes. *Angewandte Chemie International Edition* 40, 3799 (2001).

90. C. Albayrak, N. Özkan, O. Dag, Origin of Lyotropic Liquid Crystalline Mesophase Formation and Liquid Crystalline to Mesostructured Solid Transformation in the Metal Nitrate Salt−Surfactant Systems. *Langmuir* 27, 870 (2011/02/01, 2010).

91. A. F. Demirörs, B. E. Eser, Ö. Dag, Liquid Crystalline Mesophases of Pluronics (L64, P65, and P123) and Transition Metal Nitrate Salts ([M(H2O)6](NO3)2). *Langmuir* 21, 4156 (2005/04/01, 2005).

92. Ö. Dag, O. Samarskaya, C. Tura, A. Günay, Ö. Çelik, Spectroscopic Investigation of Nitrate−Metal and Metal−Surfactant Interactions in the Solid AgNO3/C12EO10 and Liquid-Crystalline [M(H2O)n](NO3)2/C12EO10 Systems. *Langmuir* 19, 3671 (2003/04/01, 2003).

93. Ö. Dag, S. Alayoğlu, İ. Uysal, Effects of Ions on the Liquid Crystalline Mesophase of Transition-Metal Salt:Surfactant (CnEOm). *The Journal of Physical Chemistry B* 108, 8439 (2004/06/01, 2004).

94. C. Albayrak, A. M. Soylu, O. Dag, Lyotropic Liquid-Crystalline Mesophases of [Zn(H2O)6](NO3)2−C12EO10−CTAB−H2O and

[Zn(H2O)6](NO3)2−C12EO10−SDS−H2O Systems. *Langmuir* 24, 10592 (2008/10/07, 2008).

95. D. R. Clarke, Varistor Ceramics. *Journal of the American Ceramic Society* 82, 485 (1999).

96. B. K. Meyer *et al.*, Bound exciton and donor–acceptor pair recombinations in ZnO. *physica status solidi (b)* 241, 231 (2004).

97. D. C. Look, B. Claflin, P-type doping and devices based on ZnO. *physica status solidi (b)* 241, 624 (2004).

98. C. Klingshirn, The Luminescence of ZnO under High One- and Two-Quantum Excitation. *physica status solidi (b)* 71, 547 (1975).

99. S. Polarz, F. Neues, M. W. E. van den Berg, W. Grünert, L. Khodeir, Mesosynthesis of ZnO−Silica Composites for Methanol Nanocatalysis. *Journal of the American Chemical Society* 127, 12028 (2005/08/01, 2005).

100. G. Xiong, L. Luo, C. Li, X. Yang, Synthesis of Mesoporous ZnO (m-ZnO) and Catalytic Performance of the Pd/m-ZnO Catalyst for Methanol Steam Reforming. *Energy & Fuels* 23, 1342 (2009/03/19, 2009).

101. S. Polarz, A. V. Orlov, F. Schüth, A.-H. Lu, Preparation of High-Surface-Area Zinc Oxide with Ordered Porosity, Different Pore Sizes, and Nanocrystalline Walls. *Chemistry – A European Journal* 13, 592 (2007).

102. S. Lepoutre *et al.*, Nanocasted mesoporous nanocrystalline ZnO thin films. *Journal of Materials Chemistry* 20, 537 (2010).

103. Q. Jiang *et al.*, Fabrication of photoluminescent ZnO/SBA-15 through directly dispersing zinc nitrate into the as-prepared mesoporous silica occluded with template. *Journal of Materials Chemistry* 16, 1536 (2006).

104. K. Niu *et al.*, Fabrication and Photoluminescent Properties of ZnO/Mesoporous Silica Composites Templated by a Chelating Surfactant. *Langmuir* 27, 13820 (2011/11/15, 2011).

105. W.-H. Zhang, J.-L. Shi, L.-Z. Wang, D.-S. Yan, Preparation and Characterization of ZnO Clusters inside Mesoporous Silica. *Chemistry of Materials* 12, 1408 (2000/05/01, 2000).

106. M. D. Alba, Z. Luan, J. Klinowski, Titanosilicate Mesoporous Molecular Sieve MCM-41: Synthesis and Characterization. *The Journal of Physical Chemistry* 100, 2178 (1996/01/01, 1996).

107. U. Ozgur *et al.*, A comprehensive review of ZnO materials and devices. *Journal of Applied Physics* 98, 041301 (2005).

108. L. Brus, Electronic wave functions in semiconductor clusters: experiment and theory. *The Journal of Physical Chemistry* 90, 2555 (1986/06/01, 1986).

APPENDIX

(1) Reprinted from Chemistry of Materials, Vol. 23, C. Karakaya, Y. Turker, O. Dag. "Assembly of Molten Transition Metal Salt–Surfactant in a Confined Space for the Synthesis of Mesoporous Metal Oxide-Rich Metal Oxide–Silica Thin Films" 3062-3071 (2011), with permission from ACS.

(27) Reprinted from Langmuir, Vol. 18 L. Zheng, M. Suzuki, and T. Inoue " Phase Behavior of an Aqueous Mixture of Octaethylene Glycol Dodecyl Ether Revealed by DSC, FT-IR, and ^{13}C NMR Measurements" 1991-1998, (2002), with permission from ACS.

(33) Reprinted from Journal of Sol-Gel Science and Technology, Vol. 57; L. G. J. A. A. Soler-Illia , P. C. Angelomé, M. C. Fuertes, A. Calvo, A. Wolosiuk, A. Zelcer , M. G. Bellino and E. D. Martínez " Mesoporous hybrid and nanocomposite thin films. A sol–gel toolbox to create nanoconfined systems with localized chemical properties " 299-312, (2011), with permission from Springer.

(89) Reprinted from Angewandte Chemie International Edition, Vol. 113 Issue 20; Ö Çelik, Ö Dag A New Lyotropic Liquid Crystalline System: Oligo(ethylene oxide) Surfactants with $[M(H_2O)_{n]}X_m$ Transition Metal Complexes " 3915–3919, (2001), with permission from Willey

(90) Reprinted from Langmuir, Vol. 27; C. Albayrak, N. Ozkan, Ö Dag A New Lyotropic Liquid Crystalline System: " Origin of Lyotropic Liquid Crystalline Mesophase Formation and Liquid Crystalline to Mesostructured Solid Transformation in the Metal Nitrate Salt−Surfactant Systems " 870-873, (2001), with permission from ACS